Study of Intrinsic Properties of HII Galaxies at High Redshift

by

Ana Luisa González Morán

Thesis submitted as partial requirement for obtaining the degree of

MASTER OF SCIENCE IN ASTROPHYSICS

at the

Instituto Nacional de Astrofísica, Óptica y Electrónica

July 2015
Tonantzintla, Puebla

Directed by:

Dr. Elena Terlevich
Tenured Researcher INAOE, Mexico

Dr. Roberto Terlevich
Tenured Researcher INAOE, Mexico; IoA, UK

Dr. Manolis Plionis
Tenured Researcher INAOE, Mexico; AUTh, Greece

To my Family

Acknowledgements

For the realization of this thesis I had the help of many people to whom I would like to thank.

To my advisors Dra. Elena Terlevich, Dr. Roberto Terlevich and Dr. Manolis Plionis, thank you very much for being so patient and support me in everything necessary. From you I learned a lot and your help was of great importance for the realization of this work. I am also very grateful to Ricardo Chávez and David Fernández for their help and many useful comments, specifically to Ricardo Chávez for the work done in collaboration. I also would like to thank to Ricardo Amorín for providing me private data for this work.

To my thesis examiners, thanks for your comments. They helped me to improve the work presented.

I especially appreciate all the help from my husband, companion and friend Emmanuel Ríos López. You and I know the great work that has cost us to be in this academic status, thank you very much for supporting me and love me forever.

To my friends Gisela, Leticia, Raúl, Eric, Carlos, Alán and Emmanuel, you have taught me that science is more enjoyable when you argue with friends. I hope that in the future we become collaborators in many articles.

I also want to thank my parents, brothers and nephews since day to day they made an effort to give me the best education, always supporting me in my decisions with so much love. All my accomplishments will be always thanks to you.

I thank God because he has never left me and has given me the spiritual tranquillity to be happy in life. I thank also my little dog 'Doki' who every day makes me smile with his antics.

Finally, I thank CONACyT for the financial support provided, which gave me the opportunity to work on what I like in life.

Declaration

This work comes from the idea of my advisors Dra. Elena Terlevich, Dr. Roberto Terlevich and Dr. Manolis Plionis. It contains data which are the outcome of work done in collaboration with Ricardo Chávez. My work consisted in compiling and analysing a sample of possible candidates of HII galaxies at high redshift according to the equivalent widths in their emission lines with data existing from the literature in order to assess the validity of the L(Hβ) - σ relation at high redshift and its use as an accurate distance estimator. The results obtained indicate a flattening or the existence of an upper limit in the luminosity for HII Galaxies, which has not been reported before in the literature.

Abstract

I have selected a sample of 504 HII like-starburst galaxies according to the equivalent widths in their emission lines in a range of redshift of $0.1 < z < 3.4$ from the literature, in order to assess the validity of the L(Hβ) - σ relation at high redshift and its use as an accurate distance estimator. The physical parameters for the sample at high redshift, within the uncertainties, are consistent with the ones for the HIIGx at low redshift. This suggests that the physical properties for HIIGx at low and high redshift are similar.

By combining our sample at high redshift with the local sample of HIIGx from Chávez et al. (2014), I find an evident flattening that starts at approximately $\log(\sigma) = 1.8$ km s^{-1} in the L(Hβ) - σ relation. This flattening has an interesting application since it leads to a kind of standard candle for those HIIGx with $\log(\sigma) > 1.8$ km s^{-1}. This flattening or the existence of an upper limit in the luminosity of HIIGx has not been reported before. Applying this new HIIGx standard candle method to the high redshift sample we obtain good restrictions on the cosmological parameters solution space. The combination of our sample at high redshift with the local sample of 156 (HIIGx and GEHRs) dramatically improves the constraints on the plane $\{\Omega_m, w_0\}$, which are consistent with the results from SNeIa.

These results are surprisingly good considering the high uncertainties in the data at high redshift, therefore we expect better constraints on the plane $\{\Omega_m, w_0\}$ using high quality data from high resolution spectrographs at 8 m class telescopes.

Resumen

Se ha seleccionado una muestra de 504 Galaxias HII en base a los anchos equivalentes en sus líneas de emissión en un rango de redshift $0.1 < z < 3.4$ de la literatura. Esto con el objetivo de evaluar la validez de la relación L(Hβ) - σ a alto corrimiento al rojo y su uso como un estimador de distancia preciso. Los parámetros físicos de la muestra a alto corrimiento al rojo, dentro de sus incertidumbres, son consistentes con los de las Galaxias HII locales. Esto sugiere que las propiedades físicas para las Galaxias HII a bajo y alto corrimiento al rojo son similares.

Combinando nuestra muestra a alto corrimiento al rojo con la muestra local de Galaxias HII dada en Chávez et al. (2014), se encontró un aplanamiento evidente que comienza aproximadamente en $\log(\sigma) = 1.8$ km s^{-1} en la relación L(Hβ) - σ. Este aplanamiento tiene una interesante aplicación, ya que conduce a una especie de candela estándar para aquellas Galaxias HII con $\log(\sigma) > 1.8$ km s^{-1}. Este aplanamiento o la existencia de un límite superior en la luminosidad de las Galaxias HII nunca antes ha sido reportado en la literatura. Aplicando este nuevo método de candela estándar para las Galaxias HII, nosotros obtenemos buenas restricciones al espacio de solución de parámetros cosmológicos. La combinación de la muestra a alto corrimiento al rojo con la muestra local de 156 objetos (Galaxias HII y Regiones HII Extragalácticas Gigantes) mejora notablemente las restricciones en el plano $\{\Omega_m, w_0\}$, las cuales son consistentes con los resultados de SNeIa.

Los resultados obtenidos son sorprendetemente buenos considerando las altas incertidumbres en los datos a alto corrimiento al rojo, por lo tanto nosotros esperamos mejores restricciones en el plano $\{\Omega_m, w_0\}$ usando datos de alta calidad obtenidos con espectrógrafos de alta resolución en telescopios de 8 metros.

Contents

Acknowledgements III

Abstract VII

List of Figures XIII

1 Introduction 1
- 1.1 Motivation and Aims of this Work . . . 3
- 1.2 Structure of this Work . . . 4

2 General Properties of HII Galaxies 5
- 2.1 Giant Extragalactic HII Regions and HII Galaxies in the Local Universe 5
  - 2.1.1 Morphology and Structure . . . 6
  - 2.1.2 Age HII Galaxies . . . 7
  - 2.1.3 Metallicity HII Galaxies . . . 8
- 2.2 L(Hβ) - σ Relation for HII Galaxies . . . 10
- 2.3 The Physics of the L(Hβ) - σ Relation . . . 13
  - 2.3.1 Age effects . . . 14
  - 2.3.2 Extinction effects . . . 15
  - 2.3.3 Metallicity effects . . . 16
  - 2.3.4 Size effects . . . 16
  - 2.3.5 Multiparametric effects . . . 16
- 2.4 HII Galaxies as Cosmological Probes . . . 17

3 Sample and Methodology 25
- 3.1 Sample Selection . . . 25
- 3.2 Properties of the Selected Sample at High Redshift . . . 30
  - 3.2.1 Velocity Dispersion . . . 30
  - 3.2.2 Size . . . 30
  - 3.2.3 Dynamical Masses . . . 31
  - 3.2.4 Extinction and Fluxes . . . 32
  - 3.2.5 Luminosity Distance . . . 34
  - 3.2.6 Luminosities . . . 34

3.2.7 Star Formation Rates 35
3.2.8 The Oxygen Abundance 36

4 Analysis and Results **65**
4.1 L(Hβ) - σ Relation 65
4.2 Luminosity vs Redshift 67
4.3 Cosmological Parameters Solution Space 68
4.4 Luminosity - Radius and Velocity Dispersion - Radius Relations 69
4.5 Dynamical Mass vs Stellar Mass 71
4.6 Metallicity - Mass Relation 73
4.7 Metallicity-Luminosity Relation 74
4.8 Starburst or AGN? 75

5 Conclusions and future work **79**
5.1 Future work 81

Bibliography **83**

List of Figures

2.1 Spectrum of a HIIGx . . . 6
2.2 Light profiles . . . 7
2.3 Hβ equivalent width vs. time . . . 8
2.4 Distribution of oxygen abundances . . . 9
2.5 L(Hβ) - σ relation for GEHRs and HIIGx . . . 11
2.6 L(Hβ) - σ relation for HIIGx at a wide range of redshifts . . . 12
2.7 L - σ relation . . . 13
2.8 M(B)$_0$ - σ relation for GEHRs . . . 14
2.9 The fundamental plane of HIIGx . . . 15
2.10 Multiparametric effects in the L(Hβ) - σ relation . . . 17
2.11 Distance Modulus Differences . . . 18
2.12 L(Hβ) - σ relation from Terlevich et al. (2015) . . . 20
2.13 Hubble diagram from Terlevich et al. (2015) . . . 21
2.14 Comparison of restrictions on the plane (Ω_m, w$_0$) . . . 22
2.15 Cosmological Parameters Solution Space from Monte-Carlo Analysis . . 22
2.16 The 'reduction' parameter S as a function of the number of high-z tracers 23

3.1 Equivalent width distribution of the [OIII] line for the sample at low redshift from Chávez et al. 2014 . . . 26
3.2 Redshift distribution for the sample at high redshift . . . 27
3.3 Sample position on the sky . . . 28
3.4 Rest-frame equivalent width distribution of the Hα, Hβ and [OIII] emission lines for the sample at high redshift . . . 29
3.5 Velocity dispersion distribution for the sample at high redshift . . . 31
3.6 Dynamical mass distribution for the sample at high redshift . . . 32
3.7 Hβ flux distribution for the sample at high redshift . . . 33
3.8 Hβ luminosity distribution for the sample at high redshift . . . 35
3.9 Oxygen abundance distribution for the sample at high redshift . . . 38

4.1 L(Hβ) - σ relation . . . 66
4.2 Hβ luminosity vs redshift . . . 67
4.3 Hβ luminosity vs redshift for objects with log$\sigma > 1.8$ km s^{-1} . . . 68

4.4 Distance moduli as a function of redshift for HIIGx at high redshift with $\log(\sigma) > 1.8$ km s^{-1}. 70
4.5 Cosmological Parameters Solution Space for the sample at high redshift with $\log(\sigma) > 1.8$ km s^{-1}. 70
4.6 Luminosity - Radius and Velocity Dispersion - Radius Relations 71
4.7 Dynamical Mass vs Stellar Mass Relation 72
4.8 Metallicity - Stellar Mass Relation 74
4.9 Metallicity vs B-band Luminosity 75
4.10 BPT Diagram 77

Chapter 1

Introduction

The identification of a class of isolated dwarf emission-line galaxies, which showed them to be indistinguishable in their observed properties from giant HII regions in nearby galaxies, was made by Sargent & Searle (1970). They called them *Isolated Extragalactic HII Regions*. Although the compact galaxies with strong emission lines had already been discovered by Haro (1956) utilizing the technique of objective prism. Later, Searle & Sargent (1972) reported the properties of two extragalactic objects with very low heavy element abundance, IZw18 and IIZw40, they emphasised that they could be young galaxies in the process of formation, because of their extreme metal under-abundance, more then 10 times less than solar. These two galaxies are HII Galaxies (HIIGx) prototypes, the HIIGx have the advantage of being gas-rich, with spectra dominated by strong emission lines due to the presence of O, B type stars in HII regions. So they can be observed in the optical as narrow and intense emission lines superimposed on a blue stellar continuum favouring their detection at great distance. The HIIGx are interesting for understanding the processes of galaxy formation. Besides, as they are gas-rich and have an active star formation they can help us to understand the processes of massive star formation in low metallicity gas (Kunth & Östlin, 2000).

A relation between the luminosity of Hβ emission line, L(Hβ), and the velocity dispersion, σ, from ionized gas in HII regions was found and investigated by Terlevich & Melnick (1981). Later, Melnick, Terlevich, & Moles (1988) presented a detailed study of the global properties of a sample of HIIGx, selected from the *Spectrophotometric Catalogue of HII galaxies* which was published by (Terlevich et al., 1991). They found that the L-σ relation can be applied to HIIGx and they proposed this method as a distance indicator (Melnick et al., 1987; Siegel et al., 2005; Bordalo & Telles, 2011; Plionis et al., 2011; Chávez et al., 2012; Chávez et al., 2014; Terlevich et al., 2015)

On the other hand, it is known that type Ia supernovae (SNeIa) provide a standard candle that can be used to accurately measure distances of galaxies at redshifts just beyond z$\sim$1 (Riess et al., 1998; Perlmutter et al., 1999; Amanullah et al., 2010; Hicken et al., 2009; Riess et al., 2011; Suzuki et al., 2012). The combination of SNeIa results with other independent cosmological probes, such as the cosmic microwave background (CMB) fluctuations from WMAP or baryon acoustic oscillation (BAO), allows to measure cosmological parameters with high precision (Aubourg et al., 2014). Due to the fact that the maximum difference in cosmological models occurs at z = $2-3$, it becomes crucial to investigate alternative methods to determine distances to galaxies at z $>$ 2. Alternatives include Gamma-Ray Bursts (GRB), explored e.g. by (Schaefer, 2007); other types of supernovae, particularly Type IIP (for Plateau) explosions (e.g. Poznanski et al., 2009) and other methods. However observing SNeIa at redshifts above the current limit appears challenging even with the next generation of space telescopes being that SNeIa could be very rare at z $>$ 2. In contrast, due to the fact that HIIGx spectra are dominated by intense emission lines, they can be observed at great distances, this makes them powerful tools for studying galaxies at high redshift.

To demonstrate the potential of HIIGx for cosmology, in (Chávez et al., 2012) they used a sample of 89 HIIGx together with a re-calibration of the L(Hβ) - σ relation for 23 Giant HII regions in 9 nearby galaxies and obtained a value for the Hubble constant of 74.3 ± 3.1 (random) $\pm$ 2.9 (systematic) km s^{-1} Mpc^{-1} , in excellent agreement with, and independently confirming, the most recent SNeIa-based results (Riess et al., 2011) and Cepheid-based results (Freedman et al., 2012). And in Plionis et al. (2011) they estimated that similar-quality observations of 60-80 HIIGx at redshifts between 0.8 and 3 can constrain $w(z)$, the parameter of the dark energy equation of state, to about 10%. Therefore, this method provides constraints on Ω_m and Ω_Λ as good as other methods (SNeIa and CMB).

Also in Terlevich et al. (2015), they present the result of high-dispersion spectroscopy of nine HII galaxies at redshifts between 0.6 and 2.33, obtained at the VLT using XShooter. Using six of these HII galaxies they obtained broad constraints on the plane Ω_m - w_0. The addition of 19 HIIGx at high redshift from the literature, in total 25 HIIGx at high redshift, plus their local compilation of 107 HIIGx up to z = 0.16 were used to impose further constraints, which are consistent with other recent studies. Although such constraints are weaker than those for SNeIa, this is not surprising since they have a small observed sample as well as poor quality data taken from the literature of HIIGx at high redshift. Besides, in their sample most of objects are in a region of space where differences between cosmological models are almost negligible, vs. 580 SNeIa with a maximum redshift of $\sim$ 1.5. The strength of their results is that their sample includes 19 objects with z $>$ 1.5 where the differences between models reach maximum values. Therefore competitive constraints can be obtained using a larger sample (from 100 to 300) HIIGx at high redshift as was proposed by (Plionis et al., 2011).

1.1 Motivation and Aims of this Work

To have a precise cosmological model it is necessary to constrain cosmological parameters and confirm the results through different and independent methods.

It is known that SNeIa provide a standard candle that can be used to accurately measure distances of galaxies. However, due to the fact that SNIa are believed to be the result of a mass transfer process into a white dwarf thus exceeding its Chandrasekhar limit, so its core will reach the ignition temperature for carbon fusion giving as a result a supernova explosion. Thus because the time it takes to develop a binary system with a white dwarf (the star progenitor has to have less than 8 $M_{\odot}$) and the low mass star has to reach the giant branch, it is expected that the number of SNIa should be small at high z. The more distant SNeIa so far discovered is 'SN1997ff' at z$\sim$1.7 (Gilliland & Phillips, 1998; Gilliland et al., 1999; Riess et al., 2001).

Therefore it is important to investigate alternative methods to determine distances to galaxies at z $>$ 1.5. As was previously mentioned, the giant extragalactic HII regions (GEHR) and HIIGx display a correlation between the luminosity in the recombination lines, e.g. Hβ L(Hβ), and the velocity dispersion, σ, (Terlevich & Melnick, 1981; Melnick et al., 1988; Chávez et al., 2014). Due to the fact that HIIGx spectra are dominated by intense emission lines, they can be observed at great distances, this makes them powerful tools for studying galaxies at high redshift. Therefore, if we extrapolate a link between nearby HIIGx and HII-like starburst galaxies at high redshift, we can use such objects as standard candles once obtained the calibration of the L(Hβ) - σ relation. As a consequence, we can obtain luminosities for HII galaxies to intermediate and high redshift and hence luminosity distances (Terlevich et al., 2015). This method has the advantage that it can be used up to z$\sim$3, since so far these HII-like starburst galaxies have been observed with the present instrumentation up to this redshift. This opens the important possibility of applying the distance estimator and map the Hubble flow up to extremely high redshifts and simultaneously to study the behaviour of starbursts of similar luminosities over a huge redshift range.

Plionis et al. (2011) using extensive Monte Carlo simulations found that using only a few tens of HIIGx at high redshift, even with a large distance modulus uncertainty, reduce significantly the cosmological parameters solution space. In fact, they found that an expected reduction ($\sim$ 20-40 per cent) of the current level of HIIGx-based distance modulus uncertainty does not provide a significant improvement in the derived cosmological constraints. It is far more efficient to increase the number of tracers than to reduce their individual uncertainties.

There are catalogues with available data in the literature, in which we can obtain candidates to HIIGx in order to compare the intrinsic properties between low and high HIIGx, this can help us to have a better understanding of the nature of these starforming galaxies at high redshift and their possible relation with similar objects nearby. However, the high redshift candidates need more complete and homogeneous data.

The aims of this work are:

- To build a large sample of HII-like starburst galaxies at high redshift.

- To investigate the physical properties of high redshift HII galaxies and compare them with those of nearby HIIGx.

- To critically assess the use of the L(Hβ)-σ distance estimator for high redshift HII galaxies.

1.2 Structure of this Work

The organization of this thesis is as follows:

Chapter II describes the fundamental physical properties of HII galaxies in the local universe as young massive bursts of star formation. The relationship between the luminosity of Hβ in emission and ionised gas velocity dispersion (L-σ) for HII Galaxies and the effect that different intrinsic physical parameters of the star-forming regions could have on this relation are also presented. The potential use of HII galaxies as distance indicators is discussed as well in this chapter.

Chapter III describes the different parameters that characterize the sample and selection parameters that were used to select HII-like starburst galaxies at high redshift from the literature.

Chapter IV gives a global comparison between HIIGx at high and low redshift. I analyse the relationships Luminosity vs Velocity Dispersion; Luminosity vs Redshift; Stellar Mass vs Dynamical Mass; Luminosity vs Effective Radius; Velocity Dispersion vs Effective Radius; Metallicity vs Stellar Mass; Metallicity vs Luminosity and the excitation mechanism using BPT diagrammes. Besides, we explore the application of the HIIGx L(Hβ) - σ relation as a distance estimator. We use a sample of 103 HII-like starburst galaxies at high redshift with the required data from the literature combined with the local sample of 156 HIIGx to obtain constraints on the plane $\{\Omega_m, w_0\}$.

Chapter V presents the general conclusions of this thesis and delineates the future work that I plan to do.

Chapter 2

General Properties of HII Galaxies

2.1 Giant Extragalactic HII Regions and HII Galaxies in the Local Universe

GEHR and HIIGx are characterized by a large star-forming region, which due to the presence of O and B spectral type stars that ionize the gas surrounding them, their spectra are dominated by nebular emission lines. As a result, they can be observed in the optical as narrow and intense emission lines, mainly H and He recombination and forbidden lines like [OIII], [NII], [SII], superimposed on a blue stellar continuum (see Figure 2.1).

But, if both are bursts of star formation, what is the difference between GEHRs and HIIGx? Well, GEHR are massive bursts of star formation located at the outer regions of the disk of the late type galaxies. Their sizes are in the range of few hundred parsecs (Kennicutt et al., 1989; Bosch et al., 2002) and the content of ionized gas of low density (Ne $\sim$ 10 - 100 cm^3) reaches up to 10^5 M$_\odot$ (García-Benito, 2009). However, the largest ones are generally composed of various knots, only distinguishable with high spatial resolution for nearby galaxies. Some examples of GEHR are 30 Dor in the Large Magellanic Cloud (LMC) and NGC 604 in the spiral galaxy M33.

HIIGx are also massive bursts of star formation located at dwarf irregular galaxies and almost completely dominating the total luminosity output (up to 10^{43} erg s^{-1} in Hα line luminosity); with total masses that are less than 10^9 M$_\odot$, radius that are less than 2 kpc and a surface brightness $\mu_{\rm V} \geq 19$ mag arcsec^2 (García-Benito, 2009). An example of HIIGx is IZw18. The HII galaxies also are known as BCDs (Blue Compact Dwarfs), however the term HII galaxy is used for the objects that have been selected by their intense and narrow emission lines (Terlevich et al., 1991), while BCDs are selected by their blue color and for being compact. Another important aspect is that not all BCDs are dominated by HII regions in their spectra, therefore not all BCDs are

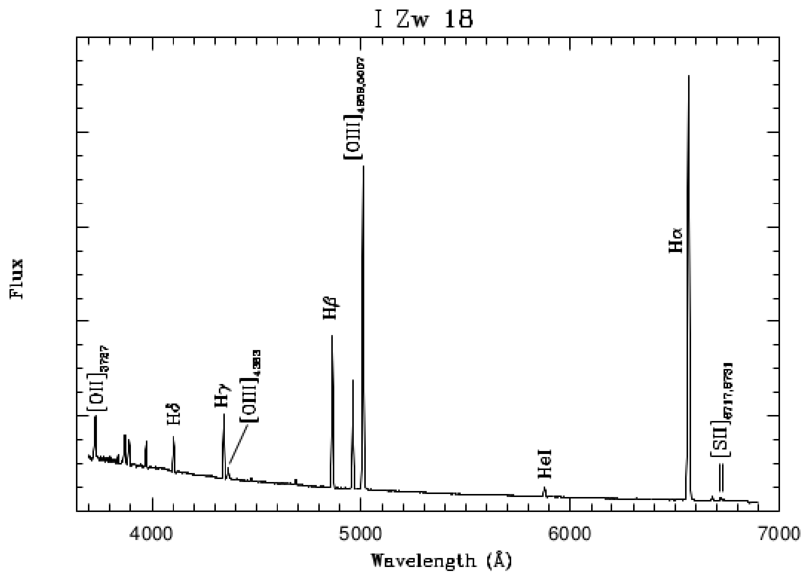

Figure 2.1: Spectrum of a HIIGx (IZw18) with the most important emission lines labelled. In this spectrum you can see the very blue continuum. Taken from Kunth & Östlin (2000).

HII galaxies. Hence, both GEHRs and HIIGx offer an important opportunity to study violent and intense episodes of star formation. Besides as they are gas-rich with active star formation, one motivation to study them has been the hope to better understand the processes of massive star formation in low metallicity gas.

2.1.1 Morphology and Structure

Earlier morphological studies have suggested that a large proportion of the HII galaxies observed are compact and isolated (Melnick, 1987). Nevertheless, when we study the morphological properties of HII galaxies is very important to remember that, although all HIIGx have at least one giant region of star formation which may or may not be in the center, HIIGx present a variety of morphologies. On the basis of the shape of outer isophotes, Telles, Melnick, & Terlevich (1997) have classified HIIGx in two types: Type I and Type II. The type I objects have disturbed morphologies and irregular outer structure, also tend to be more luminous than type II objects. The type II objects are symmetric and regular HII galaxies regardless of the multiplicity of the starburst regions. This classification is only applicable to HIIGx at low redshift due to the fact that individual star-forming regions can only be resolved in nearby galaxies, while morphological details can not be appreciated at high redshift.
Regarding the structural properties of HII Galaxies, Telles, Melnick, & Terlevich (1997) found three main types of light profiles illustrated in Figure 2.2: **d.** A single exponential

fit represents well the whole range of radii of the profile. **dd.** Double profile with a platform due to the double morphology. An exponential law is well fitted to the outer regions. **bd.** A steep bright central region and a disk-like component. The exponential fit represents well the outer component only. Therefore, the outer parts of the luminosity profiles of HII galaxies are well represented by an exponential scaling law.

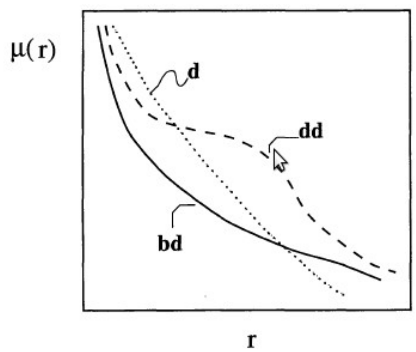

Figure 2.2: Light profiles taken from Telles, Melnick, & Terlevich (1997).

2.1.2 Age HII Galaxies

Dottori (1981) investigated the variation of the equivalent width of Hβ, EW(Hβ), as a function of the evolution of the ionizing stars in HII regions. Subsequently, measurements of the EW(Hβ) and age determinations in 29 HII regions of the LMC and 2 of SMC, respectively, were made by Dottori & Bica (1981). They found that the age maximum frequency in HII regions corresponds to the range 6.2 to 7.2 Myr, but older HII regions are practically undetectable.

In general two models for the star formation time evolution are used to estimate the age of young bursts of star formation: An instantaneous starburst model, which assumes that all stars are formed simultaneously in a short-living starburst episode, and a continuous starburst model, which assumes active star formation being constant in time. The first model is generally applied to individual low mass star clusters, whereas the second model is assumed to be a galaxy wide average properties. The continuous star formation could also be understood as a sequence of very small bursts localized within another small region in space and separated by short time intervals. Anyway, both models describe the evolution of the EW(Hβ) as a function of time, as can be seen in Figure 2.3. From this figure, it can be seen that the *Starburst99* models (Leitherer et al., 1999) with a defined Salpeter IMF, gives as results that an instantaneous burst with EW(Hβ) $>$ 50 Å has to be younger than about 5 Myr. However, Terlevich et al. (2003) have showed that HII galaxies have a star formation history that is closer to that predicted by a continuous starburst model, indicating that while the observed emission lines track the present burst, the underlying continuum contains the whole star formation history of the HIIGx.

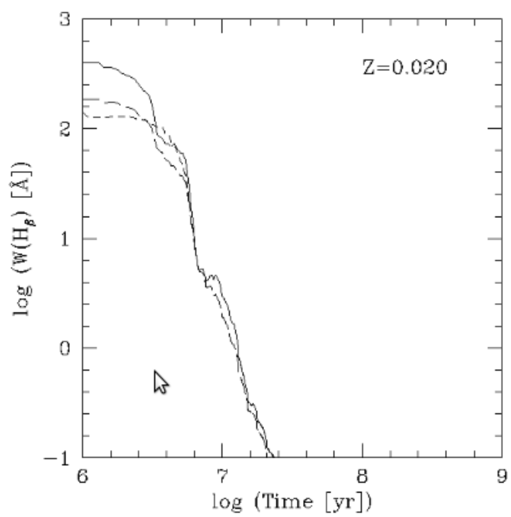

Figure 2.3: Hβ equivalent width vs. time; Left: Instantaneous star formation law: solid line α=2.35, M$_{up}$=100 M$_\odot$; long-dashed line, α=3.30, M$_{up}$=100 M$_\odot$; short-dashed line, α=2.35, M$_{up}$=30 M$_\odot$. Right: Same characteristics but for a continuous star formation law.

2.1.3 Metallicity HII Galaxies

While it is true that the average metallicity of the Universe must have increased as it evolved, the situation is more complex than a simple thought where high redshift means metal-poor, and low redshift metal-rich. Objects with high and low metallicities are found at all redshifts. Surely we expect objects that in the local Universe appear as metal deficient to be even more deficient at high redshift, if we could observe their precursors. As HII galaxies are metal-poor systems with abundances of metals in the range between 1/2 Z$_\odot$ and 1/50 Z$_\odot$, they are the survivors who form the local metal-poor galaxies population. As a consequence, they may be the principal building blocks of the Universe on large scales (Kunth & Östlin, 2000).

Observationally the HII galaxies have an advantage of being gas-rich, with spectra dominated by strong emission lines superimposed on a blue stellar continuum. From the analysis and interpretation of the ratios of two or more bright nebular emission lines, it is possible to estimate several parameters such as the electron density and temperature, the chemical abundances for different species, ionizing conditions, etc. It is also possible to characterize the ages, masses and temperature of the ionizing star cluster.

In HII regions, the oxygen is the most abundant of the metals that constitute them and it is the most reliably determined element, since the most important ionisation stages can all be observed. Therefore, the oxygen abundance is normally considered as representative of the metallicity of HII galaxies. Also, the oxygen has the property that the [OIII]λ4363 line allows an accurate determination of the electron temperature (Pagel et al., 1979). For other species apart from Sulphur, in general, one does not observe all the ionisation stages expected to be present in the photoionization region and an ionisation correction factor must be applied to derive the total abundance of the element in question.

When the electron temperature cannot be determined, empirical relations for estimating the oxygen abundance are used. These empirical relations use the line ratios between the strengths of [OII]λ3727 and [OIII]$\lambda\lambda$4959, 5007 lines relative to Hβ, though with lower accuracy (Pagel et al., 1979). A detailed discussion on these empirical relations is given in subsection 3.3.7.

Nowadays there are good quality data for more than 100 HIIGx, which show abundance in the range $7.1 \leq 12 + \log(O/H) \leq 8.3$. Pérez-Montero & Díaz (2003) analysed 12 HIIGx whose oxygen abundance are in a range of $7.68 \leq 12 + \log(O/H) \leq 8.20$. Chávez et al. (2014) calculated the oxygen abundance for a sample of 100 HIIGx and GEHR at $0.02 < z < 0.2$, finding a median value of $12 + \log(O/H) = 8.08$. The distribution of oxygen abundances for the Chávez et al. (2014) sample is shown in Figure 2.4.

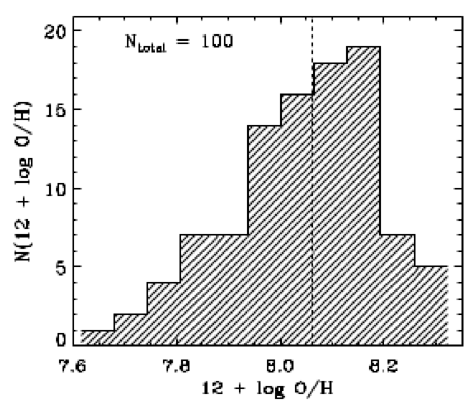

Figure 2.4: Distribution of oxygen abundances for 100 HIIGx and GEHR at low redshift. The dashed line shows the median (Chávez et al., 2014).

2.2 L(Hβ) - σ Relation for HII Galaxies

Melnick (1978) found a correlation between the average turbulent velocity of HII regions in spirals and irregular galaxies and the parent galaxy absolute magnitude. However, the physics of this relationship was not clear. Terlevich & Melnick (1981) analysed the relation between Hβ luminosity, linewidth, metallicity and size for GEHRs and HII galaxies finding the following correlations:

$$luminosity \propto (linewidth)^4 \tag{2.1}$$

$$size \propto (linewidth)^2 \tag{2.2}$$

which are valid for stellar systems supported by pressure as elliptical galaxies, bulbs of spiral galaxies, globular clusters. Therefore, they concluded that HII galaxies and GEHRs are self-gravitating systems in which the observed emission-line profile widths represent the velocity dispersion of gas clouds in the gravitational potential well. They also found that the scatter in the L(Hβ) - σ relation is correlated with the metallicity.

An analysis of properties of GEHRs was made by Melnick et al. (1987) in which they found that de Hβ emission line luminosity, velocity dispersion and core radii of giant HII regions are strongly correlated as:

$$R_c \sim \sigma^{2.5\pm0.5} \tag{2.3}$$

$$L(H\beta) \sim \sigma^{5.0\pm0.5} \tag{2.4}$$

where part of the scatter in the relations is due to a metallicity effect and that such relationships provide a powerful method to determine distances to GEHRs. Also they found that the relationships are best explained by a model in which GEHRs are assumed to be virialized clusters of large numbers of discrete gas fragments ionized by a central star cluster that contains most of the mass.

Subsequent work by Melnick, Terlevich, & Moles (1988) was devoted to obtain a calibration of the L(Hβ)-σ relation for HII galaxies in order to make it suitable for distance measurements. The relation found for HII galaxies alone is:

$$logL(H\beta) = (4.70 \pm 0.30) log\sigma + (33.61 \pm 0.50) \quad \textbf{with} \quad \delta logL(H\beta) = 0.29 \tag{2.5}$$

which is represented by a dashed line in Figure 2.5. A Hubble constant of $H_0 = 100$ km s^{-1} Mpc^{-1} was selected for the calculation of L(Hβ).

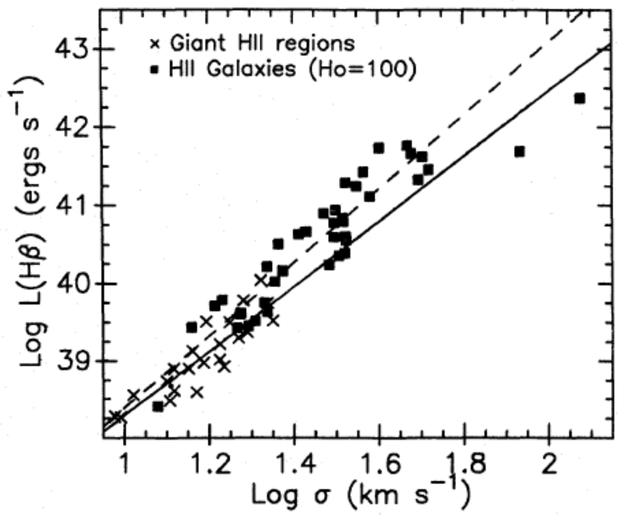

Figure 2.5: L(Hβ) - σ relation for GEHRs and HIIGx. The solid line shows a least squares fit to GEHRs and the dashed line, the corresponding fit for HIIGx (Melnick, Terlevich, & Moles, 1988).

Also Melnick, Terlevich, & Moles (1988) found that the metallicity is effectively an important component of the scatter in the L(Hβ) - σ relation. Therefore, the distance indicator defined as

$$M_z = \frac{\sigma^5}{O/H} \tag{2.6}$$

with O/H, the oxygen abundance of the nebular gas, provides the predicted luminosity from the relation

$$logL(H\beta) = (1.0 \pm 0.04) logM_z + (41.32 \pm 0.08) \quad \textbf{with} \quad \delta logL(H\beta) = 0.271 \tag{2.7}$$

where a Hubble constant of H_0 = 90 km s^{-1} Mpc^{-1} was selected for the calculation of L(Hβ).

Melnick, Terlevich, & Terlevich (2000) showed that HII-like starburst galaxies up to z ∼ 3, albeit for a small sample, satisfy the L(Hβ) - σ relation, opening the possibility of using the relation to measure cosmological parameters (see Figure 2.6). The relation derived was:

$$logL(H\beta) = logM_z + 29.5 \tag{2.8}$$

from which the distance modulus relation for HII galaxies was:

$$\mu = 2.5log[\sigma^5/F(H\beta)] - 2.5log(O/H) - A(H\beta) + Z_0 \tag{2.9}$$

where F(Hβ) and A(Hβ) are the flux and extinction in Hβ, respectively. The determined zero-point was $Z_0 = -26.44$ and the rms scatter in the distance modulus was found to be $\sim$ 0.52 mag. Although, such rms scatter is larger than what is obtained with SNeIa, the advantage of using HII galaxies is that we can reach a much larger redshift limit, z $\sim$ 3 versus z $\sim$ 1.5 (Siegel et al., 2005) where the maximum difference in cosmological models occurs.

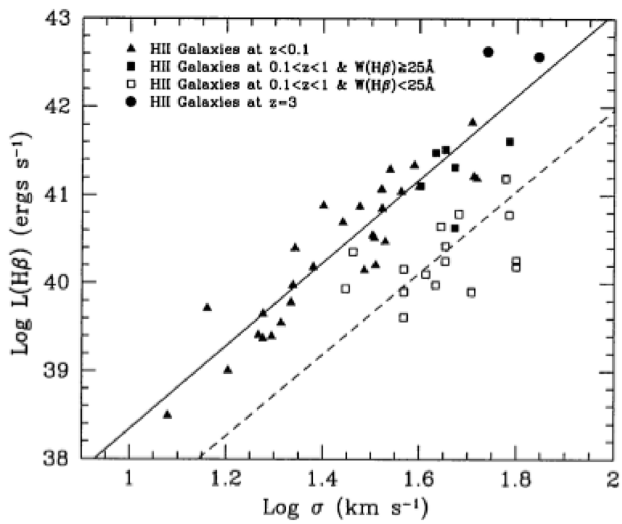

Figure 2.6: L(Hβ) - σ relation for HIIGx at a wide range of redshifts. The solid line shows the maximum-likelihood fit to the young HII galaxies in the local Universe. The dashed line shows the predicted L(Hβ) - σ relation for an evolved population of HII galaxies. A cosmology with H_0 = 65; q0 = 0 and $\Lambda = 0$ is assumed in this figure. (Melnick, Terlevich, & Terlevich, 2000).

Using recent galaxy distance determinations Plionis et al. (2011) determined the zero-point of the distance indicator, Z_0 repeating the original analysis of Melnick, Terlevich, & Moles (1988, 2000), using Cepheid and RR Lyrae distance determinations and indeed the rms scatter of the distance indicator relation was reduced by $\sim$ 7% while P_0 = 29.44.

A sample of 128 local HII galaxies, with high equivalent widths of their Balmer emission lines, was constructed by Chávez et al. (2014) with the objective of assessing the validity of the L(Hβ) - σ relation and its use as an accurate distance estimator. To this end they obtained high S/N high-dispersion ESO VLT and Subaru echelle spectroscopy, in order to accurately measure the ionized gas velocity dispersion. Additionally, they obtained integrated Hβ fluxes from low dispersion wide aperture spectrophotometry, using the 2.1m telescopes at Cananea and San Pedro Mártir Mexico. They found that L(Hβ) - σ relation for 107 HIIGx, since they only included those systems with log σ < 1.8 and remove objects with low quality data, is:

$$logL(H\beta) = 4.65\ log\sigma + 33.71 \tag{2.10}$$

with rms scatter of δlogL(Hβ) = 0.332 (see Figure 2.7).

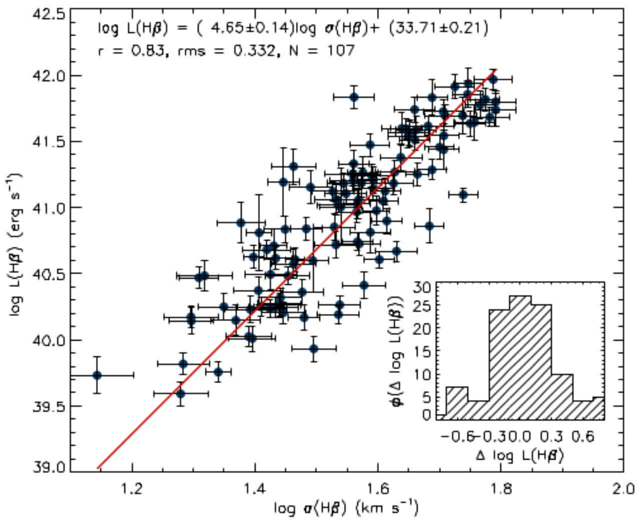

Figure 2.7: L(Hβ) - σ relation for the sample of 107 HIIGx with good determination of Luminosity and σ. The inset shows the distribution of the residuals of the fit. Taken from Chávez et al. (2014).

2.3 The Physics of the L(Hβ) - σ Relation

The physics that holds the L(Hβ) - σ relation for HII galaxies stems from the fact that as one increases the mass of the young stellar component not only the ionizing output increases but also the turbulent velocity of the gas, which is indicative of supersonic motions in the gas in the stellar gravitational potential, becomes larger. This effect induces a correlation between the integrated luminosity in a hydrogen recombination line, e.g. L(Hβ), which is proportional to the number of ionizing photons, and the velocity dispersion, σ, obtained through the linewidth.

The first ones to propose a model in which the nature of such relation is gravitation were Terlevich & Melnick (1981). They analysed the correlations between Hβ luminosities, linear diameters and the widths of the global emission-line profiles of GEHRs and found that the correlations L(Hβ) $\propto \sigma^4$ and R $\propto \sigma^2$ observed in HIIGx are similar to those valid for elliptical galaxies, bulges of spiral galaxies and globular clusters. These results strongly suggest that GEHRs are self-gravitating systems where the emission-line profile widths reflect the motions in the gravitational potential well. Terlevich & Melnick (1981) compared the relationship between luminosity and velocity dispersion of GEHRs with gravitationally bound systems (as elliptical galaxies, bulges of spiral galaxies and globular clusters). They evolved ionising stellar clusters as closed systems (i.e at constant mass) until their M/L ratios become similar to M/L ratios of gravitationally bound systems. As can be seen in Figure 2.8, the resulting $M(B)_0$ - σ relation for GEHRs is consistent with the corresponding to virialized systems, which gives a strong support to the gravitational origin of velocity dispersion in GEHRs.

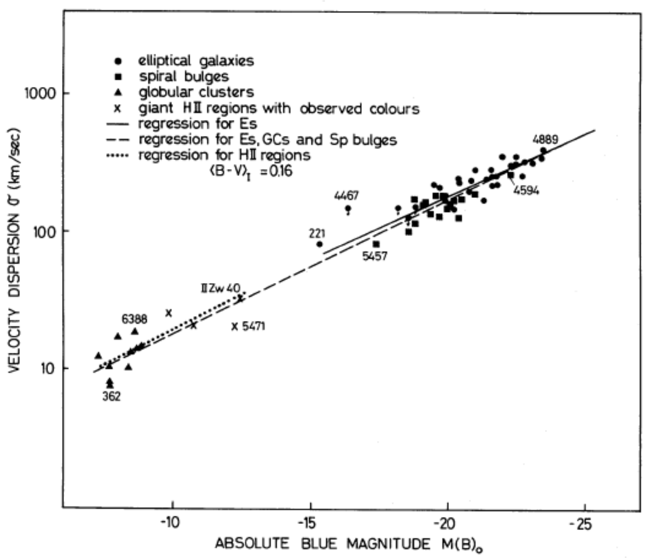

Figure 2.8: Correlation between absolute blue magnitude and velocity dispersion for elliptical galaxies, bulges of spiral galaxies and globular clusters with GEHRs. The dashed line represents the linear fit to all the data. The solid line represents a fit for elliptical galaxies alone. And the dotted line represents the fit to the GEHRs. Taken from Terlevich & Melnick (1981).

Telles (1995) showed that HIIGx define a fundamental plane that is similar to that defined by normal elliptical galaxies (see Figure 2.9). This result lends strong support to the interpretation of Terlevich & Melnick (1981) and Melnick, Terlevich, & Moles (1988) that the emission-line profile widths of GEHRs directly measure the total mass of these systems within the measuring radius. Therefore, besides systematic effects, the scatter in the L(Hβ) - σ relation depends on the existence of a second parameter. For example, on possible variations of the initial mass function (IMF), on the presence of additional sources of broadening (e.g. rotation), and on the duration of the burst of star formation that powers the emission lines (Melnick, Terlevich, & Terlevich, 2000).

2.3.1 Age effects

In order to minimize systematic effects caused by the rapid evolution of the ionizing stars, Melnick, Terlevich, & Moles (1988) restricted their sample to galaxies with EW(Hβ) $>$ 25 Å. In fact, this restriction has a double purpose, which is particularly relevant for objects at high redshift: it selects the youngest starbursts, and eliminates

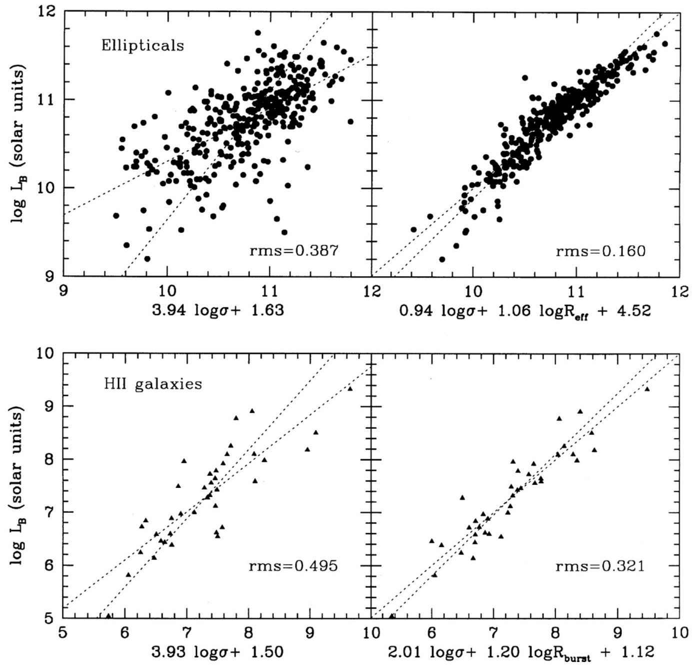

Figure 2.9: The fundamental plane of HIIGx and normal elliptical galaxies. The radii and magnitudes of HIIGx are measured from continuum images. The velocity dispersions are the widths of the emission lines. Taken from Telles (1995).

objects with significant underlying old stellar populations. The latter is critical because an old stellar population may widen the emission lines in a way that is uncorrelated with the luminosity of the young component.

The luminosity evolution of a young starburst during the first 10^7 yr proceeds as a rapid decay of the emission line flux after the first 3 Myr at roughly constant continuum flux until about 6 Myr. Thus, in this range of ages the age-dimming in L(Hβ) can be directly estimated from the change in equivalent widths (Terlevich & Melnick, 1981; Copetti et al., 1986). Chávez et al. (2014) studied the age effect in the L(Hβ) - σ relation, from their results it was clear that age should play a role in the scatter but very small.

2.3.2 Extinction effects

The dust present in the interstellar medium strongly attenuates rest-frame ultraviolet and optical fluxes in a wavelength-dependent manner. Therefore, the extinction have a systematic effect for the L(Hβ) - σ relation. Two possible sources of extinction must be considered: dust in our galaxy and dust in the HII galaxies themselves.

In practice, the most reliable technique to estimate interstellar extinction is to measure the flux ratio of two nebular Balmer emission lines such as Hα/Hβ (i.e., the Balmer decrement). Extinction corrections for local HII galaxies are determined in a straightforward manner from the Balmer decrements (Melnick, Terlevich, & Moles, 1988). While in HIIGx at intermediate and high-redshift it is rather difficult to measure the Balmer decrement because of low signal-to-noise ratio (S/N). This is now possible with observations using 8-m class telescopes which ideally include weaker Balmer lines permitting direct estimates of the reddening in HIIGx at high redshift (Erb et al., 2006a,b).

2.3.3 Metallicity effects

Terlevich & Melnick (1981) showed that other possible parameter that has an effect over the L(Hβ) - σ relation is the metallicity. Nevertheless the HIIGx, due to their nature, have a very low metallicity whose dynamical range is very narrow (see Figure 2.4). Chávez et al. (2014) showed that the metallicity plays a role as a second parameter although relatively small.

2.3.4 Size effects

If the L(Hβ) - σ correlation is a consequence of young massive clusters being in virial equilibrium, then the strongest candidate for a second parameter is the size of the star forming region (Terlevich & Melnick, 1981; Melnick et al., 1987). Chávez et al. (2014) explored this possibility using the SDSS measured radii at the u, g, r, i and z bands. They used the SDSS measured effective Petrosian radii and corrected for seeing also available from SDSS. In particular, using as second parameter either size, oxygen abundance O/H (using the empirical methods N2 or R23), EW or continuum colour, they found that the scatter in the L(Hβ) - σ relation is considerably reduced. Being the size in the u-*band* which more reduces scattering,

$$logL(H\beta) = 3.08\, log\sigma + 0.76 logR_u + 34.04 \tag{2.11}$$

with rms scatter of δlogL(Hβ) = 0.261.

2.3.5 Multiparametric effects

Chávez et al. (2014) also investigated which parameters in addition to the size can further reduce the scatter in the L(Hβ) - σ relation. They found, using multiparametric fits, that including as a third parameter the (u - i) colour or the equivalent width of a Balmer emission line, and as a fourth parameter the metallicity does significantly reduce further the scatter. Therefore, their best multiparametric distance estimator is:

$$logL(H\beta) = 2.79\; log\sigma + 0.95 logR_u + 0.63 logEW(H\beta) + 0.28 logN_2 + 33.15 \quad (2.12)$$

with rms scatter of δlogL(Hβ) = 0.233 (see Figure 2.10).

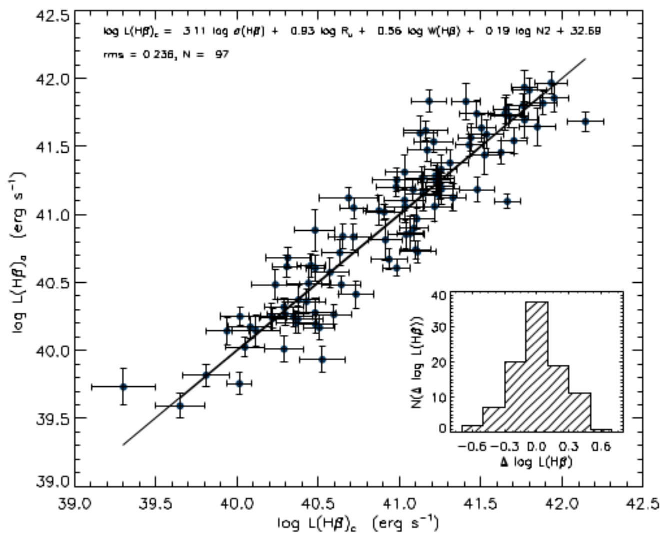

Figure 2.10: Observed L(Hβ) [L(Hβ)$_o$] vs. L(Hβ) calculated using the best Bayesian multiparametric fitting corresponding to the expression displayed on the top of the figure. The 1:1 line is shown (Chávez et al., 2014).

2.4 HII Galaxies as Cosmological Probes

As mentioned before HII galaxies, compact extragalactic objects experiencing massive bursts of star formation, have a high-luminosity per unit mass, in large part concentrated in a few strong emission lines in the optical rest frame. This ensures that the requirement for a standard candle to be usable at very large distances is met. The potential use of HII galaxies as distance indicators, as an alternative to the traditionally used SNeIa, is based on the following facts:

(a) Local and HIIGx at high redshift define a relationship between Hβ luminosity and velocity dispersion which remains valid at cosmological distances. Thus, HIIGx at high redshift can be used as alternative tracers of the Hubble expansion.

(b) HIIGx can be observed at much larger redshifts than those currently probed by SNeIa samples.

(c) It is at higher redshifts in which the differences between the predictions of the different cosmological models are stronger, as is showed in Figure 2.11.

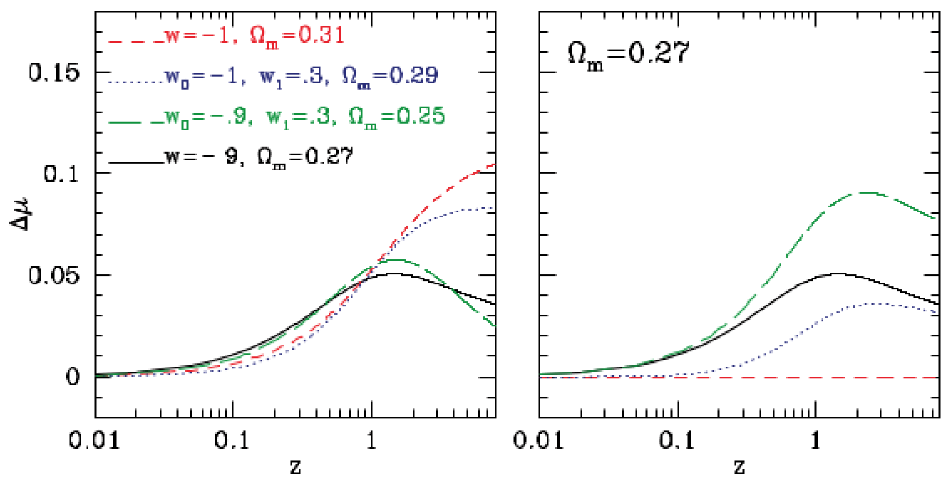

Figure 2.11: Left-hand panel: the expected distance modulus difference between the dark energy models shown and the reference model ($w = -1$) with $\Omega_m = 0.27$. Right-hand panel: the expected distance modulus differences once the $w(z)$ degeneracy is broken (imposing the same Ω_m value as in the comparison model). Plot taken from Plionis et al. (2011).

In Figure 2.11 we can see the difference between some cosmological models for which their parameters are indicated. Such difference is obtained when we compare different models to one taken as reference. We define:

$$\Delta\mu = \mu_\Lambda - \mu_{model} \tag{2.13}$$

where μ_Λ is the distance modulus given by the reference model using concordance ΛCDM cosmology and μ_{model} is the one given by any other model.

The distance modulus is defined as:

$$\mu = 5logD_L + 25 \tag{2.14}$$

where D_L is the luminosity distance expressed in Mpc, for a flat universe ($\Omega_k = 0$) and an insignificant value of Ω_r is given by:

$$D_L = \frac{c(1+z)}{H_0}\int_0^z \frac{dz}{\sqrt{\Omega_m(1+z)^3 + (1-\Omega_m)(1+z)^{3(1+w_0+w_1)}\exp(\frac{-3w_1 z}{1+z})}}, \tag{2.15}$$

for which it has been used the CPL (Chevallier & Polarski, 2001; Linder, 2003) model to parametrize the value of the dark energy equation of state parameter $w(z)$,

$$w(z) = w_0 + w_1 f(z) \tag{2.16}$$

being $w_0 = w(z = 0)$ and $f(z)$ an increasing function of redshift, such as $f(z) = z/(1+z)$ (Chevallier & Polarski, 2001; Linder, 2003; Peebles & Ratra, 2003; Dicus & Repko, 2004; Wang & Mukherjee, 2006).

Taking the concordance ΛCDM cosmology as the reference model, Terlevich et al. (2015) calculated the distances and hence the luminosities for local and high redshift HIIGx. Figure 2.12 shows the L(Hβ) - σ relation for the 25 high-z sample of HIIGx [6 high-z HIIGx observed with XShooter (red stars) and 19 high-z HIIGx from the literature (green triangles)], and the local sample of GHIIRs and HIIGx from Chávez et al. (2014). The result is a remarkably tight correlation that justifies the use of the L(Hβ) - σ relation as a distance estimator over a wide range of redshift, basically from the local group of galaxies (LMC, SMC, NGC 6822, M 33) up to at least z $\sim$ 2.3.

The L(Hβ) - σ relation found, for the joint local HIIGx (107 objects) and GEHRs (24 objects) samples, is

$$logL(H\beta) = (5.05 \pm 0.097) log\sigma(H\alpha) + (33.11 \pm 0.145) \tag{2.17}$$

Although here they are only considering the two dimensional L(Hβ) - σ relation, the scatter can be substantially reduced if additional observables in the L(Hβ) - σ relation are included. According to Chávez et al. (2014), observables like the size of the ionized gas region, the equivalent width of either Hβ or Hα and the ionized gas metallicity or the continuum colour reduce substantially the scatter (from a rms $\sim$ 0.35 to a rms $\sim$ 0.23) in the L(Hβ) - σ relation. The importance of this reduction in the scatter of the distance estimator can not be neglected.

Figure 2.13 shows the Hubble diagram for the combined sample of local and high-z systems from Terlevich et al. (2015). The distance moduli were obtained from:

$$\mu^{obs} = 2.5 logL(H\beta)_\sigma - 2.5 logF(H\beta) - 100.2 \tag{2.18}$$

where L(Hβ)$_\sigma$ was estimated from equation (2.17).

The continuous lines show the behaviour of the theoretical distance modulus with redshift computed for three different cosmological models using the equation (2.14).
This is a remarkable and unique Hubble diagram in the sense that it covers a huge dynamical range with a single distance estimator. It connects galaxies in the local group to galaxies at z $\sim$ 2.3, a range of almost 30 magnitudes in distance modulus or

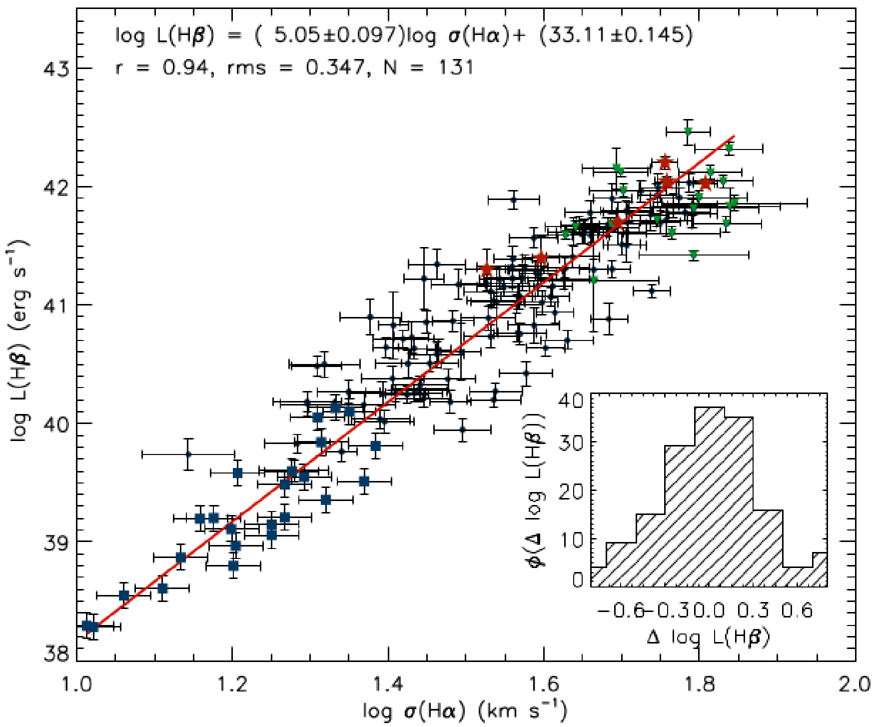

Figure 2.12: L(Hβ) - σ relation for the combined local (131 HIIGx and GEHRs) and high-z (25 HIIGx) samples, the fit corresponds only to the local sample of 131 objects. Blue squares: GEHRs. Blue dots: local HIIGx. Red stars: HIIGx at high z with XShooter observations. Green triangles: data from the literature. Plot taken from Terlevich et al. (2015).

more than 5 dex in redshift.

To restrict the set of cosmological parameters they minimised the Likelihood function,

$$\chi^2(\mathbf{p}) = \sum_{i=1}^{n} \frac{[\mu_i^{obs}(\sigma_i, f_i) - \mu_i^{th}(\mathbf{p}, z_i)]^2}{\sigma^2_{\mu_i^{obs}}} \tag{2.19}$$

where $\mu^{obs}(\sigma_i, f_i)$ are 'observed' distance moduli obtained from equation (2.18); σ_i are the measured velocity dispersions and f_i are the measured Hβ fluxes for each object. μ^{th} $(\mathbf{p},\ z_i)$ are the 'theoretical' distance moduli from equation (2.14) obtained from the measured redshifts by using a particular set of cosmological parameters, $\mathbf{p}$. $\sigma_{\mu_i^{obs}}$ are the errors in 'observed' distances moduli propagated from the uncertainties in σ_i and f_i and the slope and intercept of the distance estimator in equation (2.17). The summation is over the combined sample of HIIGx.

Figure 2.14 shows the comparison for the space p = (Ω_m, w$_0$) obtained in Terlevich et al. (2015) joining the high-z with the local HIIGx samples (see left panel), using the

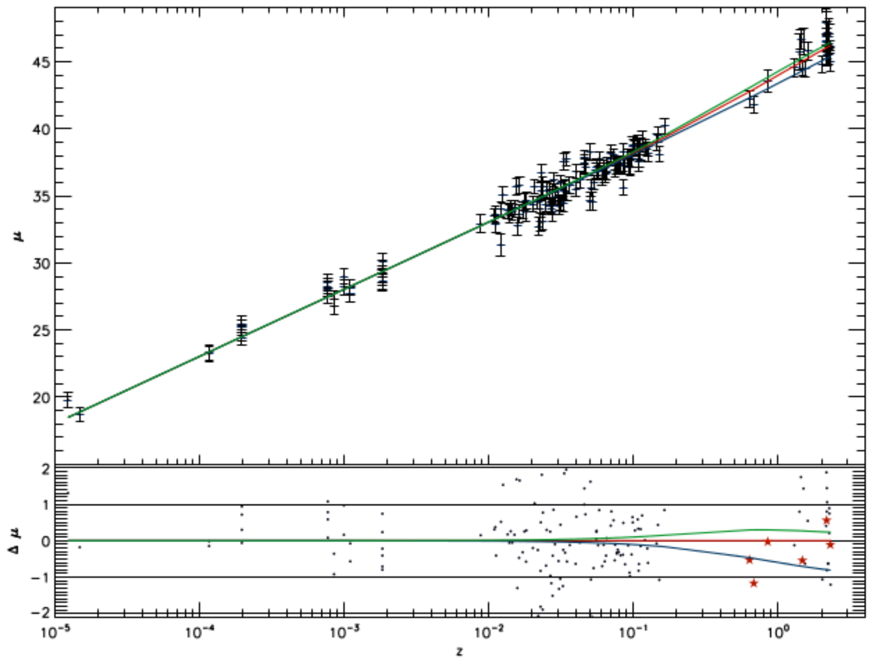

Figure 2.13: Hubble diagram for our sample of low and high-z HIIG for three different cosmologies. The solid red line indicates the concordance ΛCDM cosmology with Ω_m = 0.3; w_0 = -1.0 and H_0 = 74.3. The solid green line shows a cosmology with Ω_m = 0.3 and w_0 = -2.0. The solid blue line corresponds to Ω_m = 1.0. In all three cases Ω_k = 0. Residuals are plotted in the bottom panel. Note the huge dynamical range in distance modulus of almost 30 magnitudes covered with the L(Hβ) - σ distance estimator. Taken from Terlevich et al. (2015).

value of H_0 = 74.3 ± 3.1 calculated in Chávez et al. (2012) and w_1 = 0, with recent results from SNeIa, CMB and BAO (right panel). The figure shows the constrains of the properties of dark energy using SNeIa alone (Amanullah et al., 2010), the Wilkinson Microwave Anisotropy Probe data of the CMB (Komatsu et al., 2011) and the position of the BAO peak from the combined analysis of the SDSS Data Release 7 and 2dFGRS data Percival et al. (2010). The combined restrictions from SNeIa, CMB and BAO and the measurement of the Hubble constant (H_0) from Cepheids (Riess et al., 2011) are also shown.

From the comparison of the figures it can be seen that there are no systematic shifts between the HII galaxies and SNeIa solutions. The figure shows also that with a larger sample of HII galaxies with high quality data it becomes possible to achieve at least similar and probably even better results to those obtained with SNeIa (Plionis et al., 2011).

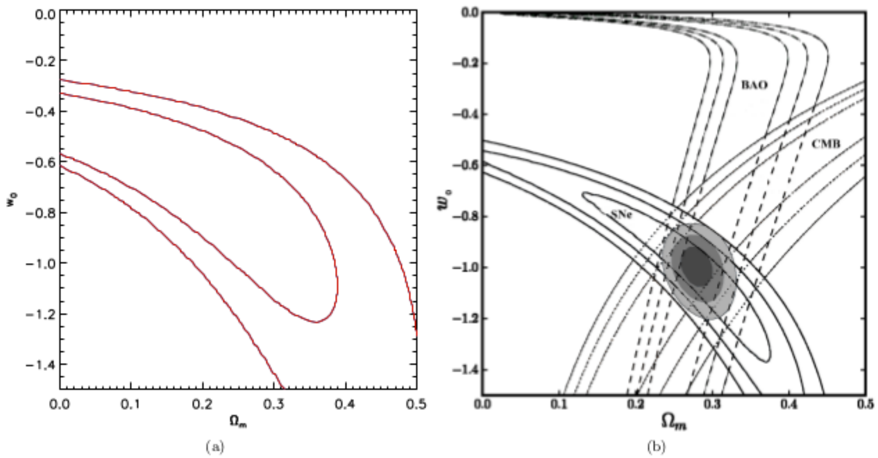

Figure 2.14: Comparison of restrictions on the plane (Ω_m, w_0). Panel (a) shows the results, obtained for the combined 25 high-z HIIGx and the local sample (131 HIIGx and GEHRs). 1 and 2σ contours are shown. Panel (b) after Suzuki et al. (2012) shows the recent results for 580 SNeIa, CMB and BAO, the 1, 2 and 3σ contours are shown. Taken from Terlevich et al. (2015).

The results shown in Figure 2.14 are consistent with simulation predictions in Plionis et al. (2011) in which they showed that a more efficient strategy to decrease the uncertainties of the cosmological parameters, based on the Hubble relation, is to use standard candles which trace also the redshift range $2 < z < 3.5$ (see Figure 2.15).

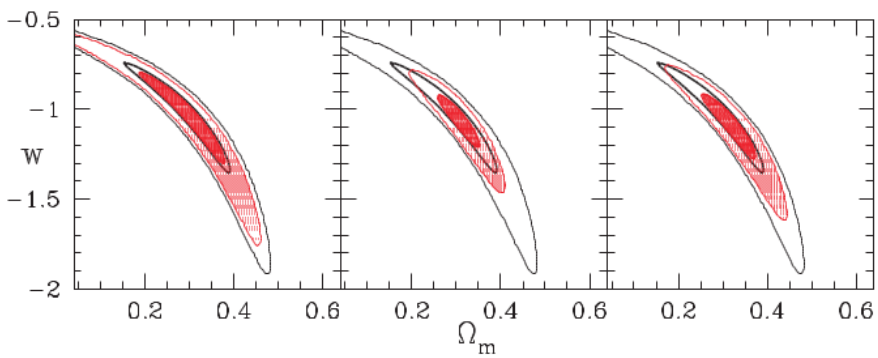

Figure 2.15: Comparison of the model Constitution SNIa constraints (black contours) with those (filled contours) derived by reducing to half their uncertainties (left-hand panel), with those derived by adding a sample of 76 high-z tracers ($2 < z < 3.5$) with a distance modulus mean uncertainty of $\sigma_\mu \simeq 0.5$ and no lensing degradation (central panel), and with those by including statistically the expected lensing degradation (right-hand panel). contours corresponding to the 1 and 3σ confidence levels are plotted. Taken from Plionis et al. (2011).

In order to study the relation between the number of high-z tracers used and the corresponding reduction of the cosmological parameter solution space, Plionis et al. (2011) used the figure of merit (FoM; Bassett, 2005; Albrecht et al., 2006; Bueno Sanchez et al., 2009), defined as the reciprocal area of the 2σ contour in the parameter space of any two degenerate cosmological parameters [e.g. (Ω_m , w) for the quintessence dark energy (QDE) model. In this way a larger FoM indicates better constrains to the cosmological parameters.
Here they use the parameter S or 'reduction factor', defined as the ratio of the FoM of the SNIa+high-z tracers Hubble relation solution to that of only the SNIa in order to study the question of how best it can be constrained the cosmological parameter space, when adding N_{high-z} high-z tracers of the Hubble relation, with respect to the best current SNIa data set as a function of the number of high-z tracers. In their results is interesting to note that the HII galaxies at high redshift could constrain cosmological parameters with the level of accuracy provided by current SNIa data sets (for $N_{high-z} > 200$) and relax the constraint that SNeIa are the only reliable tracers of the Hubble relation as has been used to-date (see Figure 2.16).

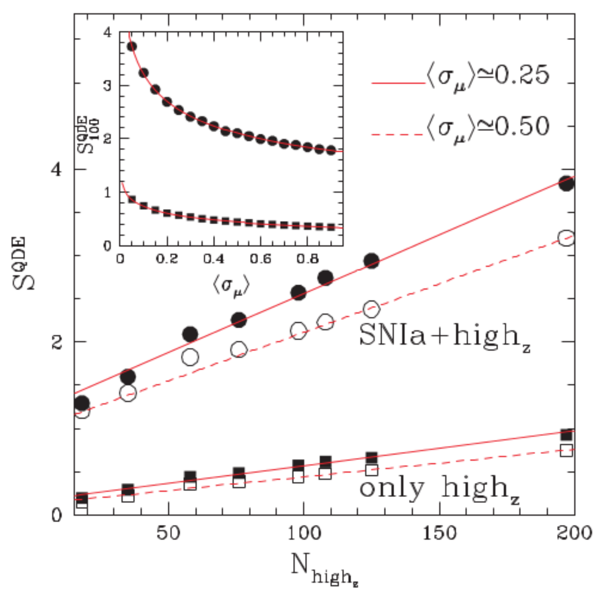

Figure 2.16: The 'reduction' parameter S, indicating the factor by which we reduce the 2σ contour area of the cosmological parameters (Ω_m , w) solution space (QDE model) as a function of the number of high-z tracers ($2 < z < 3.5$) of the Hubble relation and for two different values of the mean intrinsic distance modulus scatter (as indicated in the plot). Circular points correspond to using the high-z tracers together with the current best SNIa data set, while the squares to using only the high-z tracers (and a local $z < 0.2$ calibration sample). Inset panel: the 'reduction' parameter for the case of using 100 high-z tracers as a function of the mean distance modulus uncertainty, σ_μ. The lines correspond to logarithmic fits to the data. Taken from Plionis et al. (2011).

Chapter 3

Sample and Methodology

Large databases containing HII galaxies at high redshifts already exist and we have the possibility of selecting appropriate candidates for follow-up observations in order to achieve our scientific goals. In this chapter I will describe the parameters that characterize the sample and the selection criteria for choosing HII-like starburst galaxies at high redshift from the literature.

As already mentioned, the aim is to obtain a sample of HII-like starburst galaxies at high redshift and investigate their properties to compare them with nearby HIIGx in order to assess the L-σ relation for HIIGx as a distance estimator.

3.1 Sample Selection

The candidates were identified according to the equivalent widths (EW) in their emission lines. Synthesis models for star-forming galaxies in bursting episodes, predict that if the EW(Hβ)>50 Å or EW(Hα)>200 Å then the sample is composed by systems in which a single starburst younger than 5 Myr (Leitherer et al., 1999) dominates the total luminosity. But to account for uncertainties in the measurements of EWs reported in the literature, we relaxed the conditions so that the candidates have EW(Hβ) $>$ 25 Å or EW(Hα) $>$ 150 Å.

On the other hand, as the galaxies at the peak of cosmic star formation at z $\sim$ 2 have their emission lines shifted into the near-infrared, some objects in samples at high redshift don't have measurements of Hα. Sometimes, the Hβ line is more difficult to measure than other emission lines, for example, the [OIII]λ5007Å line. For this reason, we also need selection criteria that involve the [OIII] emission line. Now, if we suppose that rest-frame EW[OIII] in HIIGx at high redshift behaves in the same way as rest-frame EW[OIII] in HIIGx at low redshift, we can use the F[OIII]/F(Hβ) distribution of a sample of HIIGx at low redshift in order to calculate statistically the

EW[OIII] distribution through the relation:

$$EW[OIII] = \frac{F[OIII]}{F(H\beta)} \times EW(H\beta). \tag{3.1}$$

Figure 3.1 presents the equivalent width distribution obtained for [OIII]λ5007Å using the Equation (3.1) for a sample of 95 HIIGx at low redshift with F[OIII] and F(Hβ) data from Chávez et al. (2014) whose median value is 474.93 Å. Therefore, I defined a new selection criterion as EW[OIII] > 474 Å.

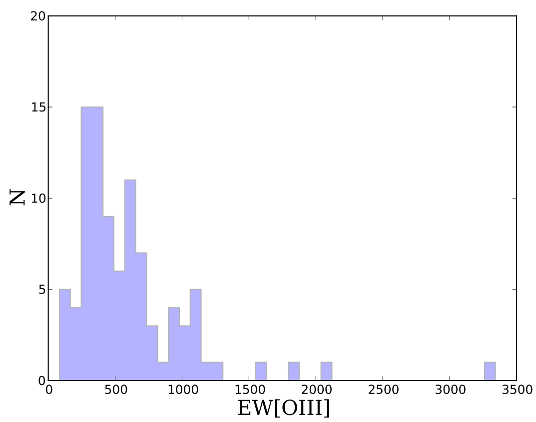

Figure 3.1: Equivalent width distribution of [OIII]λ5007Å line for the sample at low redshift from Chávez et al. (2014).

Once defined the selection parameters, EW(Hα) > 150 Å, EW(Hβ) > 25 Å or EW[OIII] > 474 Å, I found in the literature 504 HIIGx candidates in a range of redshift 0.1 < z < 3.4. Figure 3.2 shows the redshift distribution for the total sample where the dashed line represents the median value of 1.44. The purple band shows a population which was selected through broad-band photometry at 1.6 < z < 1.8 and the orange band shows an overdense region at $z = 2.23$ selected through narrow-band photometry.

The sample position on the sky is shown in Figure 3.3. From this we can see that the HIIGx at high redshift are distributed over the whole sky. Specifically, most of the HIIGx belong to the Ultra Deep Survey (UDS) in the CANDELS field, GOODS-South Deep (GSD) field and zCOSMOS survey in the COSMOS field. This has great advantages, since with the use of multiples IFUs at large telescopes, e.g. VLT-KMOS and KECK-MOSFIRE, we can observe simultaneously several objects in the same cosmological field. This increases notably the observation efficiency and in this way we take advantage of the high number density of the HIIGx.

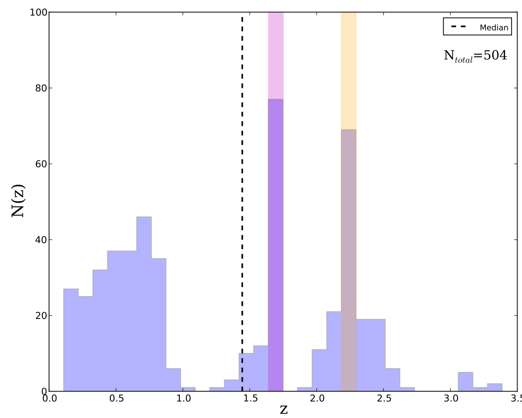

Figure 3.2: Histogram for the total sample of 504 HIIGx candidates with high rest-frame equivalent widths in their emission lines in a redshift range of $0.1 < z < 3.4$. The dashed line represents the median; the purple band shows a population which was selected through broad-band photometry at $1.6 < z < 1.8$ and the orange band shows an overdense region at $z = 2.23$ selected through narrow-band photometry

The total sample of 504 HII-like starburst galaxies at high redshift was obtained from the following sources as:

- 52 candidates at $1.4 < z < 2.6$ were selected from Erb et al. (2006a) and Erb et al. (2006b) as having EW(Hα)> 150 Å (Table 1, labelled 1 and 2 respectively).

- 16 candidates at $0.5 < z < 0.9$ were selected from Hoyos et al. (2005), as having EW(Hβ)> 25 Å (Table 1, labelled 3).

- 11 candidates at $2.1 < z < 3.3$ were selected from Siegel et al. (2005), Erb et al. (2003) and Pettini et al. (2001) as having EW(Hβ)> 25 Å (Table 1, labelled 4,5 and 6 respectively).

- 39 candidates were selected from Matsuda et al. (2011) as having EW(Hα)> 150 Å (Table 1, labelled 7).

- 16 candidates at $1.4 < z < 2.3$ were selected from Maseda et al. (2013, 2014) as having EW[OIII]λ5007 > 474 Å (Table 1, labelled 9 and 10 respectively).

- 26 candidates (13 at z$\sim$2.2 and 13 at z$\sim$1.5) were selected from Masters et al. (2014) as having EW(Hα)> 150 Å and high value of EW[OIII] (Table 1, labelled 11).

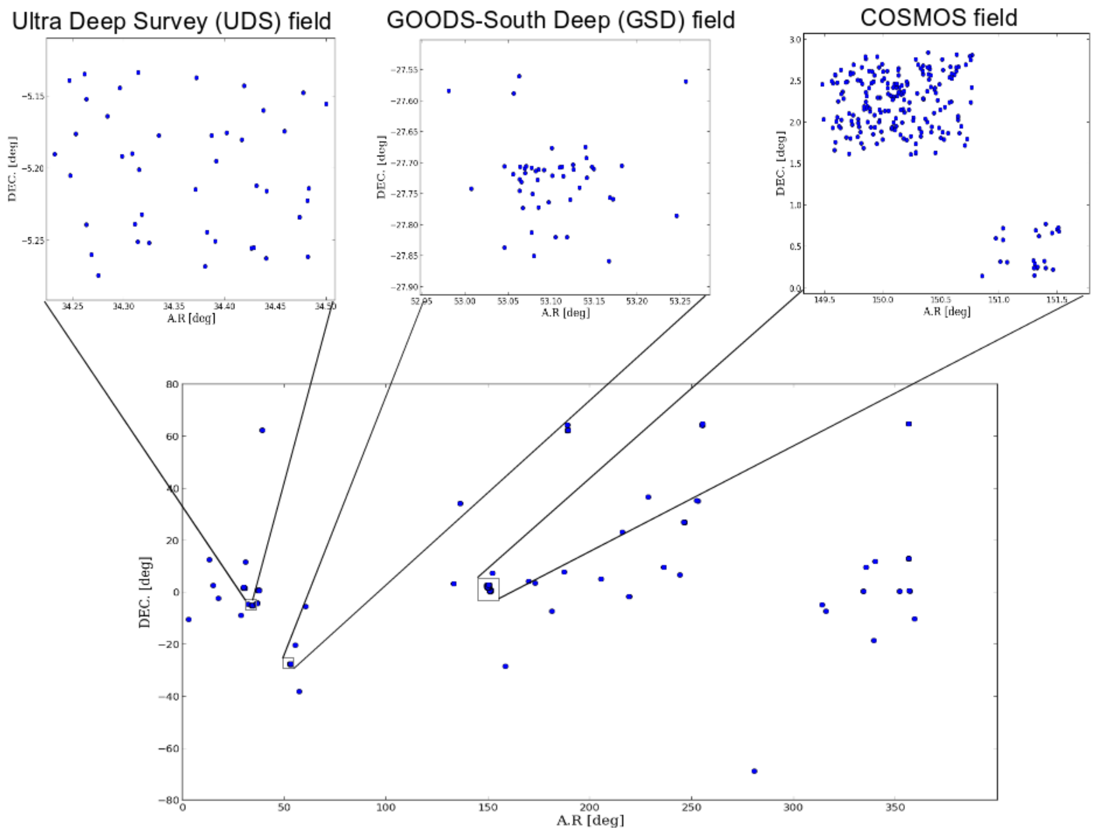

Figure 3.3: Sample position on the sky.

- 30 candidates at 0.3 < z < 0.9 were selected from Kobulnicky & Kewley (2004) and Weiner et al. (2006) as having EW(Hβ) > 25 Å (Table 1, labelled 12 and 16 respectively).

- 6 candidates at 0.6 < z < 2.1 were selected from Xia et al. (2012) as having EW(Hβ)> 25 Å (Table 1, labelled 14).

- 69 candidates at 1.6 < z < 1.8 were selected from van der Wel et al. (2011) as having EW[OIII]λ5007 > 474 Å (Table 1, labelled 17).

- 26 candidates at 1.5 < z < 2.6 were selected from Förster Schreiber et al. (2009) as having EW(Hα)> 150 Å (Table 1, labelled 18).

- 17 objects at 1.4 < z < 2.5 were selected from Mancini et al. (2011) as having EW(Hα) > 150 Å (Table 1, labelled 19).

- 165 candidates at $0.1 < z < 0.92$ were selected from Amorín et al. (2015) as having EW(Hα)> 150 Å, EW(Hβ)> 25 Å and high values of EW[OIII] (Table 1, labelled 20).

- 31 candidates at $0.21 < z < 0.86$ were selected from Amorín et al. (2014) as having EW(Hβ)> 25 Å and high values of EW[OIII] (Table 1, labelled 21).

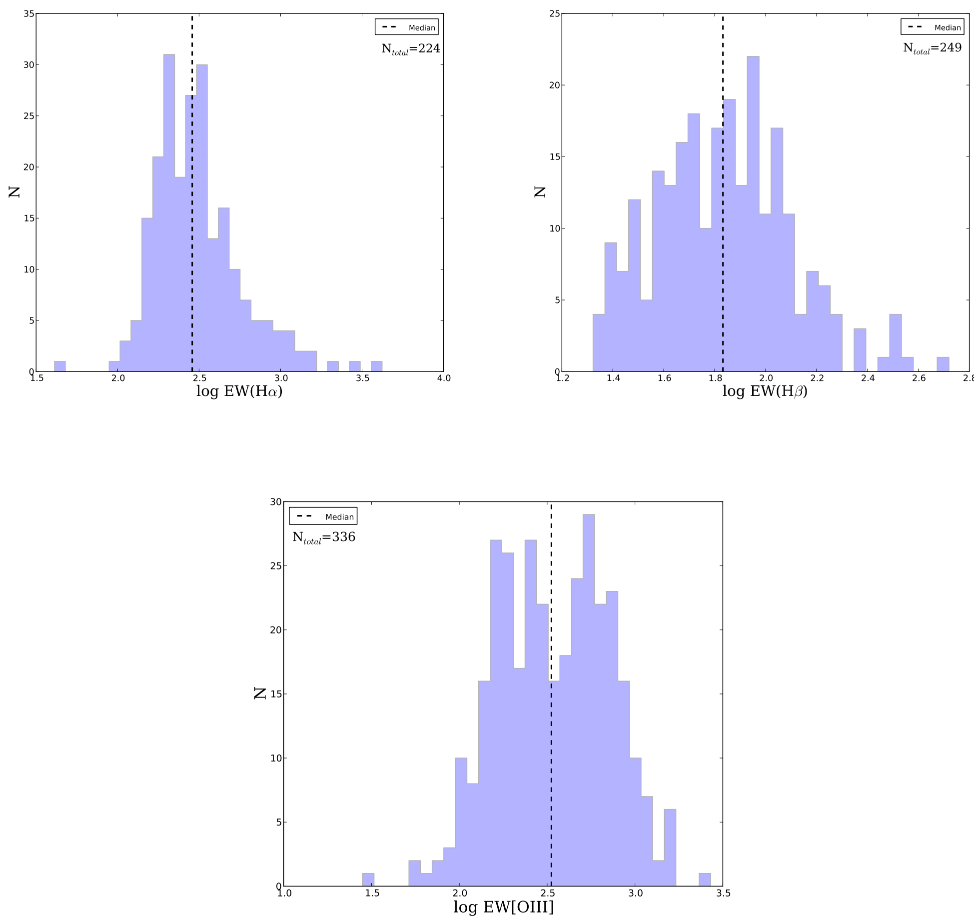

Figure 3.4: Rest-frame equivalent width distribution of the Hα, Hβ and [OIII] emission lines for the total sample. Top left panel: Histogram of the Hα emission line for 224 objects in a range of redshift $0.10 < z < 2.58$. Top right panel: Histogram of the Hβ emission line for 249 objects in a range of redshift $0.15 < z < 3.39$. Bottom panel: Histogram of the [OIII] line for 336 objects in a range of redshift $0.10 < z < 2.32$. The dashed lines represent the median in each distribution.

Due to the fact that the 504 HII-like galaxies at high redshift could satisfy just one of the three selection criteria, each one of the EWs histograms from Figure 3.4 does not have 504 objects. Therefore, those objects with EW(Hα) < 150 Å present in the left top panel from Figure 3.4 satisfy any of the other two selection criteria. The same occurs for the objects with EW(Hβ) < 25 Å and EW[OIII] < 474 Å seen in the right top histogram and central bottom histogram from Figure 3.4, respectively.

3.2 Properties of the Selected Sample at High Redshift

It is well known that the rest-frame optical spectra of star-forming galaxies at all redshifts exhibit emission lines from which detailed physical properties can be inferred. These intrinsic properties will be described in this section. Some of them were taken from the literature and others were calculated with the purpose of characterizing the sample of HII-like starburst galaxies at high redshift.

The general properties of this sample will be compared with a sample of HIIGx at low redshift from the literature in order to assess a possible connection between HIIGx at low and high redshift (see Chapter 4).

3.2.1 Velocity Dispersion

The line emission velocity dispersion (σ) reflects the dynamics of the gas in the galaxies' potential well. And because it requires only a measurement of the line width, it is therefore our most useful kinematic quantity. The velocity dispersion is calculated by:

$$\sigma = \frac{FWHM}{2\sqrt{2ln(2)}}, \tag{3.2}$$

where FWHM is the full width at half-maximum after subtraction of the nominal instrumental resolution. The values of velocity dispersions were taken from the literature and can be seen in column (7) from Table 1 in km s^{-1}. Their distribution is presented in Figure 3.5 where the dashed line represents the median value of $\sigma = 70.25$ km s^{-1}.

3.2.2 Size

The sizes of the HIIGx are defined as twice the half-light radius. The half-light radius is determined using the curves-of-growth extracted from circular apertures centered on the centroid of the line emission (i.e carried out from the spectra integrated in aperture radii that best fit to find the shape of each HIIGx), and then adjusting the radius of circular aperture until it encompasses half of the total Hα luminosity. The half-light radii also are corrected for the respective PSF FWHM[1]. The values of half-light radii

[1]The PSF FWHM corresponds to the effective spatial resolution of all observations for a given object and instrument setup. It is estimated from the combined images of the acquisition star taken regularly during the observations of a science target.

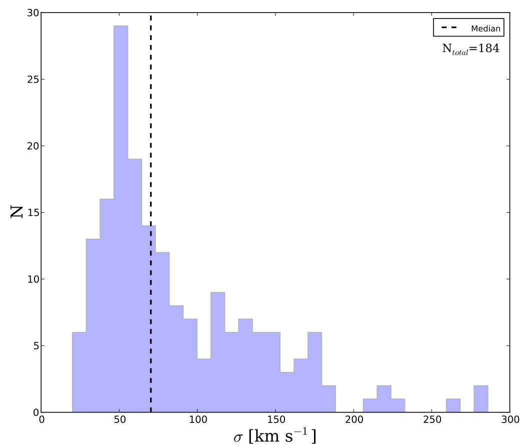

Figure 3.5: Velocity dispersion distribution for 184 sample galaxies in a range of redshift of $0.32 < z < 3.39$. The dashed line shows the median of the distribution.

were taken from the literature and can be seen in column (5) of Table 2 in kpc.

3.2.3 Dynamical Masses

If the emission-line widths reflect the relative motions of HII regions within the gravitational potential of the galaxies, dynamical masses can be calculated from the line widths via the relation:

$$M_{dyn} = \frac{C\sigma^2 r}{G} \tag{3.3}$$

where the factor C depends on the galaxy's mass distribution and therefore on the mass density profile, also on the velocity anisotropy, on random motions or rotation and finally on the assumption of a spherical or disk-like system.

The definition of the radius r is very important in the determination of dynamical masses. In most calculations of dynamical masses at high redshift C = 5 which is the ideal case of a sphere of uniform density has been used (Pettini et al., 2001; Erb et al., 2003, 2004; Shapley et al., 2004; Swinbank et al., 2004). Erb et al. (2006b) have used C $\simeq$ 3.4, instead of C = 5, under the assumption of a disk geometry.

In this thesis, I have selected the case of a sphere of uniform density, i.e. C = 5, therefore, the Equation (3.3) can be written as:

$$M_{dyn} = 1.16 \times 10^6 M_{\odot} \frac{\sigma^2}{[km/s]^2} \frac{r}{[kpc]}, \tag{3.4}$$

Taking the value of half-light radius and the velocity dispersion explained above, the dynamical masses were calculated using the Equation (3.4) and they are shown $M_\odot$ in column (6) from Table 2. Their distribution is presented in Figure 3.6 where the dashed line represents the median value of $\log(M_{dyn}) = 10.47\ M_\odot$.

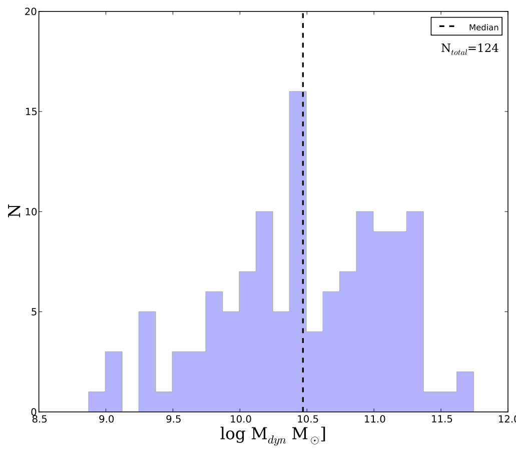

Figure 3.6: Dynamical mass distribution for 124 HII-like starburst galaxies with data on σ and radii the redshift range $0.68 < z < 2.57$. The dashed line represents the median.

3.2.4 Extinction and Fluxes

Following the empirical extinction relation found in Calzetti et al. (1994), the intrinsic fluxes at the wavelength λ, $F(\lambda)$, are given by:

$$F(\lambda) = F_{obs}(\lambda)10^{0.4k(\lambda)E(B-V)} = F_{obs}(\lambda)10^{0.4A(\lambda)} \tag{3.5}$$

where F_{obs} are the observed fluxes, $A(\lambda)$=$k(\lambda)E(B\text{-}V)$ is the extinction in magnitudes at the wavelength λ, E(B-V) is the color excess and $k(\lambda)$ is the reddening curve. We will use the reddening curve $k(\lambda)$ found in Calzetti et al. (2000) for our analysis, therefore:

$$k(\lambda) = 2.659(-1.857 + 1.040/\lambda) + \text{Rv} \qquad \textbf{for} \ \ 0.63 \leq \lambda \leq 2.20\mu m \tag{3.6}$$

$$k(\lambda) = 2.659(-2.156 + 1.509/\lambda - 0.198/\lambda^2 + 0.011/\lambda^3) + \text{Rv} \ \ \textbf{for} \ \ 0.12 \leq \lambda \leq 0.63\mu m \tag{3.7}$$

where Rv=Av/E(B-V) is the optical total-to-selective extinction ratio. We use the value of Rv=4.05±0.80 selected from Calzetti et al. (2000). The extinction in magnitudes for Hα and Hβ is:

$$A(H\alpha) = (3.32 \pm 0.80)E(B-V). \tag{3.8}$$

$$A(H\beta) = (4.60 \pm 0.80)E(B - V). \tag{3.9}$$

The values of E$(B - V)$, A(Hα) and A(Hβ) can be seen in columns (8), (9) and (10) of Table 2, respectively.

In some cases, the Hβ observed fluxes aren't available in the literature, so we estimate them by using the Equation (3.5) for Hα and Hβ. Then dividing both equations we obtain:

$$\frac{F(H\alpha)}{F(H\beta)} = \frac{F_{obs}(H\alpha)}{F_{obs}(H\beta)} 10^{0.4[A(H\alpha) - A(H\beta)]} \tag{3.10}$$

Assuming the intrinsic value of F(Hα)/F(Hβ)=2.86, corresponding to a temperature T=10^4 K and an electron density n_e=10^2 cm^{-3} for Case B recombination Osterbrock (1989), we obtain that:

$$F_{obs}(H\beta) = \frac{1}{2.86} F_{obs}(H\alpha) 10^{0.4[A(H\alpha) - A(H\beta)]} \tag{3.11}$$

Once the Hβ and Hα observed fluxes are obtained, Equation (3.5) is used to calculate the Hβ and Hα intrinsic fluxes, respectively. The results are presented in columns 8, 9, 11 and 12 of Table 1, where the uncertainties for the fluxes have been estimated propagating the error. The Hβ flux distribution is presented in Figure 3.7, where the dashed line represents the median value of log F(Hβ) = - 16.23 erg s^{-1} cm^{-2}.

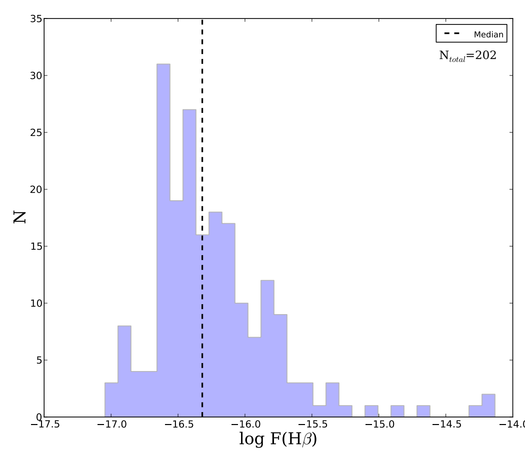

Figure 3.7: Hβ flux distribution for 202 HII-like starburst galaxies from our total sample in a range of redshift of 0.21 < z < 3.39. From these 202 objects, 132 have corrected Hβ flux as described in the text and the rest of them have observed Hβ flux. The dashed line represents the median.

3.2.5 Luminosity Distance

In the matter dominated era, the Hubble relation depends on the cosmological parameters via the following expression (derived from Friedmann's equation):

$$\frac{\dot{R}}{R} = H_0[\Omega_m(1+z)^3 + \Omega_r(1+z)^4 + \Omega_k(1+z)^2 + \Omega_\Lambda]^{1/2}, \tag{3.12}$$

then

$$H(z) = H_0 E(z), \tag{3.13}$$

where

$$H(z) = \frac{\dot{R}}{R}, \qquad \Omega_\Lambda \equiv \frac{\Lambda c^2}{3H_0^2}, \qquad \Omega_k \equiv \frac{-kc^2}{R_0^2 H_0^2}. \tag{3.14}$$

It is evident that at the present epoch we obtain from (3.13) that E(0)=1 and thus $\Omega_m + \Omega_r + \Omega_k + \Omega_\Lambda$=1.

In order to calculate the Hβ luminosity using the Hβ measured fluxes it is necessary to determine the luminosity distance, which is given by the following expression for a flat universe ($\Omega_k = 0$):

$$d_L = (1+z)\int_0^z \frac{c}{H(z)dz} \tag{3.15}$$

To obtain the luminosity distance I used the task *lumdist* from Python, which calculates the luminosity distance once the redshift and cosmological parameters, H_0 and Ω_m, are specified. The same results are obtained for the luminosity distance whether I use the task *lumdist* or Equation (3.15) to calculate it.
A cosmology with $H_0 = 74.3 \pm 4.3$ km s^{-1} Mpc^{-1} (Chávez et al., 2012), $\Omega_m = 0.27$ and $\Omega_\Lambda = 0.73$ is assumed in the calculation of luminosity distance.

3.2.6 Luminosities

The Hα and Hβ intrinsic luminosities were computed using the equations:

$$L(H\beta) = 4\pi d_L^2 F(H\beta), \tag{3.16}$$

and

$$L(H\alpha) = 4\pi d_L^2 F(H\alpha), \tag{3.17}$$

where d_L is the luminosity distance and F(Hβ) and F(Hα) are the reddening corrected Hβ and Hα fluxes, both parameters previously calculated. The Hβ luminosities estimated this way can be seen in column (3) of Table 2 in erg s^{-1}. Their distribution is presented in Figure 3.7, where the dashed line represents the median value of log L(Hβ) = 42.124 erg s^{-1}.

3.2.7 Star Formation Rates

In the calculation of star formation rate (SFR) we need calibrations based on evolutionary synthesis models, in which the emergent SEDs are derived for synthetic stellar populations with a prescribed age mix, chemical composition and IMF.
The extinction-corrected values of Hβ luminosities previously calculated were converted into Star Formation Rates (SFR) following the relation (cf. Kennicutt & Evans, 2012):

$$\frac{SFR}{[M_{\odot}/yr]} = 1.54 \times 10^{-41} \frac{L_{H\beta}}{[ergs^{-1}]} \tag{3.18}$$

where an IMF of Kroupa & Weidner (2003) with a Salpeter slope of α_{*} = -2.35 from 1 to 100 M$_{\odot}$ and α_{*} = -1.3 from 0.1 to 1 M$_{\odot}$ were used.

It is important to bear in mind that the concept of SFR is normally applied to whole galaxies, where the SFR does not suffer rapid changes. In general, a definition of SFR for an instantaneous burst is more difficult. Nevertheless, the SFR is useful to make comparisons with other star-forming galaxies. The SFR for the objects in our sample are presented in column (4) of Table 2. Their distribution is presented in Figure 3.8, where the dashed line represents the median value of log(SFR)=1.31 M$_{\odot}$ yr^{-1}.

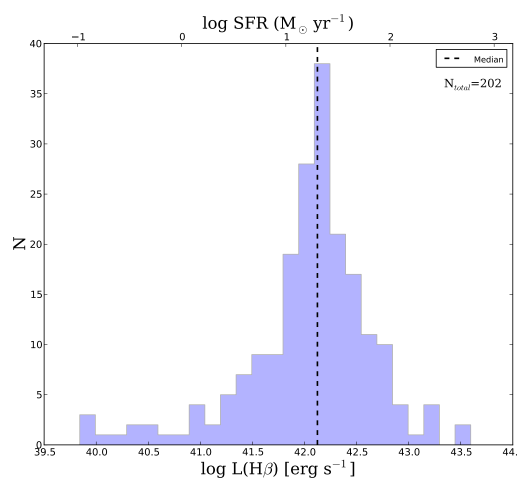

Figure 3.8: Hβ luminosity (and SFR as labelled on the top of the figure) distribution for 202 HII-like starburst galaxies from the sample in the redshift range 0.21 < z < 3.39. From this 202 objects, 132 have corrected Hβ luminosity and the rest of them have observed Hβ luminosity. The dashed line shows the median of the distribution

.

3.2.8 The Oxygen Abundance

The calculation of the oxygen abundance for HIIGx at high redshift is made under the assumption that the integrated spectra of these HIIGx can be treated in the same way as the spectra of individual local HII regions. The latter are used to calibrate the strong-line abundance indicators (see e.g. Erb et al., 2010).

In order to obtain the gas-phase oxygen abundance in HII regions it is necessary to measure the relative strengths of strong emission lines. The lines typically used are [OII]λ3727, Hβ, [OIII]$\lambda\lambda$4959, 5007, Hα, and [NII]λ6584. Different metallicity calibrators based on emission-line strengths exist (see e.g. Kewley & Ellison, 2008, for an overview). These empirical relations between strong-line ratios and chemical abundance have been calibrated using local HII regions with measured electron temperatures, in which the direct method is used to obtain the chemical abundance.

Direct Method

The direct method uses the temperature-sensitive ratio of two transitions of the same ion to determine the electron temperature. Most commonly, the auroral line [OIII]λ4363 is used. The total oxygen abundance is obtained as:

$$12 + log\left(\frac{O}{H}\right) = 12 + log\left(\frac{O^{+}}{H^{+}}\right) \; + \; 12 + log\left(\frac{O^{++}}{H^{+}}\right), \tag{3.19}$$

where the ionic oxygen abundances can be calculated from Pagel et al. (1992):

$$12 + log(O^{++}/H^{+}) = log\frac{I(4959) + I(5007)}{H\beta} + 6.174 + \frac{1.251}{t} - 0.55\, log(t) \tag{3.20}$$

and

$$\begin{aligned} 12 + log(O^{+}/H^{+}) = log\frac{I(3726) + I(3729)}{H\beta} + 5.890 + \frac{1.676}{t_2} \\ - 0.40\, log(t) + log(1 + 1.35x), \end{aligned} \tag{3.21}$$

being t the electron temperature:

$$t = 1.432[log\, R - 0.85 + 0.03\, log\, t + log(1 + 0.0433xt^{0.06})]^{-1}, \tag{3.22}$$

in units of 10^4 K; x=10^{-4} Ne t^2, where Ne is the electron density in cm^{-3} obtained using the [SII]λ6716/λ6731 line ratio; Finally R and t_2 are defined as

$$R = \frac{I(4959) + I(5007)}{I(4363)}, \tag{3.23}$$

$$t_2^{-1} = 0.5(t^{-1} + 0.8). \tag{3.24}$$

The direct method is useful in a restricted range of abundances, since in systems with oxygen abundance between $0.2(O/H)_{\odot}$ and $0.5(O/H)_{\odot}$ the [OIII]λ 4363 Å auroral line becomes extremely weak, requiring high S/N observations to be detected (Kennicutt et al., 2003). As a consequence of this, empirical methods using strong line ratios have been developed (see e.g. Kewley & Ellison, 2008).

R_{23} Method

The R_{23} method is an empirical method that is based on the ratio R23=([OIII]λ4959, 5007 + [OII]λ3727)/Hβ, this was first proposed by Pagel et al. (1979). Several calibrations have also been produced for the parameter R23 in an effort to compensate for the effect of the stellar temperature and ionization parameter (Edmunds & Pagel, 1984; Zaritsky, Kennicutt, & Huchra, 1994; Kobulnicky, Kennicutt, & Pizagno, 1999; Pilyugin, 2001a,b,c).

A difficulty with R_{23} is that it is double-valued with (O/H). For each value of R_{23} there is a low metallicity value corresponding to the lower branch of the relation and a high metallicity estimate corresponding to the upper branch. This makes necessary to determine in which branch of the R_{23} curve is located the oxygen abundance. Other problem is that most of the observational points tend to lay close to the knee of the relation, i.e., in the region in which there is no dependence of the R_{23} parameter on metallicity. The R_{23} method is in practice a reliable abundance estimator only for the metal rich or very metal poor systems.

To break the R_{23} degeneracy the [NII]λ6584/[O II]λ3727 ratio is used as an initial guess of metallicity helping in the selection of the appropriate R_{23} branch (McCall, Rybski, & Shields, 1985). This ratio shows a weak dependence on the ionization parameter and a strong correlation with metallicity (Kewley & Dopita, 2002). Another empirical indicator based on the R23 method was proposed by Pilyugin (2001a,b,c) where the excitation parameter P is introduced to compensate for R23 variations along the region produced by differences in the ionization parameter. The upper branch applies to 12 + log (O/H) $>$ 8.2 and the lower branch to 12 + log (O/H) $<$ 8.2. Another diagnostic ratio used to distinguish the appropriate R_{23} branch is [NII]λ6584/Hα, called the N2 index (Raimann et al., 2000), calibrated in [O/H] by Denicoló, Terlevich, & Terlevich (2002) and is described below.

N2 Method

The derivation of oxygen abundance in terms of N2 method is:

$$12 + log(O/H) = 9.12 + 0.73 \times N2, \tag{3.25}$$

where the N2 index, defined by Denicoló, Terlevich, & Terlevich (2002) as N2 $\equiv$ log([NII]λ6584/Hα), was previously used by Storchi-Bergmann, Calzetti, & Kinney

(1994) as an empirical abundance estimator for star-forming galaxies. It is valid for HII regions with -2.5 < N2 < -0.3 or according with the N2 ratio from 7.50 < 12+log(O/H) < 8.75. This estimator has the advantage of increasing monotonically with metallicity below 12 + log(O/H) ∼ 9.2, but above this value it is not an ideal metallicity indicator, being sensitive to the ionization parameter (Kewley & Dopita, 2002).

O3N2 Method

Pettini & Pagel (2004) calibrated the O3N2 ratio (Alloin et al., 1979) as an abundance estimator, giving the relation

$$12 + log(O/H) = 8.73 - 0.32 \times O3N2, \tag{3.26}$$

where O3N2 ≡ log[([OIII]λ5007/Hβ)/([N II]λ6584/Hα)]. This relation is valid for HII regions with -1 < O3N2 < 1.9 or according to the O3N2 ratio from 8.12 < 12+log(O/H) < 9.05. Due to the fact that the pair of ratios are closely spaced emission lines, this method is independent of flux calibrations and uncertainties in dust extinction.

Due to the lack of spectra of the sample I can not apply any of the methods discussed above. For this work, the oxygen abundances were taken from the literature and they are presented in column (15) of Table 2, indicating in each case the method applied. Their distribution is presented in Figure 3.9, where the dashed line represents the median value of 12 + log(O/H) = 8.18.

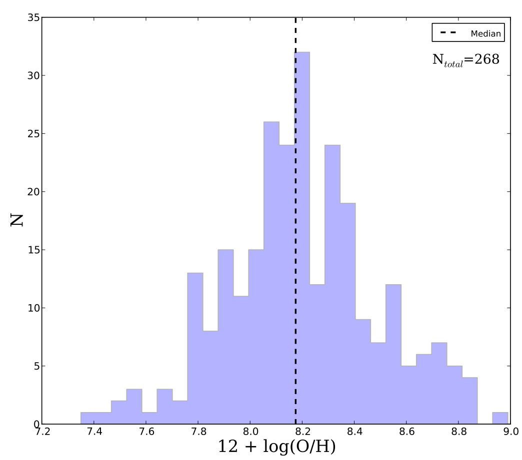

Figure 3.9: Oxygen abundance distribution for 268 HII-like starburst galaxies from the sample at high redshift in a range of redshift of 0.10 < z < 3.39. The dashed line represents the median of the distribution

.

Table 1

Index	Name	z	EW(Hα) (Å)	EW(Hβ) (Å)	EW[OIII] (Å)	σ (km s^{-1})	F($H\alpha$) Observed	F($H\beta$) Observed	F[OIII]λ5007Å Observed	F($H\alpha$) Corrected	F($H\beta$) Corrected	A.R (J2000)	DEC. (J2000)	Reference
001	HDF-BX1303	2.3003	308	...	...	...	$2.6^{+0.5}_{-0.5}$	$0.81^{+0.34}_{-0.34}$ [a]	...	$3.53^{+1.05}_{-1.05}$	$1.23^{+0.65}_{-0.65}$	12 37 11.20	+62 11 18.67	1,2
002	HDF-BX1376	2.4294	266	...	...	96^{+22}_{-24}	$2.2^{+0.2}_{-0.2}$	$0.71^{+0.20}_{-0.20}$ [a]	...	$2.73^{+0.50}_{-0.50}$	$0.95^{+0.34}_{-0.34}$	12 36 52.96	+64 15 45.55	1,2
003	HDF-BX1388	2.0317	265	...	...	140^{+21}_{-21}	$5.8^{+0.5}_{-0.5}$	$1.47^{+1.51}_{-1.51}$ [a]	...	$13.06^{+7.95}_{-7.95}$	$4.57^{+5.93}_{-5.93}$	12 36 44.84	+64 17 15.84	1,2
004	HDF-BX1409	2.2452	207	...	...	158^{+18}_{-18}	$8.5^{+0.6}_{-0.6}$	$2.12^{+2.34}_{-2.34}$ [a]	...	$20.66^{+13.66}_{-13.66}$	$7.22^{+10.24}_{-10.24}$	12 36 47.41	+64 17 28.70	1,2
005	Q1623-BX429	2.0160	219	...	...	57^{+22}_{-27}	$5.1^{+0.5}_{-0.5}$	$1.55^{+0.72}_{-0.72}$ [a]	...	$7.36^{+2.13}_{-2.13}$	$2.58^{+1.53}_{-1.53}$	16 25 48.65	+26 45 14.47	1,2
006	Q1623-BX432	2.1817	427	72	...	54^{+15}_{-16}	$5.4^{+0.3}_{-0.3}$	$1.76^{+0.41}_{-0.41}$ [a]	...	$6.49^{+0.95}_{-0.95}$	$2.27^{+0.68}_{-0.68}$	16 25 48.73	+26 46 47.28	1,2,4,5
007	Q1623-BX455	2.4074	1172	...	...	187^{+15}_{-15}	$18.8^{+1.1}_{-1.1}$	$4.82^{+4.88}_{-4.88}$ [a]	...	$42.33^{+25.62}_{-25.62}$	$14.80^{+19.21}_{-19.21}$	16 25 51.66	+26 46 54.88	1,2
008	Q1623-BX502	2.1558	1536	...	...	75^{+8}_{-8}	$13.2^{+0.4}_{-0.4}$	$3.57^{+2.99}_{-2.99}$ [a]	...	$25.90^{+12.94}_{-12.94}$	$9.05^{+9.72}_{-9.72}$	16 25 54.38	+26 44 09.25	1,2
009	Q1623-BX511	2.2421	325	...	...	152^{+34}_{-36}	$3.4^{+0.3}_{-0.3}$	$0.90^{+0.81}_{-0.81}$ [a]	...	$6.98^{+3.76}_{-3.76}$	$2.44^{+2.80}_{-2.80}$	16 25 56.11	+26 44 44.57	1,2
010	Q1623-BX543	2.5211	229	...	...	148^{+24}_{-26}	$8.6^{+0.7}_{-0.7}$	$2.10^{+2.44}_{-2.44}$ [a]	...	$21.89^{+15.21}_{-15.21}$	$7.65^{+11.38}_{-11.38}$	16 25 57.70	+26 50 08.59	1,2
011	Q1623-BX599	2.3304	303	...	...	162^{+8}_{-8}	$18.1^{+0.4}_{-0.4}$	$5.47^{+2.62}_{-2.62}$ [a]	...	$26.54^{+7.58}_{-7.58}$	$9.28^{+5.69}_{-5.69}$	16 26 02.54	+26 45 31.90	1,2
012	Q1623-MD107	2.5373	858	21	...	< 43	$3.7^{+0.4}_{-0.4}$	$1.21^{+0.30}_{-0.30}$ [a]	...	$4.45^{+0.77}_{-0.77}$	$1.55^{+0.48}_{-0.48}$	16 25 53.87	+26 45 15.46	1,2,4,5
013	Q1623-MD66	2.1075	482	...	...	120^{+4}_{-4}	$19.7^{+0.3}_{-0.3}$	$5.23^{+4.66}_{-4.66}$ [a]	...	$40.47^{+21.51}_{-21.51}$	$14.15^{+16.18}_{-16.18}$	16 25 40.39	+26 50 08.88	1,2
014	Q1700-BX490	2.3960	310	...	...	110^{+9}_{-9}	$17.7^{+0.6}_{-0.6}$	$4.43^{+4.82}_{-4.82}$ [a]	...	$42.38^{+27.48}_{-27.48}$	$14.82^{+20.66}_{-20.66}$	17 01 14.83	+64 09 51.69	1,2
015	Q1700-BX530	1.9429	208	...	...	< 37	$12.2^{+0.7}_{-0.7}$	$4.05^{+0.74}_{-0.74}$ [a]	...	$14.00^{+1.66}_{-1.66}$	$4.90^{+1.13}_{-1.13}$	17 00 36.86	+64 10 17.38	1,2
016	Q1700-BX691	2.1895	257	...	...	170^{+14}_{-14}	$7.7^{+0.3}_{-0.3}$	$2.32^{+1.12}_{-1.12}$ [a]	...	$11.29^{+3.25}_{-3.25}$	$3.95^{+2.43}_{-2.43}$	17 01 06.00	+64 12 10.27	1,2
017	Q1700-BX717	2.4353	410	25	...	< 47	$3.8^{+0.4}_{-0.4}$	$1.20^{+0.43}_{-0.43}$ [a]	...	$5.01^{+1.15}_{-1.15}$	$1.75^{+0.79}_{-0.79}$	17 00 56.99	+64 12 23.76	1,2,4,5
018	Q1700-MD109	2.2942	246	...	...	93^{+24}_{-26}	$8.9^{+0.7}_{-0.7}$	$2.53^{+1.69}_{-1.69}$ [a]	...	$15.21^{+6.13}_{-6.13}$	$5.32^{+4.54}_{-4.54}$	17 01 04.48	+64 12 09.29	1,2
019	Q2343-BM133	1.4774	2245	...	...	55^{+4}_{-6}	$28.7^{+0.8}_{-0.8}$	$8.77^{+3.87}_{-3.87}$ [a]	...	$40.82^{+10.76}_{-10.76}$	$14.27^{+8.06}_{-8.06}$	23 46 16.18	+12 48 09.31	1,2
020	Q2343-BX341	2.5749	231	...	...	...	$4.0^{+0.6}_{-0.6}$	$1.09^{+0.89}_{-0.89}$ [a]	...	$7.61^{+3.80}_{-3.80}$	$2.66^{+2.76}_{-2.76}$	23 46 23.24	+64 47 07.97	1,2
021	Q2343-BX378	2.0441	606	...	...	...	$4.5^{+1.0}_{-1.0}$	$1.30^{+0.87}_{-0.87}$ [a]	...	$7.46^{+3.26}_{-3.26}$	$2.61^{+2.19}_{-2.19}$	23 46 33.90	+64 47 26.20	1,2
022	Q2343-BX389	2.1716	253	...	...	111^{+8}_{-8}	$12.0^{+0.4}_{-0.4}$	$3.13^{+2.98}_{-2.98}$ [a]	...	$25.81^{+14.65}_{-14.65}$	$9.02^{+11.01}_{-11.01}$	23 46 28.90	+64 47 33.55	1,2
023	Q2343-BX390	2.2313	293	...	...	78^{+21}_{-24}	$4.9^{+0.5}_{-0.5}$	$1.44^{+0.83}_{-0.83}$ [a]	...	$7.76^{+2.75}_{-2.75}$	$2.71^{+2.00}_{-2.00}$	23 46 24.72	+64 47 33.80	1,2
024	Q2343-BX391	2.1740	537	...	...	...	$4.2^{+0.2}_{-0.2}$	$1.17^{+0.86}_{-0.86}$ [a]	...	$7.63^{+3.38}_{-3.38}$	$2.67^{+2.53}_{-2.53}$	23 46 28.07	+64 47 31.82	1,2
025	Q2343-BX418	2.3052	1639	...	...	66^{+6}_{-6}	$8.0^{+0.2}_{-0.2}$	$2.68^{+0.36}_{-0.36}$ [a]	...	$8.91^{+0.73}_{-0.73}$	$3.11^{+0.53}_{-0.53}$	23 46 18.57	+64 47 47.38	1,2
026	Q2343-BX429	2.1751	632	...	...	51^{+16}_{-20}	$4.8^{+0.3}_{-0.3}$	$1.35^{+0.96}_{-0.96}$ [a]	...	$8.46^{+3.60}_{-3.60}$	$2.96^{+2.68}_{-2.68}$	23 46 25.25	+64 47 51.20	1,2
027	Q2343-BX435	2.1119	200	...	...	60^{+12}_{-14}	$8.1^{+0.4}_{-0.4}$	$2.18^{+1.87}_{-1.87}$ [a]	...	$16.14^{+8.29}_{-8.29}$	$5.64^{+6.22}_{-6.22}$	23 46 26.36	+64 47 55.06	1,2
028	Q2343-BX436	2.3277	345	...	...	63^{+10}_{-12}	$7.2^{+0.4}_{-0.4}$	$2.32^{+0.63}_{-0.63}$ [a]	...	$8.92^{+1.50}_{-1.50}$	$3.12^{+1.08}_{-1.08}$	23 46 09.06	+64 47 56.00	1,2
029	Q2343-BX461	2.5662	760	...	...	139^{+22}_{-24}	$7.0^{+0.7}_{-0.7}$	$1.83^{+1.75}_{-1.75}$ [a]	...	$15.05^{+8.66}_{-8.66}$	$5.26^{+6.44}_{-6.44}$	23 46 32.96	+64 48 08.15	1,2
030	Q2343-BX493	2.3396	497	...	...	155^{+39}_{-42}	$5.3^{+0.9}_{-0.9}$	$1.37^{+1.35}_{-1.35}$ [a]	...	$11.57^{+6.96}_{-6.96}$	$4.05^{+5.07}_{-5.07}$	23 46 14.46	+64 48 21.64	1,2
031	Q2343-BX529	2.1129	230	...	...	...	$3.5^{+0.5}_{-0.5}$	$1.03^{+0.59}_{-0.59}$ [a]	...	$5.46^{+1.96}_{-1.96}$	$1.91^{+1.38}_{-1.38}$	23 46 09.72	+64 48 40.33	1,2
032	Q2343-BX537	2.3396	365	...	...	...	$5.2^{+0.3}_{-0.3}$	$1.56^{+0.78}_{-0.78}$ [a]	...	$7.74^{+2.32}_{-2.32}$	$2.71^{+1.72}_{-1.72}$	23 46 25.55	+64 48 44.54	1,2
033	Q2343-BX660	2.1735	488	...	...	< 40	$9.4^{+0.4}_{-0.4}$	$3.25^{+0.18}_{-0.18}$ [a]	...	$9.69^{+0.47}_{-0.47}$	$3.39^{+0.22}_{-0.22}$	23 46 29.43	+64 49 45.54	1,2
034	Q2343-MD80	2.0138	206	...	...	74^{+16}_{-16}	$3.2^{+0.3}_{-0.3}$	$1.09^{+0.13}_{-0.13}$ [a]	...	$3.40^{+0.35}_{-0.35}$	$1.19^{+0.16}_{-0.16}$	23 46 10.79	+64 48 33.24	1,2
035	Q2346-BX220	1.9677	482	...	...	143^{+14}_{-14}	$10.3^{+0.6}_{-0.6}$	$3.38^{+0.72}_{-0.72}$ [a]	...	$12.19^{+1.66}_{-1.66}$	$4.26^{+1.16}_{-1.16}$	23 48 46.10	+00 22 20.95	1,2
036	Q2346-BX404	2.0282	273	...	...	102^{+3}_{-3}	$13.9^{+0.3}_{-0.3}$	$4.35^{+1.56}_{-1.56}$ [a]	...	$18.59^{+4.00}_{-4.00}$	$6.50^{+3.00}_{-3.00}$	23 48 21.40	+00 24 43.07	1,2
037	Q2346-BX405	2.0300	358	...	...	50^{+4}_{-4}	$14.0^{+0.2}_{-0.2}$	$4.84^{+0.20}_{-0.20}$ [a]	...	$14.44^{+0.39}_{-0.39}$	$5.05^{+0.26}_{-0.26}$	23 48 21.22	+00 24 45.46	1,2
038	Q2346-BX416	2.2404	287	...	...	126^{+12}_{-14}	$12.1^{+0.7}_{-0.7}$	$3.37^{+2.50}_{-2.50}$ [a]	...	$21.99^{+9.77}_{-9.77}$	$7.69^{+7.30}_{-7.30}$	23 48 18.21	+00 24 55.30	1,2
039	HDF-BX1322	2.4443	197.00	...	...	< 47	$2.0^{+0.2}_{-0.2}$	$0.63^{+0.22}_{-0.22}$ [a]	...	$2.59^{+0.57}_{-0.57}$	$0.91^{+0.39}_{-0.39}$	12 37 06.54	+62 12 24.94	1,2
040	Q1623-BX376	2.4085	308.00	...	...	261^{+54}_{-54}	$5.3^{+0.7}_{-0.7}$	$1.51^{+1.02}_{-1.02}$ [a]	...	$9.06^{+3.78}_{-3.78}$	$3.17^{+2.73}_{-2.73}$	16 25 45.59	+26 46 49.26	1,2

Continuation on the next page.

Table 1 Continued

Index	Name	z	EW(Hα) (Å)	EW(Hβ) (Å)	EW[OIII] (Å)	σ (km s^{-1})	F($H\alpha$) Observed	F($H\beta$) Observed	F[OIII]λ5007Å Observed	F($H\alpha$) Corrected	F($H\beta$) Corrected	A.R (J2000)	DEC. (J2000)	Reference
041	Q1623-BX447	2.1481	154.00	...	...	174^{+15}_{-15}	$5.6^{+0.3}_{-0.3}$	$1.85^{+0.36}_{-0.36}$ [a]	...	$6.53^{+0.82}_{-0.82}$	$2.28^{+0.57}_{-0.57}$	16 25 50.37	+26 47 14.28	1,2
042	Q1623-BX449	2.4185	196.00	...	...	< 72	$3.5^{+0.9}_{-0.9}$	$1.08^{+0.53}_{-0.53}$ [a]	...	$4.90^{+1.76}_{-1.76}$	$1.71^{+1.02}_{-1.02}$	16 25 50.53	+26 46 59.97	1,2
043	Q1623-BX453	2.1816	187.00	...	...	61^{+4}_{-4}	$13.8^{+0.2}_{-0.2}$	$3.50^{+3.65}_{-3.65}$ [a]	...	$32.04^{+19.94}_{-19.94}$	$11.20^{+15.00}_{-15.00}$	16 25 50.84	+26 49 31.40	1,2
044	Q1623-BX586	2.1045	192.00	...	...	124^{+18}_{-20}	$5.1^{+0.4}_{-0.4}$	$1.42^{+1.05}_{-1.05}$ [a]	...	$9.27^{+4.15}_{-4.15}$	$3.24^{+3.08}_{-3.08}$	16 26 01.52	+26 45 41.58	1,2
045	Q1700-BX523	2.4756	171.00	...	...	130^{+26}_{-26}	$4.7^{+0.5}_{-0.5}$	$1.21^{+1.21}_{-1.21}$ [a]	...	$10.42^{+6.24}_{-6.24}$	$3.64^{+4.64}_{-4.64}$	17 00 41.71	+64 10 14.88	1,2
046	Q1700-BX536	1.9780	150.00	...	...	89^{+14}_{-15}	$11.3^{+0.7}_{-0.7}$	$3.45^{+1.53}_{-1.53}$ [a]	...	$16.07^{+4.33}_{-4.33}$	$5.62^{+3.19}_{-3.19}$	17 01 08.94	+64 10 24.95	1,2
047	Q1700-BX794	2.2473	183.00	...	...	80^{+14}_{-14}	$6.8^{+0.4}_{-0.4}$	$2.04^{+1.02}_{-1.02}$ [a]	...	$10.13^{+3.04}_{-3.04}$	$3.54^{+2.26}_{-2.26}$	17 00 47.30	+64 13 18.70	1,2
048	Q2343-BX169	2.2094	152.00	...	...	...	$4.7^{+0.3}_{-0.3}$	$1.42^{+0.68}_{-0.68}$ [a]	...	$6.89^{+2.01}_{-2.01}$	$2.41^{+1.49}_{-1.49}$	23 46 05.03	+12 45 40.77	1,2
049	Q2343-BX182	2.2879	168.00	...	...	...	$2.4^{+0.3}_{-0.3}$	$0.75^{+0.30}_{-0.30}$ [a]	...	$3.26^{+0.84}_{-0.84}$	$1.14^{+0.57}_{-0.57}$	23 46 18.04	+12 45 51.11	1,2
050	Q2343-BX236	2.4348	150.00	...	...	148^{+40}_{-42}	$3.1^{+0.6}_{-0.6}$	$0.98^{+0.37}_{-0.37}$ [a]	...	$4.02^{+1.10}_{-1.10}$	$1.41^{+0.65}_{-0.65}$	23 46 18.71	+12 46 15.97	1,2
051	Q2343-BX513	2.1092	192.00	...	...	150^{+9}_{-9}	$10.1^{+0.4}_{-0.4}$	$3.01^{+1.54}_{-1.54}$ [a]	...	$15.27^{+4.69}_{-4.69}$	$5.34^{+3.51}_{-3.51}$	23 46 11.13	+12 48 32.14	1,2
052	Q2343-BX601	2.3769	199.00	...	...	105^{+12}_{-12}	$7.4^{+0.4}_{-0.4}$	$2.23^{+1.08}_{-1.08}$ [a]	...	$10.85^{+3.15}_{-3.15}$	$3.79^{+2.34}_{-2.34}$	23 46 20.40	+12 49 12.91	1,2
053	DEEP2-1	0.8510	...	98±5	...	40±14	...	...	...	...	...	23 29 08.20	+00 20 40.70	3
054	DEEP2-2	0.7300	...	90±5	...	25±6	...	...	...	...	...	02 29 33.65	+00 26 08.00	3
055	DEEP2-3	0.7490	...	96±5	...	30±14	...	...	...	...	...	16 53 03.49	+34 58 48.90	3
056	DEEP2-4	0.6310	...	88±5	...	32±4	...	...	...	...	...	23 28 47.84	...	3
057	DEEP2-5	0.6360	...	96±5	...	28±4	...	...	...	...	...	23 28 41.65	+00 18 20.00	3
058	DEEP2-6	0.5300	...	160±20	...	34±5	...	...	...	...	...	...	...	3
059	DEEP2-7	0.7060	...	70±5	...	41±4	...	...	...	...	...	16 50 05.43	+35 06 30.40	3
060	DEEP2-8	0.6590	...	70±10	...	50±10	...	...	...	...	...	02 31 17.32	+00 37 28.20	3
061	DEEP2-9	0.7500	...	91±5	...	40±10	...	...	...	...	...	02 30 20.03	+00 42 49.70	3
062	DEEP2-10	0.6570	...	60±10	...	60±16	...	...	...	...	...	02 28 38.46	+00 28 52.30	3
063	DEEP2-11	0.5510	...	81±9	...	20±20	...	...	...	...	...	02 28 40.39	+00 36 07.70	3
064	DEEP2-12	0.6800	...	110±15	...	32±2	...	...	...	...	...	02 28 45.05	+00 41 32.80	3
065	DEEP2-13	0.7020	...	91±3	...	30±16	...	...	...	...	...	02 30 02.06	+00 47 34.70	3
066	DEEP2-14	0.7250	...	59±5	...	37±5	...	...	...	...	...	02 30 12.32	+00 36 52.50	3
067	TKRS-1	0.8550	...	150±20	...	57±6	...	...	...	...	...	02 36 42.83	+62 20 01.58	3
068	TKRS-2	0.6810	...	100±15	...	48±4	...	...	...	...	...	02 36 33.02	+62 15 37.52	3
069	Q0201-B13	2.1663	...	23	...	62±29	$2.54^{+0.56}_{-0.56}$ [c]	$0.88^{+0.20}_{-0.20}$ [c]	...	$2.57^{+0.57}_{-0.57}$	$0.90^{+0.20}_{-0.20}$	02 03 49.25	+11 36 10.58	4,5
070	Q1700-MD103	2.3148	...	47	...	75±21	$3.46^{+1.31}_{-1.31}$ [c]	$0.93^{+0.29}_{-0.29}$ [c]	...	$6.86^{+2.84}_{-2.84}$	$2.4^{+0.60}_{-0.60}$	17 01 00.20	+64 44 56.00	4,5
071	CDFaC1	3.1110	...	28	...	≤ 63	$6.94^{+1.00}_{-1.00}$ [c]	$2.13^{+0.18}_{-0.18}$ [c]	...	$9.72^{+1.60}_{-1.60}$	$3.40^{+0.10}_{-0.10}$	00 53 34.07	+12 30 30.00	4,6
072	Q0347-383C5	3.2360	...	≤ 27	...	69±4	$4.15^{+0.28}_{-0.28}$ [c]	$1.36^{+0.05}_{-0.05}$ [c]	...	$4.86^{+0.37}_{-0.37}$	$1.70^{+0.00}_{-0.00}$	03 49 43.05	-38 10 05.00	4,6
073	SSA22a-MD46	3.0810	...	≤ 31	...	67±6	$6.11^{+0.19}_{-0.19}$ [c]	$2.08^{+0.04}_{-0.04}$ [c]	...	$6.58^{+0.23}_{-0.23}$	$2.30^{+0.00}_{-0.00}$	22 17 27.03	+00 18 10.00	4,6
074	B20902+343C6	3.0800	...	40	...	55±15	$7.10^{+2.43}_{-2.43}$ [c]	$2.31^{+0.78}_{-0.78}$ [c]	...	$8.58^{+2.96}_{-2.96}$	$3.00^{+1.00}_{-1.00}$	09 05 20.05	+34 09 08.00	4,6
075	B20902+343C12	3.3866	...	37	...	87±12	...	...	...	$7.72^{+0.86}_{-0.86}$	$2.70^{+0.30}_{-0.30}$	09 05 43.80	+34 11 08.00	4,6
076	Q1422+231D81	3.1037	...	43	...	116±8	...	...	...	$11.73^{+1.14}_{-1.14}$	$4.10^{+0.40}_{-0.40}$	14 24 31.40	+22 59 52.00	4,6
077	SSA22aD3	3.0687	...	25	...	113±7	...	...	...	$3.72^{+0.86}_{-0.86}$	$1.30^{+0.30}_{-0.30}$	22 17 32.40	+00 11 33.00	4,6
078	DSF2237+116aC2	3.3176	...	25	...	100±4	...	...	...	$10.01^{+1.14}_{-1.14}$	$3.50^{+0.40}_{-0.40}$	22 40 08.30	+11 49 05.00	4,6
079	MS1512-cB58	2.7290	...	26	...	81.00	...	...	...	$3.86^{+0.57}_{-0.57}$	$1.35^{+0.20}_{-0.20}$	15 14 22.30	+36 36 26.00	4,6
080	2QZC-C1-HAE19	2.2300	1311.76	...	...	...	08.71	...	...	...	...	10 03 24.89	+00 08 31.80	7

Continuation on the next page.

Table 1 Continued

Index	Name	z	EW(Hα) (Å)	EW(Hβ) (Å)	EW[OIII] (Å)	σ (km s^{-1})	F($H\alpha$) Observed	F($H\beta$) Observed	F[OIII]λ5007Å Observed	F($H\alpha$) Corrected	F($H\beta$) Corrected	A.R (J2000)	DEC. (J2000)	Reference
081	2QZC-C1-HAE20	2.2300	230.65	...	...	...	06.46	...	...	...	...	10 04 16.74	+00 18 33.00	7
082	2QZC-C1-HAE21	2.2300	980.5	...	...	...	07.58	...	...	...	...	10 04 02.90	+00 18 52.50	7
083	2QZC-C2-HAE1	2.2300	255.11	...	...	...	123.03	...	...	...	...	10 05 11.82	+00 14 18.30	7
084	2QZC-C2-HAE3	2.2300	454.8	...	...	...	18.62	...	...	...	...	10 05 36.81	+00 14 19.40	7
085	2QZC-C2-HAE4	2.2300	328.48	...	...	...	15.85	...	...	...	...	10 05 34.17	+00 19 32.40	7
086	2QZC-C2-HAE13	2.2300	210.53	...	...	...	07.24	...	...	...	...	10 05 12.95	+00 09 10.20	7
087	2QZC-C2-HAE14	2.2300	335.6	...	...	...	07.41	...	...	...	...	10 05 14.51	+00 17 36.50	7
088	2QZC-C2-HAE15	2.2300	444.58	...	...	...	07.58	...	...	...	...	10 05 51.55	+00 13 16.40	7
089	2QZC-C2-HAE16	2.2300	406.19	...	...	...	06.76	...	...	...	...	10 05 10.98	+00 19 55.60	7
090	2QZC-C2-HAE17	2.2300	348.3	...	...	...	06.61	...	...	...	...	10 05 18.32	+00 14 21.00	7
091	2QZC-C2-HAE18	2.2300	886.07	...	...	...	07.24	...	...	...	...	10 05 19.23	+00 15 01.50	7
092	2QZC-C3-HAE8	2.2300	220.74	...	...	...	10.23	...	...	...	...	10 06 00.01	+00 42 33.60	7
093	2QZC-C3-HAE9	2.2300	4199.69	...	...	...	12.59	...	...	...	...	10 05 36.99	+00 46 20.20	7
094	2QZC-C3-HAE11	2.2300	698.76	...	...	...	10.72	...	...	...	...	10 06 02.53	+00 43 34.80	7
095	2QZC-C3-HAE12	2.2300	706.19	...	...	...	10.72	...	...	...	...	10 06 03.90	+00 41 06.30	7
096	2QZC-C3-HAE14	2.2300	185.45	...	...	...	06.92	...	...	...	...	10 05 49.59	+00 39 53.20	7
097	2QZC-C3-HAE15	2.2300	289.16	...	...	...	07.58	...	...	...	...	10 05 16.28	+00 41 50.40	7
098	2QZC-C3-HAE19	2.2300	196.28	...	...	...	06.46	...	...	...	...	10 05 22.24	+00 37 38.40	7
099	2QZC-C4-HAE3	2.2300	366.87	...	...	...	09.12	...	...	...	...	10 03 53.81	+00 36 05.70	7
100	2QZC-C4-HAE4	2.2300	185.76	...	...	...	07.08	...	...	...	...	10 04 08.44	+00 43 09.80	7
101	2QZC-C4-HAE6	2.2300	901.86	...	...	...	07.24	...	...	...	...	10 04 08.45	+00 34 58.30	7
102	0200-C1-HAE4	2.2300	205.57	...	...	...	16.98	...	...	...	...	02 01 06.09	+01 23 30.80	7
103	0200-C1-HAE6	2.2300	182.66	...	...	...	12.02	...	...	...	...	02 00 36.58	+01 19 53.70	7
104	0200-C1-HAE7	2.2300	506.19	...	...	...	14.12	...	...	...	...	02 00 57.57	+01 19 39.20	7
105	0200-C1-HAE8	2.2300	459.75	...	...	...	13.18	...	...	...	...	02 00 43.94	+01 26 14.80	7
106	0200-C1-HAE9	2.2300	186.38	...	...	...	10.96	...	...	...	...	02 00 33.53	+01 21 28.70	7
107	0200-C1-HAE10	2.2300	1217.03	...	...	...	13.49	...	...	...	...	02 01 05.81	+01 23 50.30	7
108	0200-C1-HAE11	2.2300	267.18	...	...	...	10.23	...	...	...	...	02 00 40.04	+01 19 22.00	7
109	0200-C1-HAE12	2.2300	1064.4	...	...	...	11.48	...	...	...	...	02 01 07.72	+01 28 22.60	7
110	0200-C2-HAE7	2.2300	569.35	...	...	...	17.38	...	...	...	...	02 02 46.26	+01 21 46.20	7
111	0200-C2-HAE9	2.2300	235.91	...	...	...	11.75	...	...	...	...	02 03 05.95	+01 28 22.90	7
112	0200-C2-HAE11	2.2300	197.83	...	...	...	10.96	...	...	...	...	02 02 19.56	+01 30 54.00	7
113	0200-C2-HAE12	2.2300	308.98	...	...	...	11.22	...	...	...	...	02 02 19.72	+01 21 32.20	7
114	0200-C2-HAE13	2.2300	1066.56	...	...	...	11.48	...	...	...	...	02 02 40.64	+01 30 18.20	7
115	0200-C2-HAE16	2.2300	323.84	...	...	...	09.55	...	...	...	...	02 03 04.90	+01 29 38.80	7
116	0200-C4-HAE7	2.2300	313.31	...	...	...	11.75	...	...	...	...	02 01 07.59	+01 44 34.10	7
117	0200-C4-HAE8	2.2300	467.18	...	...	...	12.02	...	...	...	...	02 01 05.52	+01 48 03.10	7
118	0200-C4-HAE11	2.2300	191.02	...	...	...	08.51	...	...	...	...	02 00 51.62	+01 47 20.20	7
119	COSMOS-15144	1.4120	325±230	...	1130±274	43.3±8.9	...	...	16.3±3.58	...	...	10 00 37.62	+02 21 38.88	9,10
120	COSMOS-13848	1.4440	41±345	...	888±351	46.7±14.4	...	...	8.76±3.46	...	...	10 00 42.48	+02 20 43.40	9,10

Continuation on the next page.

Table 1 Continued

Index	Name	z	EW(Hα) (Å)	EW(Hβ) (Å)	EW[OIII] (Å)	σ (km s^{-1})	F($H\alpha$) Observed	F($H\beta$) Observed	F[OIII]λ5007Å Observed	F($H\alpha$) Corrected	F($H\beta$) Corrected	A.R (J2000)	DEC. (J2000)	Reference
121	COSMOS-12807	1.5830	...	...	628±152	38.2±10.0	...	...	5.99±3.61	...	...	10 00 38.29	+02 19 59.88	9,10
122	UDS-7444	1.6210	...	...	713±42	71.1±5.7	...	...	...	...	...	02 17 53.73	-05 14 03.24	9,10
123	COSMOS-16207	1.6490	...	...	536±20	47.7±9.5	...	...	20.5±0.77	...	...	10 00 43.94	+02 22 22.61	9,10
124	UDS-3760	1.6640	...	...	731±86	48.2±5.9	...	...	...	...	...	02 17 42.86	-05 15 19.14	9,10
125	UDS-3646	1.6870	...	...	701±95	54.7±6.1	...	...	...	...	...	02 17 42.36	-05 15 20.77	9,10
126	GOODS-S-17892	1.6870	...	...	693±47	52.3±5.7	...	...	7.36±2.99	...	...	03 32 41.26	-27 45 32.92	9,10
127	GOODS-S-26816	1.7380	...	...	861±66	54.4±4.5^{a}	...	...	16.9±0.88	...	...	03 32 17.11	-27 42 20.89	9,10
128	UDS-11484	2.1850	...	...	723±95	54.2±9.4	...	...	21.5±2.82	...	...	02 17 43.54	-05 12 43.63	9,10
129	COSMOS-11212	2.1990	...	...	598±189	40.3±8.9	...	...	11.5±2.94	...	...	10 00 29.82	+02 18 49.22	9,10
130	COSMOS-8991	2.2200	...	...	714±85	30.9±9.0	...	...	11.8±0.89	...	...	10 00 22.88	+02 17 14.09	9,10
131	UDS-14655	2.2970	...	...	503±34	61.0±10.8	...	...	21.9±3.09	...	...	02 17 33.93	-05 11 43.12	9,10
132	UDS-4501	2.2980	...	...	803±162	57.8±9.7	...	...	13.7±2.76	...	...	02 17 33.78	-05 15 02.89	9,10
133	COSMOS-12102	1.4630	360±18	...	630±29	230.8±14.7	...	...	49.4±2.28	...	...	10 00 23.35	+02 18 09.07	10
134	COSMOS-17118	1.6560	...	...	493±169	46.5±8.8	...	...	12.3±4.22	...	...	10 00 36.27	+02 21 14.76	10
135	WISP159-134	1.3000	314±36	...	...	64.9±4.3	$14.2^{+1.0}_{-1.0}$	$4.74^{+4.97}_{-1.06}$ ^{a}	...	$16.05^{+9.91}_{-2.32}$	$5.61^{+7.57}_{-1.59}$	20 56 30.91	-04 47 56.3	11
136	WISP134-171	1.3540	266±11	...	124±6	71.5±2.1	$22.60^{+0.78}_{-0.78}$	...	...	...	...	18 42 33.21	-68 58 37.4	11
137	WISP50-65	1.4370	202±15	...	...	145.5±3.8	$10.0^{+0.9}_{-0.9}$	$1.44^{+2.73}_{-2.52}$ ^{a}	...	$102.57^{+118.89}_{-110.77}$	$35.86^{+86.95}_{-80.37}$	22 22 15.86	+09 36 47.1	11
138	WISP173-205	1.4440	603±42	...	982±146	61.3±1.4	$11.2^{+0.6}_{-0.6}$	$3.78^{+1.02}_{-0.64}$ ^{a}	...	$12.28^{+2.01}_{-1.33}$	$4.29^{+1.47}_{-0.91}$	01 55 23.64	-09 03 10.2	11
139	WISP9-73	1.4540	221±12	...	233±9	79.0±1.0	$18.7^{+0.8}_{-0.8}$	$4.60^{+1.74}_{-1.74}$ ^{a}	...	$46.87^{+12.02}_{-12.02}$	$16.39^{+7.70}_{-7.70}$	12 29 43.35	+07 48 35.9	11
140	WISP43-75	1.4820	137±14	...	...	...	$29.6^{+3.7}_{-3.7}$	$8.78^{+5.32}_{-5.32}$ ^{a}	...	$45.45^{+16.99}_{-16.99}$	$15.89^{+12.26}_{-12.26}$	21 04 06.18	-07 22 28.6	11
141	WISP25-53	1.4860	130±7	...	...	75.9±1.2	$15.0^{+0.7}_{-0.7}$	$5.24^{+0.86}_{-0.24}$ ^{a}	...	$15.00^{+1.54}_{-0.70}$	$5.24^{+1.09}_{-0.24}$	10 08 44.82	+07 10 20.4	11
142	WISP46-75	1.5040	245±28	...	...	69.4±3.9	$13.6^{+1.3}_{-1.3}$	$4.48^{+3.32}_{-1.27}$ ^{a}	...	$15.85^{+6.99}_{-2.92}$	$5.54^{+5.26}_{-1.97}$	22 37 56.48	-18 42 46.1	11
143	WISP126-90	1.5360	...	...	...	78.1±1.5	...	...	...	...	...	13 41 49.16	+05 03 06.2	11
144	WISP22-111	1.5410	...	...	87±15	68.3±1.9	$7.58^{+0.16}_{-0.16}$	$2.65^{+2.22}_{-0.05}$ ^{a}	...	$7.58^{+3.72}_{-0.16}$	$2.65^{+2.85}_{-0.06}$	08 52 46.09	+03 09 19.4	11
145	WISP22-216	1.5430	...	...	99±8	48.2±1.7	$9.58^{+0.46}_{-0.46}$	$3.35^{+0.72}_{-0.16}$ ^{a}	...	$9.58^{+1.26}_{-0.46}$	$3.35^{+0.92}_{-0.16}$	08 52 46.29	+03 08 45.9	11
146	WISP64-2056	1.6100	...	...	...	58.5±1.9	$7.68^{+0.17}_{-0.17}$	...	...	...	...	14 37 30.20	-01 50 51.4	11
147	WISP81-83	1.6770	...	...	122±11	...	$1.14^{+0.01}_{-0.01}$	...	...	...	...	01 10 06.69	-02 23 06.5	11
148	WISP138-173	2.1580	...	...	286±22	60.5±6.4	$9.43^{+0.78}_{-0.78}$	$1.61^{+1.45}_{-1.45}$ ^{a}	...	$61.10^{+35.83}_{-35.83}$	$21.36^{+24.02}_{-24.02}$	15 45 31.03	+09 33 30.0	11
149	WISP170-106	2.1650	...	...	154±7	55.2±3.2	$6.89^{+0.24}_{-0.24}$	$1.70^{+0.96}_{-0.96}$ ^{a}	...	$17.27^{+6.13}_{-6.13}$	$6.04^{+4.33}_{-4.33}$	00 12 28.18	-10 28 33.6	11
150	WISP64-210	2.1770	...	...	143±14	74.5±4.7	$7.77^{+0.32}_{-0.32}$	$1.84^{+0.93}_{-0.93}$ ^{a}	...	$21.35^{+6.98}_{-6.98}$	$7.47^{+4.73}_{-4.73}$	14 37 28.34	-01 49 54.4	11
151	WISP204-133	2.1910	...	...	226±44	54.9±11.2	$3.61^{+0.36}_{-0.36}$	$1.26^{+0.12}_{-0.12}$ ^{a}	...	$3.61^{+0.36}_{-0.36}$	$1.26^{+0.12}_{-0.12}$	11 19 46.37	+04 10 30.8	11
152	WISP27-95	2.1920	...	...	150±14	109.6±3.0	$12.0^{+0.2}_{-0.2}$	$2.88^{+0.14}_{-0.14}$ ^{a}	...	$31.98^{+8.51}_{-8.51}$	$11.18^{+5.47}_{-5.47}$	11 33 08.67	+03 28 27.0	11
153	WISP147-72	2.1960	...	...	131±16	186.7±7.24	$8.27^{+0.29}_{-0.29}$	...	...	...	...	23 58 22.06	-10 14 48.7	11
154	WISP90-58	2.2120	...	...	71±4	111.9±2.9	$15.4^{+0.4}_{-0.4}$	$4.06^{+1.33}_{-1.33}$ ^{a}	...	$32.12^{+6.96}_{-6.96}$	$11.23^{+4.59}_{-4.59}$	01 00 56.20	+02 25 54.0	11
155	WISP70-253	2.2150	...	...	257±23	51.2±3.2	$3.38^{+0.13}_{-0.13}$	$1.18^{+0.04}_{-0.04}$ ^{a}	...	$3.38^{+0.13}_{-0.13}$	$1.18^{+0.04}_{-0.04}$	04 02 02.50	-05 37 19.5	11
156	WISP175-124	2.2160	...	...	271±18	85.1±4.5	$9.53^{+0.33}_{-0.33}$	...	...	...	...	03 42 19.72	-20 33 17.1	11
157	WISP96-158	2.2340	...	...	238±10	50.7±3.2	$6.09^{+0.25}_{-0.25}$	$1.21^{+1.18}_{-1.18}$ ^{a}	...	$26.50^{+16.05}_{-16.05}$	$9.26^{+11.48}_{-11.48}$	02 09 26.37	-04 43 29.0	11
158	WISP138-160	2.2640	...	...	116±4	56.5±0.8	$13.3^{+0.1}_{-0.1}$	$3.9^{+2.13}_{-2.13}$ ^{a}	...	$21.06^{+6.86}_{-6.86}$	$7.36^{+5.15}_{-5.15}$	15 45 36.29	+09 34 26.7	11
159	WISP56-210	2.3040	...	...	372±13	84.0±23.3	$10.3^{+1.6}_{-1.6}$	$3.60^{+3.06}_{-0.56}$ ^{a}	...	$10.3^{+5.30}_{-1.60}$	$3.60^{+3.92}_{-0.56}$	16 16 50.44	+06 36 38.0	11
160	WISP206-261	2.3150	...	...	210±28	39.4±1.7	$5.57^{+0.17}_{-0.17}$	$1.37^{+0.61}_{-0.61}$ ^{a}	...	$13.96^{+4.04}_{-4.04}$	$4.88^{+2.72}_{-2.72}$	10 34 17.56	-28 30 49.8	11

Continuation on the next page.

Table 1 Continued

Index	Name	z	EW(Hα) (Å)	EW(Hβ) (Å)	EW[OIII] (Å)	σ (km s^{-1})	F($H\alpha$) Observed	F($H\beta$) Observed	F[OIII]λ5007Å Observed	F($H\alpha$) Corrected	F($H\beta$) Corrected	A.R (J2000)	DEC. (J2000)	Reference
121	COSMOS-12807	1.5830	...	...	628±152	38.2±10.0	...	...	5.99±3.61	...	...	10 00 38.29	+02 19 59.88	9,10
161	TKRS7889	0.51241	...	50.4±1.0	178.9±1.3	45.39	...	...	...	...	...	12 36 17.737	62 8 18.9888	12,16
162	TKRS10625	0.51309	...	48.9±2.0	373.0±2.9	52.60	...	...	...	...	...	12 37 27.348	62 13 18.7788	12,16
163	TKRS7887	0.59449	...	63.1±2.5	387.2±2.7	47.86	...	...	...	...	...	12 36 24.9581	62 9 12.5604	12,16
164	TKRS7878	0.84173	...	54.4±4.0	131.4±4.3	42.27	...	...	...	...	...	12 37 19.177	62 15 30.06	12,16
165	TKRS2882	0.87506	...	49.8±3.1	168.0±6.7	40.83	...	...	...	...	...	12 36 58.951	62 19 16.0284	12,16
166	TKRS10350	0.90716	...	50.7±1.9	173.0±2.8	69.02	...	...	...	...	...	12 37 8.688	62 11 28.2588	12,16
167	TKRS7105	0.32930	...	33.9±2.3	255.3±3.2	43.65±1.21	...	...	...	...	...	12 37 15.8201	62 15 59.4216	12,16
168	TKRS2246	0.38741	...	33.2±2.8	141.8±3.4	25.12±1.58	...	...	...	...	...	12 36 52.3459	62 19 9.8004	12,16
169	TKRS2336	0.38990	...	31.9±3.7	61.9±4.0	46.88±1.23	...	...	...	...	...	12 36 5.4941	62 13 30.99	12,16
170	TKRS4648	0.39740	...	31.0±1.4	135.9±1.3	36.48±1.20	...	...	...	...	...	12 36 19.843	62 12 29.3112	12,16
171	TKRS3741	0.43720	...	30.1±1.8	169.4±2.2	25.12±1.58	...	...	...	...	...	12 36 16.638	62 13 10.5492	12,16
172	TKRS5621	0.45652	...	30.9±0.7	97.7±1.3	52.6±1.07	...	...	...	...	...	12 36 58.385	62 15 48.5784	12,16
173	TKRS5634	0.45694	...	25.1±0.9	58.9±1.8	55.46±1.14	...	...	...	...	...	12 36 31.158	62 12 36.2988	12,16
174	TKRS3272	0.45724	...	29.6±1.6	88.4±2.8	25.12±1.58	...	...	...	...	...	12 36 5.0359	62 12 25.6212	12,16
175	TKRS7843	0.50858	...	27.4±1.1	109.1±1.5	35.81±1.09	...	...	...	...	...	12 36 15.293	62 8 8.0484	12,16
176	TKRS3130	0.51604	...	28.2±1.0	184.3±1.5	36.90±1.09	...	...	...	...	...	12 36 55.044	62 18 24.5088	12,16
177	TKRS10183	0.55639	...	25±2.4	56.0±3.1	59.57±1.09	...	...	...	...	...	12 37 13.027	62 12 9.2016	12,16
178	TKRS4375	0.66031	...	28.6±1.2	100.6±3.1	52.84±1.07	...	...	...	...	...	12 37 0.5081	62 17 33.3996	12,16
179	TKRS1953	0.68536	...	38.4±2.7	197.3±16.9	40.36±1.11	...	...	...	...	...	12 36 13.704	62 14 52.9908	12,16
180	TKRS4389	0.69442	...	28.4±0.8	102.0±0.8	54.08±1.08	...	...	...	...	...	12 36 19.813	62 12 51.7896	12,16
181	TKRS8126	0.69780	...	24.2±1.9	95.1±3.3	66.37±1.09	...	...	...	...	...	12 37 20.603	62 15 19.7712	12,16
182	TKRS5167	0.74411	...	38.9±5.2	108.4±3.7	36.48±1.07	...	...	...	...	...	12 37 2.479	62 16 45.0192	12,16
183	TKRS1468	0.79803	...	42.3±2.7	142.2±4.0	55.59±1.07	...	...	...	...	...	12 36 18.45	62 16 1.5312	12,16
184	TKRS11643	0.82058	...	28.2±1.0	130.1±0.9	52.48±1.10	...	...	...	...	...	12 37 14.149	62 10 44.3316	12,16
185	TKRS4332	0.83567	...	30.5±2.9	113.5±2.6	36.14±1.16	...	...	...	...	...	12 36 50.6741	62 16 28.74	12,16
186	TKRS3021	0.83571	...	33.0±2.9	104.0±1.9	93.54±1.12	...	...	...	...	...	12 37 5.5411	62 19 50.6784	12,16
187	TKRS6786	0.83977	...	25.2±1.6	74.1±1.9	88.10±1.07	...	...	...	...	...	12 37 6.3	62 15 18	12,16
188	TKRS7075	0.83987	...	29.7±2.6	133.4±2.9	43.85±1.09	...	...	...	...	...	12 37 14.0441	62 15 49.2012	12,16
189	TKRS9211	0.84092	...	31.3±3.1	91.0±4.5	73.11±1.09	...	...	...	...	...	12 37 27.599	62 14 58.8588	12,16
190	TKRS6596	0.85182	...	23.0±2.9	28.1±2.5	82.04±1.07	...	...	...	...	...	12 37 15.431	62 16 32.5308	12,16
191	PEARS123301	0.6020	...	61	334	...	$780.53^{+1684.16}_{-1684.16}$ [c]	$192.02^{+278.22}_{-278.22}$ [c]	23739.5±562.4 [b]	$1956.53^{+4608.89}_{-4608.89}$	$684.10^{+451.90}_{-451.90}$	03 32 18.56	-27 42 29.51	14
192	PEARS119341	0.6960	...	352	1605	...	$597.44^{+277.88}_{-183.32}$ [c]	$201.68^{+68.99}_{-52.82}$ [c]	1219.1±69.2 [b]	$654.94^{+327.87}_{-210.28}$	$229.00^{+52.20}_{-52.20}$	03 32 16.80	-27 42 59.72	14
193	PEARS122206	0.9980	...	525	729	...	$1920.93^{+1214.89}_{-1012.47}$ [c]	$648.45^{+355.57}_{-325.68}$ [c]	2419.1±474.8 [b]	$2105.82^{+1387.70}_{-1127.63}$	$736.30^{+357.40}_{-357.40}$	03 32 20.57	-27 42 40.82	14
194	PEARS-364	0.6420	...	38	248	...	$1313.58^{+1602.54}_{-329.37}$ [c]	$443.43^{+344.12}_{-85.65}$ [c]	3086.1±95.9	$1440.01^{+1928.14}_{-385.87}$	$503.50^{+72.40}_{-72.40}$	03 32 16.64	-27 42 32.72	14
195	PEARS-103	1.6820	...	45	193	...	$234.18^{+277.14}_{-209.29}$ [c]	$76.32^{+73.80}_{-63.69}$ [c]	528.3±103.3	$281.42^{+351.62}_{-257.08}$	$98.40^{+78.10}_{-78.10}$	03 32 15.20	-27 43 38.22	14
196	PEARS-242	2.0700	...	25	143	...	$213.99^{+285.19}_{-285.19}$ [c]	$59.89^{+58.29}_{-58.29}$ [c]	794.6±111.9	$382.95^{+550.58}_{-550.58}$	$133.90^{+85.70}_{-85.70}$	03 32 19.71	-27 42 49.52	14
197	GSD1	1.6-1.8	...	...	459±40	...	...	...	...	...	...	03 32 40.10	-27 51 32.17	17
198	GSD2	1.6-1.8	...	...	569±67	...	...	...	...	...	...	03 32 19.28	-27 51 02.06	17
199	GSD3	1.6-1.8	...	...	507±75	...	...	...	...	...	...	03 32 11.04	-27 50 14.36	17
200	GSD4	1.6-1.8	...	...	769±143	...	...	...	...	...	...	03 32 25.22	-27 49 11.91	17

Continuation on the next page.

Table 1 Continued

Index	Name	z	EW(Hα) (Å)	EW(Hβ) (Å)	EW[OIII] (Å)	σ (km s^{-1})	F($H\alpha$) Observed	F($H\beta$) Observed	F[OIII]λ5007Å Observed	F($H\alpha$) Corrected	F($H\beta$) Corrected	A.R (J2000)	DEC. (J2000)	Reference
201	GSD5	1.6-1.8	...	...	566±74	...	...	...	...	...	...	03 32 16.20	-27 46 24.94	17
202	GSD6	1.6-1.8	...	...	700±53	...	...	...	...	...	...	03 32 23.40	-27 45 50.11	17
203	GSD7	1.6-1.8	...	...	535±99	...	...	...	...	...	...	03 32 29.31	-27 45 34.35	17
204	GSD8	1.6-1.8	...	...	693±45	...	...	...	...	...	...	03 32 41.26	-27 45 32.92	17
205	GSD9	1.6-1.8	...	...	468±32	...	...	...	...	...	...	03 32 18.90	-27 45 01.04	17
206	GSD10	1.6-1.8	...	...	759±134	...	...	...	...	...	...	03 32 15.28	-27 44 45.07	17
207	GSD11	1.6-1.8	...	...	534±76	...	...	...	...	...	...	03 32 01.80	-27 44 30.72	17
208	GSD12	1.6-1.8	...	...	641±139	...	...	...	...	...	...	03 32 27.51	-27 43 19.12	17
209	GSD13	1.6-1.8	...	...	490±29	...	...	...	...	...	...	03 32 24.36	-27 43 15.18	17
210	GSD14	1.6-1.8	...	...	501±65	...	...	...	...	...	...	03 32 13.42	-27 43 07.69	17
211	GSD15	1.6-1.8	...	...	820±288	...	...	...	...	...	...	03 32 35.89	-27 42 37.03	17
212	GSD16	1.6-1.8	...	...	582±80	...	...	...	...	...	...	03 32 35.43	-27 42 25.52	17
213	GSD17	1.6-1.8	...	...	465±43	...	...	...	...	...	...	03 32 15.41	-27 42 23.48	17
214	GSD18	1.6-1.8	...	...	861±66	...	...	...	...	...	...	03 32 17.11	-27 42 20.89	17
215	GSD19	1.6-1.8	...	...	1002±245	...	...	...	...	...	...	03 32 43.67	-27 42 18.14	17
216	GSD20	1.6-1.8	...	...	496±82	...	...	...	...	...	...	03 32 33.80	-27 41 32.60	17
217	GSD21	1.6-1.8	...	...	935±139	...	...	...	...	...	...	03 32 24.22	-27 40 36.13	17
218	GSD22	1.6-1.8	...	...	870±198	...	...	...	...	...	...	03 32 28.43	-27 49 11.71	17
219	GSD23	1.6-1.8	...	...	1512±338	...	...	...	...	...	...	03 32 18.62	-27 48 46.06	17
220	GSD24	1.6-1.8	...	...	698±318	...	...	...	...	...	...	03 32 31.91	-27 44 24.37	17
221	GSD25	1.6-1.8	...	...	562±164	...	...	...	...	...	...	03 32 20.25	-27 43 40.51	17
222	GSD26	1.6-1.8	...	...	650±106	...	...	...	...	...	...	03 32 33.96	-27 43 29.57	17
223	GSD27	1.6-1.8	...	...	954±262	...	...	...	...	...	...	03 32 27.02	-27 42 25.52	17
224	GSD28	1.6-1.8	...	...	1009±293	...	...	...	...	...	...	03 32 11.07	-27 42 20.17	17
225	GSD29	1.6-1.8	...	...	1314±557	...	...	...	...	...	...	03 32 33.59	-27 40 30.50	17
226	UDS1	1.6-1.8	...	...	576±90	...	...	...	...	...	...	02 17 06.07	-05 16 28.18	17
227	UDS2	1.6-1.8	...	...	1081±147	...	...	...	...	...	...	02 17 45.78	-05 15 45.24	17
228	UDS3	1.6-1.8	...	...	507±95	...	...	...	...	...	...	02 17 55.72	-05 15 41.04	17
229	UDS4	1.6-1.8	...	...	614±83	...	...	...	...	...	...	02 17 04.48	-05 15 36.23	17
230	UDS5	1.6-1.8	...	...	701±95	...	...	...	...	...	...	02 17 42.36	-05 15 20.77	17
231	UDS6	1.6-1.8	...	...	731±86	...	...	...	...	...	...	02 17 42.86	-05 15 19.14	17
232	UDS7	1.6-1.8	...	...	656±43	...	...	...	...	...	...	02 17 18.16	-05 15 06.27	17
233	UDS8	1.6-1.8	...	...	728±153	...	...	...	...	...	...	02 17 15.36	-05 15 03.77	17
234	UDS9	1.6-1.8	...	...	478±64	...	...	...	...	...	...	02 17 31.82	-05 14 40.63	17
235	UDS10	1.6-1.8	...	...	541±64	...	...	...	...	...	...	02 17 03.25	-05 14 21.96	17
236	UDS11	1.6-1.8	...	...	735±94	...	...	...	...	...	...	02 17 14.71	-05 14 20.24	17
237	UDS12	1.6-1.8	...	...	713±42	...	...	...	...	...	...	02 17 53.73	-05 14 03.23	17
238	UDS13	1.6-1.8	...	...	716±68	...	...	...	...	...	...	02 17 16.35	-05 13 56.28	17
239	UDS14	1.6-1.8	...	...	602±96	...	...	...	...	...	...	02 17 55.58	-05 13 21.00	17
240	UDS15	1.6-1.8	...	...	843±111	...	...	...	...	...	...	02 17 29.08	-05 12 53.29	17

Continuation on the next page.

Table 1 Continued

Index	Name	z	EW(Hα) (Å)	EW(Hβ) (Å)	EW[OIII] (Å)	σ (km s^{-1})	F($H\alpha$) Observed	F($H\beta$) Observed	F[OIII]λ5007Å Observed	F($H\alpha$) Corrected	F($H\beta$) Corrected	A.R (J2000)	DEC. (J2000)	Reference
241	UDS6	1.6-1.8	...	...	662±87	...	...	...	...	...	...	02 17 55.90	-05 12 51.07	17
242	UDS17	1.6-1.8	...	...	469±63	...	...	...	...	...	...	02 16 59.40	-05 12 19.19	17
243	UDS18	1.6-1.8	...	...	739±136	...	...	...	...	...	...	02 17 15.71	-05 12 03.25	17
244	UDS19	1.6-1.8	...	...	543±106	...	...	...	...	...	...	02 17 11.73	-05 11 30.48	17
245	UDS20	1.6-1.8	...	...	648±55	...	...	...	...	...	...	02 16 55.70	-05 11 25.40	17
246	UDS21	1.6-1.8	...	...	609±66	...	...	...	...	...	...	02 17 14.14	-05 11 24.32	17
247	UDS22	1.6-1.8	...	...	1070±307	...	...	...	...	...	...	02 17 40.02	-05 10 49.59	17
248	UDS123	1.6-1.8	...	...	591±74	...	...	...	...	...	...	02 17 32.88	-05 10 38.06	17
249	UDS24	1.6-1.8	...	...	779±140	...	...	...	...	...	...	02 17 00.68	-05 10 34.90	17
250	UDS25	1.6-1.8	...	...	507±39	...	...	...	...	...	...	02 17 36.51	-05 10 31.27	17
251	UDS26	1.6-1.8	...	...	552±59	...	...	...	...	...	...	02 17 50.21	-05 10 28.01	17
252	UDS27	1.6-1.8	...	...	576±139	...	...	...	...	...	...	02 17 08.21	-05 09 50.70	17
253	UDS28	1.6-1.8	...	...	519±100	...	...	...	...	...	...	02 18 00.06	-05 09 20.14	17
254	UDS29	1.6-1.8	...	...	1003±150	...	...	...	...	...	...	02 17 03.18	-05 09 07.83	17
255	UDS30	1.6-1.8	...	...	533±103	...	...	...	...	...	...	02 17 54.66	-05 08 51.08	17
256	UDS31	1.6-1.8	...	...	546±88	...	...	...	...	...	...	02 17 11.12	-05 08 39.90	17
257	UDS32	1.6-1.8	...	...	721±138	...	...	...	...	...	...	02 17 40.62	-05 08 34.41	17
258	UDS33	1.6-1.8	...	...	553±85	...	...	...	...	...	...	02 16 59.23	-05 08 20.83	17
259	UDS34	1.6-1.8	...	...	586±50	...	...	...	...	...	...	02 17 29.26	-05 08 14.18	17
260	UDS35	1.6-1.8	...	...	1125±315	...	...	...	...	...	...	02 17 15.53	-05 08 01.23	17
261	UDS36	1.6-1.8	...	...	658±76	...	...	...	...	...	...	02 17 02.82	-05 08 04.82	17
262	UDS37	1.6-1.8	...	...	832±249	...	...	...	...	...	...	02 17 31.34	-05 16 05.18	17
263	UDS38	1.6-1.8	...	...	912±208	...	...	...	...	...	...	02 17 45.95	-05 12 57.47	17
264	UDS39	1.6-1.8	...	...	594±145	...	...	...	...	...	...	02 17 20.37	-05 10 37.79	17
265	UDS40	1.6-1.8	...	...	677±157	...	...	...	...	...	...	02 17 45.14	-05 09 36.25	17
266	GMASS-167	2.5730	353^{+88}_{-85}	...	...	68^{+14}_{-17}	$6.6^{+1.1}_{-0.9}$	$1.94^{+0.73}_{-0.70}$ [a]	...	$10.38^{+2.75}_{-2.56}$	$3.63^{+1.66}_{-1.63}$	...	...	18
267	GMASS-2562	2.5400	161^{+52}_{-46}	...	...	87^{+27}_{-33}	$3.0^{+0.7}_{-0.6}$	$0.74^{+0.41}_{-0.40}$ [a]	...	$7.43^{+2.94}_{-2.80}$	$2.60^{+1.76}_{-1.73}$	...	...	18
268	Q1623-BX528	2.2683	132±26	...	...	141±8	$11.4^{+0.4}_{-0.4}$	$3.35^{+1.13}_{-1.13}$ [a]	...	$17.94^{+3.75}_{-3.75}$	$6.27^{+2.69}_{-2.69}$	16 25 56.44	+26 50 15.44	18
269	Q1623-BX663	2.4332	309±62	...	...	172±22	$16.7^{+0.9}_{-0.9}$	$4.63^{+1.82}_{-1.82}$ [a]	...	$30.63^{+7.59}_{-7.59}$	$10.71^{+5.32}_{-5.32}$	16 25 04.58	+26 48 00.20	18
270	SSA22a-MD41	2.1704	512±170	...	...	118^{+6}_{-7}	$14.4^{+0.6}_{-0.6}$	$3.77^{+1.68}_{-1.68}$ [a]	...	$30.69^{+8.65}_{-8.65}$	$10.73^{+6.04}_{-6.04}$	22 17 39.97	+00 17 11.04	18
271	Q2343-BX610	2.2103	268^{+53}_{-52}	...	...	176^{+10}_{-11}	$30.5^{+1.3}_{-1.1}$	$8.46^{+3.31}_{-3.30}$ [a]	...	$55.94^{+13.74}_{-13.68}$	$19.56^{+9.69}_{-9.68}$	23 46 09.43	+12 49 19.21	18
272	K20-ID5	2.2243	641±128	...	...	281^{+29}_{-30}	$26.9^{+1.5}_{-1.5}$	$5.27^{+4.06}_{-4.06}$ [a]	...	$122.16^{+60.72}_{-60.72}$	$42.71^{+41.37}_{-41.37}$	...	...	18
273	K20-ID6	2.2345	150±31	...	...	91^{+14}_{-7}	$5.4^{+0.4}_{-0.4}$	$1.41^{+0.64}_{-0.64}$ [a]	...	$11.51^{+3.32}_{-3.32}$	$4.02^{+2.28}_{-2.28}$	...	...	18
274	K20-ID7	2.2241	313±61	...	...	173^{+8}_{-9}	$19.7^{+0.7}_{-0.7}$	$5.16^{+2.29}_{-2.29}$ [a]	...	$41.98^{+11.80}_{-11.80}$	$14.68^{+8.25}_{-8.25}$	...	...	18
275	K20-ID8	2.2235	179±36	...	...	132^{+10}_{-11}	$10.7^{+0.6}_{-0.6}$	$2.97^{+1.16}_{-1.16}$ [a]	...	$19.62^{+4.87}_{-4.87}$	$6.86^{+3.41}_{-3.41}$	...	...	18
276	K20-ID9	2.0343	420±88	...	...	167^{+15}_{-13}	$9.4^{+0.6}_{-0.7}$	$2.19^{+1.25}_{-1.26}$ [a]	...	$27.13^{+9.98}_{-10.03}$	$9.49^{+6.83}_{-6.84}$	...	...	18
277	Deep3a-4751	2.2656	147^{+34}_{-33}	...	...	86^{+13}_{-10}	$6.8^{+0.6}_{-0.5}$	$1.78^{+0.80}_{-0.80}$ [a]	...	$14.49^{+4.24}_{-4.18}$	$5.07^{+2.88}_{-2.87}$	...	...	18
278	Deep3a-6004	2.3867	354±71	...	...	129±7	$19.5^{+0.8}_{-0.7}$	$4.05^{+2.85}_{-2.85}$ [a]	...	$75.98^{+34.35}_{-34.32}$	$26.57^{+23.53}_{-23.52}$	...	...	18
279	Deep3a-15504	2.3826	274±55	...	...	148±9	$24.9^{+0.9}_{-0.8}$	$6.52^{+2.90}_{-2.90}$ [a]	...	$53.06^{+14.92}_{-14.90}$	$18.55^{+10.43}_{-10.43}$	...	...	18
280	GMASS-1084	1.5521	223^{+48}_{-47}	...	...	114^{+16}_{-11}	$2.1^{+0.2}_{-0.2}$	$0.31^{+0.34}_{-0.34}$ [a]	...	$20.32^{+14.79}_{-14.79}$	$7.11^{+9.99}_{-9.99}$	...	...	18

Continuation on the next page.

Table 1 Continued

Index	Name	z	EW(Hα) (Å)	EW(Hβ) (Å)	EW[OIII] (Å)	σ (km s^{-1})	F($H\alpha$) Observed	F($H\beta$) Observed	F[OIII]λ5007Å Observed	F($H\alpha$) Corrected	F($H\beta$) Corrected	A.R (J2000)	DEC. (J2000)	Reference
281	GMASS-1146	1.5385	324^{+73}_{-70}	...	...	133^{+23}_{-22}	$5.0^{+0.6}_{-0.4}$	$0.98^{+0.76}_{-0.76}$ [a]	...	$22.71^{+11.54}_{-11.36}$	$7.94^{+7.74}_{-7.70}$	...	...	18
282	GMASS-2113W	1.6120	118^{+29}_{-28}	...	...	217^{+208}_{-65}	$1.7^{+0.2}_{-0.2}$	$0.30^{+0.27}_{-0.27}$ [a]	...	$10.42^{+6.21}_{-6.21}$	$3.64^{+4.18}_{-4.18}$	03 32 22.00	-27 42 43.50	18
283	GMASS-2252	2.4085	217^{+47}_{-46}	...	...	141±25	$7.1^{+0.6}_{-0.5}$	$1.86^{+0.84}_{-0.83}$ [a]	...	$15.13^{+4.41}_{-4.35}$	$5.29^{+3.00}_{-2.99}$	...	...	18
284	GMASS-2303	2.4507	220^{+48}_{-47}	...	...	109±8	$6.6^{+0.4}_{-0.4}$	$2.05^{+0.62}_{-0.62}$ [a]	...	$8.94^{+1.68}_{-1.68}$	$3.12^{+1.20}_{-1.20}$	...	...	18
285	GMASS-2363	2.4518	171^{+44}_{-43}	...	...	135^{+61}_{-49}	$2.9^{+0.5}_{-0.4}$	$0.72^{+0.38}_{-0.38}$ [a]	...	$7.18^{+2.62}_{-2.51}$	$2.51^{+1.67}_{-1.65}$	...	...	18
286	GMASS-2438	1.6135	245±50	...	...	170^{+16}_{-18}	$7.6^{+0.3}_{-0.3}$	$1.67^{+1.06}_{-1.06}$ [a]	...	$25.48^{+10.37}_{-10.37}$	$8.91^{+7.12}_{-7.12}$	03 32 26.41	-27 42 28.40	18
287	GMASS-2540	1.6146	127^{+29}_{-28}	...	...	80^{+12}_{-9}	$10.5^{+1.1}_{-0.8}$	$3.09^{+1.08}_{-1.06}$ [a]	...	$16.52^{+3.82}_{-3.63}$	$5.78^{+2.54}_{-2.51}$	03 32 30.33	-27 42 40.30	18
288	GMASS-2550	1.6030	115^{+31}_{-32}	...	...	$64^{+132.5}_{-50}$	$4.1^{+0.7}_{-0.8}$	$1.14^{+0.48}_{-0.49}$ [a]	...	$7.52^{+2.23}_{-2.34}$	$2.63^{+1.37}_{-1.40}$	03 32 30.08	-27 42 12.20	18
289	zCOSMOS-772759	2.1733	590^{+133}_{-126}	...	...	125^{+18}_{-15}	$15.4^{+2.0}_{-1.4}$	$3.59^{+2.09}_{-2.06}$ [a]	...	$44.44^{+17.10}_{-16.60}$	$15.54^{+11.32}_{-11.23}$	10 00 45.10	+02 07 05.20	18
290	zCOSMOS-782941	2.1814	444±88	...	...	171^{+12}_{-8}	$22.5^{+0.9}_{-0.8}$	$5.56^{+2.83}_{-2.83}$ [a]	...	$55.71^{+18.04}_{-18.01}$	$19.48^{+12.51}_{-12.51}$	09 59 56.00	+02 06 51.30	18
291	GDDSSA12-6339	2.2969	849^{+276}_{-275}	...	...	93^{+7}_{-6}	$12.2^{+0.7}_{-0.6}$	$2.39^{+1.84}_{-1.84}$ [a]	...	$55.40^{+27.55}_{-27.50}$	$19.37^{+18.76}_{-18.76}$	12 05 32.70	-07 23 38.00	18
292	zCOSMOS-400528	2.3876	144^{+14}_{-19}	...	...	221^{+72}_{-62}	$15.6^{+1.5}_{-2.0}$	$3.93^{+1.36}_{-1.39}$ [a]	...	$36.78^{+9.03}_{-9.55}$	$12.86^{+5.42}_{-5.53}$	09 59 47.60	+01 44 19.00	19
293	zCOSMOS-400569	2.2405	157^{+15}_{-17}	...	...	207^{+34}_{-39}	$16.1^{+1.5}_{-1.8}$	$3.65^{+1.56}_{-1.57}$ [a]	...	$50.01^{+15.12}_{-15.44}$	$17.48^{+9.13}_{-9.19}$	10 01 08.70	+01 44 28.30	19
294	zCOSMOS-403741	1.4455	186^{+8}_{-7}	...	...	86^{+7}_{-4}	$12.0^{+0.1}_{-0.1}$	$2.56^{+1.19}_{-1.19}$ [a]	...	$43.44^{+14.03}_{-14.03}$	$15.19^{+8.70}_{-8.70}$	10 00 18.40	+01 55 08.10	19
295	zCOSMOS-404221	2.2201	231^{+25}_{-29}	...	...	96^{+37}_{-19}	$8.66^{+0.60}_{-0.85}$	$2.6^{+0.57}_{-0.60}$ [a]	...	$12.90^{+1.93}_{-2.13}$	$4.51^{+1.22}_{-1.26}$	10 01 41.30	+01 56 42.80	19
296	zCOSMOS-404987	2.1239	332^{+63}_{-94}	...	...	131^{+43}_{-61}	$7.04^{+1.02}_{-1.80}$	$1.88^{+0.60}_{-0.72}$ [a]	...	$14.24^{+3.43}_{-4.56}$	$4.98^{+1.91}_{-2.18}$	10 00 40.40	+01 59 27.70	19
297	zCOSMOS-405081	2.2344	248^{+50}_{-58}	...	...	64^{+24}_{-21}	$5.01^{+0.71}_{-0.93}$	$1.44^{+0.44}_{-0.48}$ [a]	...	$8.43^{+1.90}_{-2.15}$	$2.95^{+1.10}_{-1.16}$	10 00 22.70	+01 59 46.20	19
298	zCOSMOS-405501	2.1543	300^{+52}_{-46}	...	...	124^{+32}_{-18}	$11.2^{+1.6}_{-1.3}$	$3.13^{+0.91}_{-0.87}$ [a]	...	$20.04^{+4.41}_{-4.08}$	$7.01^{+2.43}_{-2.36}$	09 59 53.70	+02 01 08.80	19
299	zCOSMOS-406690	2.1949	391^{+13}_{-12}	...	...	138±4	$61.5^{+1.4}_{-1.1}$	$16.62^{+4.63}_{-4.62}$ [a]	...	$120.66^{+22.65}_{-22.58}$	$42.19^{+14.62}_{-14.61}$	09 58 59.10	+02 05 04.20	19
300	zCOSMOS-407928	2.4309	371^{+83}_{-85}	...	...	178^{+185}_{-86}	$7.94^{+1.52}_{-1.57}$	$1.95^{+0.82}_{-0.83}$ [a]	...	$19.90^{+6.31}_{-6.39}$	$6.96^{+3.52}_{-3.54}$	09 59 53.40	+02 08 41.50	19
301	zCOSMOS-410041	2.4539	988^{+268}_{-255}	...	...	154^{+80}_{-60}	$13.4^{+2.9}_{-2.7}$	$3.79^{+1.24}_{-1.20}$ [a]	...	$23.26^{+6.28}_{-6.00}$	$8.13^{+3.05}_{-2.98}$	10 00 44.30	+02 15 58.40	19
302	zCOSMOS-410542	1.4049	187^{+14}_{-20}	...	...	286^{+39}_{-64}	$18.4^{+1.4}_{-2.0}$	$3.89^{+1.87}_{-1.89}$ [a]	...	$68.68^{+23.25}_{-23.86}$	$24.02^{+14.16}_{-14.28}$	09 59 54.70	+02 17 48.30	19
303	zCOSMOS-411737	2.4443	391^{+66}_{-60}	...	...	106^{+30}_{-15}	$9.63^{+0.95}_{-0.69}$	$2.76^{+0.71}_{-0.68}$ [a]	...	$16.21^{+2.98}_{-2.77}$	$5.67^{+1.77}_{-1.73}$	10 00 32.40	+02 21 20.90	19
304	zCOSMOS-412369	2.0283	271^{+17}_{-16}	...	...	133±9	$21.7^{+1.0}_{-1.0}$	$5.09^{+1.99}_{-1.99}$ [a]	...	$61.48^{+16.65}_{-16.65}$	$21.50^{+10.33}_{-10.33}$	10 01 46.90	+02 23 24.60	19
305	zCOSMOS-413507	2.4794	208^{+82}_{-39}	...	...	63^{+124}_{-35}	$4.73^{+1.81}_{-0.75}$	$1.15^{+0.60}_{-0.45}$ [a]	...	$12.22^{+5.56}_{-3.58}$	$4.27^{+2.51}_{-2.02}$	10 00 24.20	+02 27 41.30	19
306	zCOSMOS-413597	2.4498	310^{+61}_{-59}	...	...	73^{+22}_{-48}	$7.07^{+1.22}_{-1.16}$	$1.72^{+0.68}_{-0.68}$ [a]	...	$18.27^{+5.49}_{-5.41}$	$6.39^{+3.04}_{-3.03}$	09 59 36.40	+02 27 59.10	19
307	zCOSMOS-415087	2.2986	102^{+41}_{-32}	...	...	96^{+29}_{-42}	$2.44^{+0.93}_{-0.69}$	$0.64^{+3.32}_{-3.32}$ [a]	...	$5.25^{+2.31}_{-1.88}$	$1.83^{+1.04}_{-0.93}$	10 00 32.40	+02 33 40.60	19
308	zCOSMOS-415876	2.4362	118^{+24}_{-19}	...	...	116^{+28}_{-23}	$3.52^{+0.62}_{-0.44}$	$0.87^{+0.34}_{-0.32}$ [a]	...	$8.82^{+2.62}_{-2.38}$	$3.08^{+1.44}_{-1.39}$	10 00 09.40	+02 36 58.30	19
309	zCOSMOS-700882	0.4640	...	98	475	...	...	...	...	...	...	10 01 23.88	+02 16 32.94	20
310	zCOSMOS-701051	0.3450	400	78	252	...	...	...	...	...	...	09 59 25.67	+02 14 45.54	20
311	zCOSMOS-701741	0.5040	...	228	423	...	...	...	...	...	...	10 01 34.56	+02 34 44.05	20
312	zCOSMOS-800984	0.5950	...	280	1506	...	...	...	...	...	...	10 01 08.75	+01 37 26.12	20
313	zCOSMOS-801094	0.5460	...	89	296	...	...	...	...	...	...	10 00 58.08	+01 36 36.51	20
314	zCOSMOS-802275	0.6350	...	104	317	...	...	...	...	...	...	09 58 50.83	+01 36 58.35	20
315	zCOSMOS-803226	0.5700	...	75	387	...	...	...	...	...	...	10 02 49.30	+01 43 01.09	20
316	zCOSMOS-803892	0.4390	300	48	237	...	...	...	...	...	...	10 02 06.43	+01 47 14.44	20
317	zCOSMOS-804130	0.4290	303	36	164	...	...	...	...	...	...	10 01 48.58	+01 37 56.51	20
318	zCOSMOS-804791	0.6030	...	78	265	...	...	...	...	...	...	10 01 08.77	+01 38 00.02	20
319	zCOSMOS-805200	0.4720	815	153	820	...	...	...	...	...	...	10 00 49.35	+01 46 56.38	20
320	zCOSMOS-806881	0.7510	...	163	520	...	...	...	...	...	...	09 59 20.15	+01 41 03.54	20

Continuation on the next page.

Table 1 Continued

Index	Name	z	EW(Hα) (Å)	EW(Hβ) (Å)	EW[OIII] (Å)	σ (km s^{-1})	F($H\alpha$) Observed	F($H\beta$) Observed	F[OIII]λ5007Å Observed	F($H\alpha$) Corrected	F($H\beta$) Corrected	A.R (J2000)	DEC. (J2000)	Reference
321	zCOSMOS-806958	0.5310	...	85	409	...	...	...	...	...	...	09 59 15.89	+01 44 30.38	20
322	zCOSMOS-807965	0.8030	...	198	840	...	...	...	...	...	...	09 58 22.05	+01 45 23.66	20
323	zCOSMOS-807990	0.5690	...	53	324	...	...	...	...	...	...	09 58 20.20	+01 39 36.77	20
324	zCOSMOS-809215	0.1240	1270	...	1236	...	...	...	...	...	...	10 02 54.02	+01 47 54.15	20
325	zCOSMOS-809399	0.4460	272	57	261	...	...	...	...	...	...	10 02 42.07	+01 56 49.18	20
326	zCOSMOS-809463	0.6450	...	90	406	...	...	...	...	...	...	10 02 38.44	+01 51 48.54	20
327	zCOSMOS-809944	0.1230	332	...	209	...	...	...	...	...	...	10 02 15.08	+01 51 49.55	20
328	zCOSMOS-810153	0.5400	...	110	527	...	...	...	...	...	...	10 02 04.13	+01 52 34.12	20
329	zCOSMOS-810220	0.7000	...	75	300	...	...	...	...	...	...	10 02 00.13	+01 48 40.68	20
330	zCOSMOS-810304	0.3740	219	37	168	...	...	...	...	...	...	10 01 55.81	+01 55 45.64	20
331	zCOSMOS-810646	0.1750	163	39	125	...	...	...	...	...	...	10 01 40.30	+01 52 45.71	20
332	zCOSMOS-811012	0.8390	...	98	558	...	...	...	...	...	...	10 01 19.44	+01 52 47.07	20
333	zCOSMOS-811024	0.8110	...	133	315	...	...	...	...	...	...	10 01 18.88	+01 49 36.67	20
334	zCOSMOS-811075	0.7240	...	128	292	...	...	...	...	...	...	10 01 16.23	+01 55 21.08	20
335	zCOSMOS-811415	0.6210	...	85	402	...	...	...	...	...	...	10 00 58.10	+01 49 35.82	20
336	zCOSMOS-811842	0.6710	...	54	203	...	...	...	...	...	...	10 00 36.90	+01 50 58.86	20
337	zCOSMOS-812047	0.2650	708	122	637	...	...	...	...	...	...	10 00 27.76	+01 57 04.05	20
338	zCOSMOS-812087	0.3220	292	50	184	...	...	...	...	...	...	10 00 25.36	+01 54 18.72	20
339	zCOSMOS-812195	0.4380	146	42	175	...	...	...	...	...	...	10 00 19.16	+01 56 14.34	20
340	zCOSMOS-812207	0.1680	306	85	360	...	...	...	...	...	...	10 00 18.56	+01 55 47.75	20
341	zCOSMOS-812599	0.2200	166	35	197	...	...	...	...	...	...	09 59 56.99	+01 53 12.37	20
342	zCOSMOS-812879	0.2510	435	120	595	...	...	...	...	...	...	09 59 40.28	+01 51 21.61	20
343	zCOSMOS-812971	0.1330	204	...	204	...	...	...	...	...	...	09 59 35.47	+01 56 06.24	20
344	zCOSMOS-813334	0.4190	420	80	380	...	...	...	...	...	...	09 59 14.38	+01 52 50.82	20
345	zCOSMOS-813400	0.4370	154	46	162	...	...	...	...	...	...	09 59 10.95	+01 56 36.76	20
346	zCOSMOS-813444	0.1260	550	...	401	...	...	...	...	...	...	09 59 08.52	+01 49 14.92	20
347	zCOSMOS-813723	0.3540	248	64	243	...	...	...	...	...	...	09 58 53.35	+01 48 10.95	20
348	zCOSMOS-813894	0.3620	508	86	424	...	...	...	...	...	...	09 58 44.53	+01 48 46.19	20
349	zCOSMOS-814092	0.4030	821	225	1396	...	...	...	...	...	...	09 58 33.03	+01 55 59.36	20
350	zCOSMOS-814148	0.2610	213	39	198	...	...	...	...	...	...	09 58 29.88	+01 56 59.92	20
351	zCOSMOS-814386	0.1850	246	47	210	...	...	...	...	...	...	09 58 16.87	+01 55 44.37	20
352	zCOSMOS-815797	0.6570	...	71	359	...	...	...	...	...	...	10 02 35.77	+02 03 32.32	20
353	zCOSMOS-815800	0.8400	...	333	793	...	...	...	...	...	...	10 02 35.56	+02 01 24.87	20
354	zCOSMOS-815804	0.5740	...	106	260	...	...	...	...	...	...	10 02 35.36	+02 04 15.11	20
355	zCOSMOS-816839	0.3000	150	67	277	...	...	...	...	...	...	10 01 46.25	+02 06 43.20	20
356	zCOSMOS-817226	0.5630	...	105	520	...	...	...	...	...	...	10 01 31.56	+01 59 53.25	20
357	zCOSMOS-817306	0.3730	124	47	184	...	...	...	...	...	...	10 01 27.98	+02 02 09.76	20
358	zCOSMOS-817804	0.9080	...	170	422	...	...	...	...	...	...	10 01 03.52	+02 03 00.96	20
359	zCOSMOS-817820	0.6380	...	47	150	...	...	...	...	...	...	10 01 02.71	+02 01 14.72	20
360	zCOSMOS-819298	0.1860	450	70	335	...	...	...	...	...	...	09 59 43.34	+02 05 02.24	20

Continuation on the next page.

Table 1 Continued

Index	Name	z	EW(Hα) (Å)	EW(Hβ) (Å)	EW[OIII] (Å)	σ (km s^{-1})	F($H\alpha$) Observed	F($H\beta$) Observed	F[OIII]λ5007Å Observed	F($H\alpha$) Corrected	F($H\beta$) Corrected	A.R (J2000)	DEC. (J2000)	Reference
361	zCOSMOS-819574	0.7660	...	118	720	...	...	...	...	...	...	09 59 29.02	+02 00 04.66	20
362	zCOSMOS-820061	0.6940	...	111	380	...	...	...	...	...	...	09 58 56.76	+01 58 08.84	20
363	zCOSMOS-820087	0.6470	...	84	248	...	...	...	...	...	...	09 58 55.40	+02 00 57.04	20
364	zCOSMOS-820163	0.7500	...	85	289	...	...	...	...	...	...	09 58 50.28	+02 06 00.68	20
365	zCOSMOS-820424	0.3410	206	42	190	...	...	...	...	...	...	09 58 34.65	+02 01 33.35	20
366	zCOSMOS-820575	0.5010	...	185	1180	...	...	...	...	...	...	09 58 26.26	+02 03 27.21	20
367	zCOSMOS-820600	0.6470	...	70	370	...	...	...	...	...	...	09 58 24.57	+02 00 26.49	20
368	zCOSMOS-821098	0.2090	191	38	129	...	...	...	...	...	...	09 57 57.85	+02 02 04.58	20
369	zCOSMOS-821693	0.6050	...	142	622	...	...	...	...	...	...	10 03 01.86	+02 14 18.90	20
370	zCOSMOS-822429	0.5560	...	52	254	...	...	...	...	...	...	10 02 21.06	+02 14 46.97	20
371	zCOSMOS-822504	0.8200	...	92	510	...	...	...	...	...	...	10 02 17.66	+02 14 02.20	20
372	zCOSMOS-822723	0.2290	245	42	170	...	...	...	...	...	...	10 02 08.01	+02 10 51.70	20
373	zCOSMOS-822960	0.8390	...	60	191	...	...	...	...	...	...	10 01 58.93	+02 08 56.97	20
374	zCOSMOS-823087	0.8150	...	116	401	...	...	...	...	...	...	10 01 53.20	+02 15 49.40	20
375	zCOSMOS-823693	0.5920	...	64	282	...	...	...	...	...	...	10 01 23.78	+02 17 01.83	20
376	zCOSMOS-823694	0.5930	...	66	230	...	...	...	...	...	...	10 01 23.78	+02 17 02.86	20
377	zCOSMOS-824210	0.1140	340	...	410	...	...	...	...	...	...	10 00 55.22	+02 14 13.22	20
378	zCOSMOS-824225	0.1900	484	110	464	...	...	...	...	...	...	10 00 54.65	+02 09 00.41	20
379	zCOSMOS-824503	0.6790	...	70	317	...	...	...	...	...	...	10 00 41.86	+02 09 12.56	20
380	zCOSMOS-824584	0.4750	148	50	158	...	...	...	...	...	...	10 00 37.40	+02 08 46.75	20
381	zCOSMOS-825278	0.1540	523	100	400	...	...	...	...	...	...	10 00 04.65	+02 08 09.22	20
382	zCOSMOS-825921	0.6340	...	45	194	...	...	...	...	...	...	09 59 34.09	+02 07 43.12	20
383	zCOSMOS-825959	0.6900	...	66	190	...	...	...	...	...	...	09 59 32.33	+02 09 55.39	20
384	zCOSMOS-826050	0.8840	...	66	200	...	...	...	...	...	...	09 59 28.15	+02 11 41.72	20
385	zCOSMOS-826076	0.1650	195	40	160	...	...	...	...	...	...	09 59 26.63	+02 09 49.57	20
386	zCOSMOS-826191	0.3550	270	74	196	...	...	...	...	...	...	09 59 21.68	+02 09 06.04	20
387	zCOSMOS-826195	0.8900	...	147	288	...	...	...	...	...	...	09 59 21.52	+02 11 17.78	20
388	zCOSMOS-827073	0.2520	515	90	500	...	...	...	...	...	...	09 58 38.87	+02 16 51.94	20
389	zCOSMOS-827326	0.8390	...	141	268	...	...	...	...	...	...	09 58 27.56	+02 14 57.07	20
390	zCOSMOS-828338	0.8220	...	126	283	...	...	...	...	...	...	10 03 03.61	+02 25 02.73	20
391	zCOSMOS-829725	0.7440	...	119	462	...	...	...	...	...	...	10 01 57.12	+02 27 15.74	20
392	zCOSMOS-829868	0.5790	...	310	1610	...	...	...	...	...	...	10 01 50.09	+02 21 05.38	20
393	zCOSMOS-829923	0.2160	180	40	156	...	...	...	...	...	...	10 01 47.90	+02 24 44.28	20
394	zCOSMOS-830132	0.4010	431	65	323	...	...	...	...	...	...	10 01 39.18	+02 25 22.96	20
395	zCOSMOS-830321	0.8500	...	130	805	...	...	...	...	...	...	10 01 32.01	+02 22 19.17	20
396	zCOSMOS-830751	0.2490	730	148	805	...	...	...	...	...	...	10 01 10.72	+02 20 49.08	20
397	zCOSMOS-831158	0.1900	206	54	184	...	...	...	...	...	...	10 00 51.53	+02 27 28.96	20
398	zCOSMOS-831178	0.2650	400	70	444	...	...	...	...	...	...	10 00 50.62	+02 26 57.39	20
399	zCOSMOS-831397	0.9130	...	173	852	...	...	...	...	...	...	10 00 39.44	+02 26 31.94	20
400	zCOSMOS-831498	0.5380	...	170	917	...	...	...	...	...	...	10 00 34.66	+02 24 48.46	20

Continuation on the next page.

Table 1 Continued

Index	Name	z	EW(Hα) (Å)	EW(Hβ) (Å)	EW[OIII] (Å)	σ (km s^{-1})	F($H\alpha$) Observed	F($H\beta$) Observed	F[OIII]λ5007Å Observed	F($H\alpha$) Corrected	F($H\beta$) Corrected	A.R (J2000)	DEC. (J2000)	Reference
401	zCOSMOS-831622	0.8370	...	84	533	...	...	...	...	...	...	10 00 28.45	+02 24 56.07	20
402	zCOSMOS-831713	0.4180	229	64	239	...	...	...	...	...	...	10 00 24.36	+02 27 14.88	20
403	zCOSMOS-831791	0.2600	220	46	237	...	...	...	...	...	...	10 00 21.92	+02 25 07.66	20
404	zCOSMOS-831824	0.6880	...	107	504	...	...	...	...	...	...	10 00 20.90	+02 18 32.43	20
405	zCOSMOS-831940	0.1200	150	...	150	...	...	...	...	...	...	10 00 16.12	+02 19 18.25	20
406	zCOSMOS-832077	0.5960	...	99	276	...	...	...	...	...	...	10 00 10.78	+02 20 24.43	20
407	zCOSMOS-832097	0.1340	278	...	243	...	...	...	...	...	...	10 00 09.99	+02 24 36.63	20
408	zCOSMOS-832539	0.7310	...	118	376	...	...	...	...	...	...	09 59 49.42	+02 17 38.60	20
409	zCOSMOS-832898	0.4070	356	89	272	...	...	...	...	...	...	09 59 32.22	+02 24 24.24	20
410	zCOSMOS-833022	0.4270	...	105	467	...	...	...	...	...	...	09 59 26.77	+02 18 59.32	20
411	zCOSMOS-833044	0.3130	196	75	174	...	...	...	...	...	...	09 59 25.48	+02 21 20.73	20
412	zCOSMOS-833222	0.4800	...	69	300	...	...	...	...	...	...	09 59 17.52	+02 27 30.09	20
413	zCOSMOS-834100	0.8680	...	191	323	...	...	...	...	...	...	09 58 37.36	+02 21 44.83	20
414	zCOSMOS-834172	0.5010	...	79	225	...	...	...	...	...	...	09 58 34.33	+02 20 15.82	20
415	zCOSMOS-834906	0.3360	590	60	345	...	...	...	...	...	...	09 57 55.26	+02 27 16.60	20
416	zCOSMOS-836042	0.6780	...	81	200	...	...	...	...	...	...	10 02 31.60	+02 36 41.36	20
417	zCOSMOS-836108	0.3510	490	74	457	...	...	...	...	...	...	10 02 28.30	+02 34 04.48	20
418	zCOSMOS-836228	0.1680	259	71	259	...	...	...	...	...	...	10 02 22.31	+02 31 37.21	20
419	zCOSMOS-836232	0.3300	290	44	188	...	...	...	...	...	...	10 02 22.19	+02 35 08.43	20
420	zCOSMOS-836338	0.7610	...	103	219	...	...	...	...	...	...	10 02 18.06	+02 32 14.37	20
421	zCOSMOS-836632	0.4710	351	92	352	...	...	...	...	...	...	10 02 04.93	+02 37 27.78	20
422	zCOSMOS-837240	0.3830	441	91	515	...	...	...	...	...	...	10 01 39.15	+02 33 48.60	20
423	zCOSMOS-837330	0.2200	220	39	141	...	...	...	...	...	...	10 01 35.13	+02 30 55.02	20
424	zCOSMOS-837582	0.7310	...	103	625	...	...	...	...	...	...	10 01 23.77	+02 34 30.06	20
425	zCOSMOS-837610	0.4920	...	80	402	...	...	...	...	...	...	10 01 22.27	+02 36 59.88	20
426	zCOSMOS-838357	0.7790	...	108	551	...	...	...	...	...	...	10 00 49.23	+02 29 17.29	20
427	zCOSMOS-838843	0.3690	273	55	202	...	...	...	...	...	...	10 00 29.23	+02 27 41.34	20
428	zCOSMOS-839293	0.1090	207	...	163	...	...	...	...	...	...	10 00 10.32	+02 28 09.75	20
429	zCOSMOS-839458	0.7480	...	86	289	...	...	...	...	...	...	10 00 02.68	+02 31 40.37	20
430	zCOSMOS-839488	0.2190	320	63	209	...	...	...	...	...	...	10 00 01.01	+02 36 34.81	20
431	zCOSMOS-839539	0.3800	321	63	269	...	...	...	...	...	...	09 59 58.88	+02 29 47.49	20
432	zCOSMOS-840004	0.4070	330	50	182	...	...	...	...	...	...	09 59 40.94	+02 29 17.12	20
433	zCOSMOS-840051	0.2500	418	84	345	...	...	...	...	...	...	09 59 39.63	+02 28 38.14	20
434	zCOSMOS-840109	0.2470	...	35	150	...	...	...	...	...	...	09 59 37.95	+02 36 34.94	20
435	zCOSMOS-840247	0.7630	...	89	280	...	...	...	...	...	...	09 59 31.68	+02 36 51.22	20
436	zCOSMOS-840599	0.4800	...	49	144	...	...	...	...	...	...	09 59 13.52	+02 29 59.35	20
437	zCOSMOS-840688	0.3200	280	50	182	...	...	...	...	...	...	09 59 08.74	+02 30 29.54	20
438	zCOSMOS-840845	0.2470	294	70	327	...	...	...	...	...	...	09 58 59.14	+02 35 22.79	20
439	zCOSMOS-840962	0.1200	2780	...	2700	...	...	...	...	...	...	09 58 53.40	+02 34 37.32	20
440	zCOSMOS-840971	0.4400	387	121	568	...	...	...	...	...	...	09 58 53.08	+02 35 39.93	20

Continuation on the next page.

Table 1 Continued

Index	Name	z	EW(Hα) (Å)	EW(Hβ) (Å)	EW[OIII] (Å)	σ (km s^{-1})	F($H\alpha$) Observed	F($H\beta$) Observed	F[OIII]λ5007Å Observed	F($H\alpha$) Corrected	F($H\beta$) Corrected	A.R (J2000)	DEC. (J2000)	Reference
441	zCOSMOS-840973	0.2000	287	62	298	...	...	...	...	...	...	09 58 53.02	+02 34 33.65	20
442	zCOSMOS-841104	0.1700	190	49	174	...	...	...	...	...	...	09 58 46.53	+02 29 08.70	20
443	zCOSMOS-841150	0.3140	905	125	440	...	...	...	...	...	...	09 58 44.10	+02 28 43.87	20
444	zCOSMOS-841493	0.1880	170	51	208	...	...	...	...	...	...	09 58 26.03	+02 28 37.24	20
445	zCOSMOS-841554	0.2750	252	39	202	...	...	...	...	...	...	09 58 21.20	+02 33 56.48	20
446	zCOSMOS-841564	0.1670	187	43	171	...	...	...	...	...	...	09 58 21.46	+02 34 19.00	20
447	zCOSMOS-841642	0.8520	...	74	208	...	...	...	...	...	...	09 58 17.70	+02 28 08.60	20
448	zCOSMOS-841690	0.4820	...	188	1105	...	...	...	...	...	...	09 58 14.85	+02 29 39.10	20
449	zCOSMOS-842700	0.1700	306	62	247	...	...	...	...	...	...	10 03 01.91	+02 45 01.11	20
450	zCOSMOS-842947	0.1250	290	...	409	...	...	...	...	...	...	10 02 51.35	+02 41 32.20	20
451	zCOSMOS-843208	0.4720	187	66	271	...	...	...	...	...	...	10 02 36.89	+02 39 53.92	20
452	zCOSMOS-843329	0.5060	...	144	815	...	...	...	...	...	...	10 02 31.44	+02 39 42.83	20
453	zCOSMOS-843573	0.8510	...	115	231	...	...	...	...	...	...	10 02 19.60	+02 40 01.16	20
454	zCOSMOS-843933	0.6760	...	78	295	...	...	...	...	...	...	10 02 02.59	+02 45 24.28	20
455	zCOSMOS-844465	0.6670	...	60	200	...	...	...	...	...	...	10 01 37.20	+02 38 33.51	20
456	zCOSMOS-844480	0.6110	...	76	240	...	...	...	...	...	...	10 01 36.54	+02 40 02.45	20
457	zCOSMOS-844783	0.5280	...	90	285	...	...	...	...	...	...	10 01 23.36	+02 40 36.12	20
458	zCOSMOS-844972	0.6210	...	128	481	...	...	...	...	...	...	10 01 12.78	+02 41 38.12	20
459	zCOSMOS-845045	0.2290	314	80	286	...	...	...	...	...	...	10 01 08.16	+02 45 18.72	20
460	zCOSMOS-845785	0.3610	278	57	214	...	...	...	...	...	...	10 00 32.62	+02 38 49.26	20
461	zCOSMOS-845804	0.7260	...	74	269	...	...	...	...	...	...	10 00 31.86	+02 37 45.71	20
462	zCOSMOS-846604	0.7280	...	150	1087	...	...	...	...	...	...	09 59 58.54	+02 41 59.23	20
463	zCOSMOS-846749	0.2250	352	58	218	...	...	...	...	...	...	09 59 52.10	+02 39 26.11	20
464	zCOSMOS-846799	0.7960	...	85	209	...	...	...	...	...	...	09 59 49.06	+02 47 22.46	20
465	zCOSMOS-847264	0.4800	...	108	450	...	...	...	...	...	...	09 59 24.90	+02 45 32.12	20
466	zCOSMOS-847277	0.5980	...	108	625	...	...	...	...	...	...	09 59 24.66	+02 47 20.81	20
467	zCOSMOS-847434	0.7550	...	83	316	...	...	...	...	...	...	09 59 16.38	+02 39 38.93	20
468	zCOSMOS-847735	0.3810	269	50	160	...	...	...	...	...	...	09 58 59.44	+02 41 18.47	20
469	zCOSMOS-848170	0.8620	...	65	171	...	...	...	...	...	...	09 58 33.42	+02 37 43.27	20
470	zCOSMOS-849222	0.8490	...	165	601	...	...	...	...	...	...	10 03 04.20	+02 48 30.19	20
471	zCOSMOS-849272	0.6110	...	116	475	...	...	...	...	...	...	10 03 00.34	+02 47 41.83	20
472	zCOSMOS-849619	0.2170	177	40	152	...	...	...	...	...	...	10 02 33.23	+02 48 55.31	20
473	zCOSMOS-850262	0.8160	...	113	450	...	...	...	...	...	...	10 01 33.28	+02 50 13.65	20
474	VUDS520276545	0.8614	...	45±20	119±19	...	...	$7.8^{+1.7}_{-1.7}$	33.5±1.1	...	...	02 25 09.25	-04 30 01.49	21
475	VUDS520281627	0.4033	...	37±5	160±15	...	$36.8^{+0.6}_{-0.6}$	$13.2^{+0.7}_{-0.7}$	55.9±1.1	...	...	02 25 19.84	-04 29 34.12	21
476	VUDS520290391	0.7411	...	86±25	305±47	...	...	$8.4^{+0.7}_{-0.7}$	35.2±0.7	...	...	02 25 33.71	-04 28 36.83	21
477	VUDS520246239	0.6177	...	30±9	103±13	...	...	$7.4^{+0.8}_{-0.8}$	22.6±1.3	...	...	02 25 56.55	-04 33 08.01	21
478	VUDS520327062	0.7065	...	37±25	162±30	...	...	$8.9^{+1.7}_{-1.7}$	34.6±1.7	...	...	02 26 22.22	-04 24 51.78	21
479	VUDS520388031	0.5270	...	44±10	198±23	...	...	$13.0^{+1.4}_{-1.4}$	55.7±1.8	...	...	02 26 28.28	-04 18 37.75	21
480	VUDS520420821	0.5550	...	145±30	1086±100	...	...	$17.9^{+1.2}_{-1.2}$	116.9±1.6	...	...	02 26 34.42	-04 15 16.54	21

Continuation on the next page.

Table 1 Continued

Index	Name	z	EW(Hα) (Å)	EW(Hβ) (Å)	EW[OIII] (Å)	σ (km s^{-1})	F($H\alpha$) Observed	F($H\beta$) Observed	F[OIII]λ5007Å Observed	F($H\alpha$) Corrected	F($H\beta$) Corrected	A.R (J2000)	DEC. (J2000)	Reference
481	VUDS520349673	0.5183	...	29±6	132±30	...	...	$14.3^{+1.2}_{-1.2}$	50.9±6.1	...	...	02 26 39.93	-04 22 34.80	21
482	VUDS520316717	0.6935	...	45±9	258±50	...	...	$10.2^{+0.5}_{-0.5}$	41.2±1.4	...	...	02 26 52.60	-04 25 57.40	21
483	VUDS520433508	0.8464	...	...	326±130	...	...	$7.4^{+1.8}_{-1.8}$	36.2±2.8	...	...	02 27 07.88	-04 13 51.39	21
484	VUDS520344687	0.8011	...	68±20	269±65	...	...	$9.0^{+2.7}_{-2.7}$	35.1±2.0	...	...	02 27 15.16	-04 23 03.16	21
485	VUDS530076899	0.3400	...	55±16	140±10	...	$5.8^{+0.8}_{-0.8}$	$2.0^{+0.4}_{-0.4}$	9.5±0.5	...	...	03 31 55.47	-27 35 02.27	21
486	VUDS530076254	0.2500	...	31±7	102±14	...	$20^{+1.5}_{-1.5}$	$5.7^{+0.9}_{-0.9}$	17.6±1.2	...	...	03 32 13.64	-27 35 17.58	21
487	VUDS530080539	0.8400	...	54±8	161±26	...	...	$18.4^{+1.8}_{-1.8}$	68.0±5.5	...	...	03 32 15.09	-27 33 39.18	21
488	VUDS530053182	0.3750	...	172±30	1002±20	...	$160.9^{+5.5}_{-5.5}$	$57.8^{+2.8}_{-2.8}$	342.4±5.5	...	...	03 32 15.82	-27 43 51.24	21
489	VUDS530046029	0.6700	...	...	124±20	...	...	$5.8^{+1.2}_{-1.2}$	25.0±1.8	...	...	03 32 20.50	-27 46 21.05	21
490	VUDS530048721	0.5700	...	40±10	168±15	...	...	$2.6^{+0.8}_{-0.8}$	14.5±0.9	...	...	03 32 40.38	-27 45 23.42	21
491	VUDS530043711	0.6200	...	...	125±7	...	...	$17.1^{+8.1}_{-8.1}$	55.2±1.6	...	...	03 32 59.02	-27 47 10.57	21
492	VUDS530079125	0.3800	...	59±6	264±30	...	$13.4^{+1.1}_{-1.1}$	$5.8^{+0.6}_{-0.6}$	24.2±0.7	...	...	03 33 01.56	-27 34 09.70	21
493	VUDS510830468	0.6745	...	340±30	1650±151	...	...	$26.0^{+1.7}_{-1.7}$	149.5±3.5	...	...	09 59 09.27	+02 01 52.50	21
494	VUDS510146174	0.4781	...	106±30	456±43	...	...	$3.0^{+0.9}_{-0.9}$	13.9±1.2	...	...	09 59 09.66	+01 59 17.71	21
495	VUDS511475480	0.6634	...	329±25	1595±300	...	...	$15.1^{+1.5}_{-1.5}$	93.2±1.7	...	...	09 59 43.09	+02 33 56.89	21
496	VUDS510573089	0.5472	...	50±7	397±35	...	...	$20.1^{+1.5}_{-1.5}$	147.0±3.1	...	...	09 59 44.22	+01 56 14.25	21
497	VUDS510809459	0.6614	...	85±12	349±25	...	...	$2.0^{+0.2}_{-0.2}$	10.0±0.4	...	...	09 59 52.20	+02 00 03.82	21
498	VUDS510352169	0.6282	...	233±15	957±25	...	...	$28.3^{+0.8}_{-0.8}$	133.5±2.4	...	...	09 59 59.59	+01 47 12.63	21
499	VUDS510229076	0.2197	...	37±13	163±27	...	$22^{+3.7}_{-3.7}$	$5.6^{+1.2}_{-1.2}$	19.5±1.5	...	...	10 00 11.84	+02 08 15.63	21
500	VUDS510997797	0.2837	...	46±12	148±26	...	$28.2^{+1.5}_{-1.5}$	$7.8^{+1.3}_{-1.3}$	28.2±1.5	...	...	10 00 20.21	+02 15 58.80	21
501	VUDS510175664	0.5018	...	115±30	656±45	...	...	$9.0^{+3.0}_{-3.0}$	39.8±2.0	...	...	10 00 27.14	+02 02 34.63	21
502	VUDS5120568170	0.3389	...	48±10	133±15	...	...	$3.3^{+0.7}_{-0.7}$	13.2±0.9	...	...	10 00 42.66	+01 48 11.25	21
503	VUDS5101659094	0.6782	...	22±4	188±30	...	...	$2.9^{+0.7}_{-0.7}$	13.8±1.7	...	...	10 01 18.50	+02 38 50.43	21
504	VUDS5101657178	0.5633	...	62±11	228±15	...	...	$8.0^{+0.9}_{-0.9}$	36.6±1.3	...	...	10 01 33.13	+02 39 38.69	21

Notes: All equivalent widths are quoted in the rest-frame. Flux units in 10^{-17} ergs s^{-1} cm^{-2}. Units of right ascension are hours, minutes and seconds, and units of declination are degrees, arcminutes and arcseconds.

[a] Observed flux of Hβ emission line calculated from observed flux of Hβ emission line once that they have been corrected by extinction.

[b] Corrected flux of [OIII] emission line taken from literature.

[c] Observed flux of Hα and Hβ emission lines calculated from corrected fluxes of Hβ emission line taken from literature.

References. (1) Erb et al. 2006a; (2) Erb et al 2006b; (3) Hoyos et al. 2005; (4) Siegel et al. 2005; (5) Erb et al. 2003; (6) Pettini et al. 2001; (7) Matsuda et al. 2011; (9) Maseda et al. 2013; (10) Maseda et al. 2014; (11) Masters et al. 2014; (12) Kobulnicky & kewley 2004; (14) Xia et al. 2012; (16) Weiner et al. 2006; (17) Van der Well et al. 2011; (18) Föster Schreiber et al. 2009; (19) Mancini et al. 2011; (20) Amorín et al. 2014a (private data); (21) Amorín et al. 2014b (private data).

Table 2

Index	Name	L(Hβ) Corrected	SFR(Hβ) Corrected	r_e (kpc)	M_{dyn} (10^{10} $M_\odot$)	M_* (10^8 $M_\odot$)	$E(B-V)$ (mag)	A(Hα)	A(Hβ)	M_B (mag)	R (AB)	H (AB)	K (AB)	12 + log(O/H)	Method
001	HDF-BX1303	$00.47^{+00.25}_{-00.25}$	$07.26^{+03.86}_{-03.86}$	3.40	...	$02.16^{+01.15}_{-01.15}$	$0.10^{+0.07}_{-0.07}$	$0.33^{+0.25}_{-0.25}$	$0.46^{+0.33}_{-0.33}$	...	24.72	...	...	...	...
002	HDF-BX1376	$00.42^{+00.15}_{-00.15}$	$06.41^{+02.33}_{-02.33}$	2.90	$03.11^{+01.42}_{-01.55}$	$02.11^{+00.76}_{-00.76}$	$0.07^{+0.05}_{-0.05}$	$0.23^{+0.17}_{-0.17}$	$0.32^{+0.23}_{-0.23}$	...	24.48	...	...	...	...
003	HDF-BX1388	$01.28^{+01.67}_{-01.67}$	$19.78^{+25.76}_{-25.76}$	7.90	$18.00^{+05.40}_{-05.40}$	$06.50^{+08.47}_{-08.47}$	$0.26^{+0.19}_{-0.19}$	$0.88^{+0.65}_{-0.65}$	$1.22^{+0.88}_{-0.88}$	...	24.55	...	...	...	...
004	HDF-BX1409	$02.60^{+03.69}_{-03.69}$	$40.03^{+56.81}_{-56.81}$	7.00	$20.31^{+04.63}_{-04.63}$	$15.38^{+21.83}_{-21.83}$	$0.29^{+0.20}_{-0.20}$	$0.96^{+0.71}_{-0.71}$	$1.33^{+0.96}_{-0.96}$	...	24.66	...	...	...	...
005	Q1623-BX429	$00.71^{+00.43}_{-00.43}$	$10.94^{+06.57}_{-06.57}$	6.70	$02.53^{+01.95}_{-02.40}$	$04.21^{+02.53}_{-02.53}$	$0.120^{+0.08}_{-0.08}$	$0.40^{+0.30}_{-0.30}$	$0.55^{+0.40}_{-0.40}$	...	23.63	...	...	...	...
006	Q1623-BX432	$00.76^{+00.24}_{-00.24}$	$11.71^{+03.64}_{-03.64}$	4.60	$01.56^{+00.87}_{-00.92}$	$02.71^{+00.84}_{-00.84}$	$0.06^{+0.04}_{-0.04}$	$0.20^{+0.15}_{-0.15}$	$0.28^{+0.20}_{-0.20}$	...	24.58	...	...	~8.55	R23
007	Q1623-BX455	$06.32^{+08.22}_{-08.22}$	$97.32^{+126.53}_{-126.53}$	5.00	$20.32^{+03.26}_{-03.26}$	$08.63^{+11.22}_{-11.22}$	$0.26^{+0.19}_{-0.19}$	$0.88^{+0.65}_{-0.65}$	$1.22^{+0.88}_{-0.88}$	...	24.80	...	...	...	...
008	Q1623-BX502	$02.95^{+03.18}_{-03.18}$	$45.39^{+48.91}_{-48.91}$	6.20	$04.05^{+00.86}_{-00.86}$	$02.45^{+02.64}_{-02.64}$	$0.22^{+0.15}_{-0.15}$	$0.73^{+0.54}_{-0.54}$	$1.01^{+0.73}_{-0.73}$	...	24.35	...	...	...	...
009	Q1623-BX511	$00.88^{+01.01}_{-01.01}$	$13.48^{+15.51}_{-15.51}$	6.20	$16.65^{+07.45}_{-07.89}$	$03.85^{+04.42}_{-04.42}$	$0.24^{+0.16}_{-0.16}$	$0.78^{+0.58}_{-0.58}$	$1.08^{+0.78}_{-0.78}$	...	25.37	...	...	...	...
010	Q1623-BX543	$03.66^{+05.45}_{-05.45}$	$56.34^{+83.91}_{-83.91}$	7.40	$18.84^{+06.11}_{-06.62}$	$20.84^{+31.03}_{-31.03}$	$0.31^{+0.21}_{-0.21}$	$1.01^{+0.75}_{-0.75}$	$1.40^{+1.01}_{-1.01}$	...	23.11	...	...	...	...
011	Q1623-BX599	$03.66^{+02.27}_{-02.27}$	$56.34^{+34.90}_{-34.90}$	5.80	$17.69^{+01.75}_{-01.75}$	$17.32^{+10.73}_{-10.73}$	$0.12^{+0.09}_{-0.09}$	$0.42^{+0.31}_{-0.31}$	$0.57^{+0.42}_{-0.42}$	...	23.44	...	...	...	...
012	Q1623-MD107	$00.75^{+00.24}_{-00.24}$	$11.62^{+03.75}_{-03.75}$	3.60	< 0.77	$01.33^{+00.43}_{-00.43}$	$0.06^{+0.04}_{-0.04}$	$0.20^{+0.15}_{-0.15}$	$0.28^{+0.20}_{-0.20}$	...	25.35	...	...	~8.55	R23
013	Q1623-MD66	$04.36^{+05.00}_{-05.00}$	$67.08^{+76.94}_{-76.94}$	5.30	$08.87^{+00.59}_{-00.59}$	$14.10^{+16.17}_{-16.17}$	$0.24^{+0.16}_{-0.16}$	$0.78^{+0.58}_{-0.58}$	$1.08^{+0.78}_{-0.78}$	...	23.95	...	...	...	...
014	Q1700-BX490	$06.25^{+08.73}_{-08.73}$	$96.29^{+134.48}_{-134.48}$	5.50	$07.74^{+01.26}_{-01.26}$	$28.61^{+39.96}_{-39.96}$	$0.28^{+0.20}_{-0.20}$	$0.95^{+0.70}_{-0.70}$	$1.31^{+0.95}_{-0.95}$	...	22.88	...	...	...	...
015	Q1700-BX530	$01.23^{+00.31}_{-00.31}$	$18.99^{+04.72}_{-04.72}$	6.20	< 00.99	$07.30^{+01.82}_{-01.82}$	$0.04^{+0.03}_{-0.03}$	$0.15^{+0.11}_{-0.11}$	$0.21^{+0.15}_{-0.15}$	...	23.05	...	...	...	...
016	Q1700-BX691	$01.34^{+00.83}_{-00.83}$	$20.56^{+12.76}_{-12.76}$	6.70	$22.51^{+03.71}_{-03.71}$	$07.21^{+04.47}_{-04.47}$	$0.12^{+0.09}_{-0.09}$	$0.42^{+0.31}_{-0.31}$	$0.57^{+0.42}_{-0.42}$	...	25.33	...	...	...	...
017	Q1700-BX717	$00.77^{+00.35}_{-00.35}$	$11.84^{+5.44}_{-5.44}$	4.80	< 01.23	$02.86^{+01.31}_{-01.31}$	$0.09^{+0.06}_{-0.06}$	$0.30^{+0.22}_{-0.22}$	$0.41^{+0.30}_{-0.30}$	...	24.78	...	...	~8.55	R23
018	Q1700-MD109	$02.02^{+01.73}_{-01.73}$	$31.07^{+26.68}_{-26.68}$	4.10	$04.12^{+02.13}_{-02.30}$	$10.89^{+09.35}_{-09.35}$	$0.18^{+0.12}_{-0.12}$	$0.58^{+0.43}_{-0.43}$	$0.80^{+0.58}_{-0.58}$	...	25.46	...	...	...	...
019	Q2343-BM133	$01.82^{+01.05}_{-01.05}$	$28.03^{+16.14}_{-16.14}$	7.70	$02.71^{+00.39}_{-00.59}$	$00.85^{+00.49}_{-00.49}$	$0.12^{+0.08}_{-0.08}$	$0.38^{+0.28}_{-0.28}$	$0.53^{+0.38}_{-0.38}$	...	22.59	...	...	...	...
020	Q2343-BX341	$01.34^{+01.39}_{-01.39}$	$20.62^{+21.42}_{-21.42}$	2.40	...	$07.63^{+07.92}_{-07.92}$	$0.21^{+0.15}_{-0.15}$	$0.70^{+0.52}_{-0.52}$	$0.96^{+0.70}_{-0.70}$	...	24.21	...	...	...	...
021	Q2343-BX378	$00.74^{+00.63}_{-00.63}$	$11.47^{+09.67}_{-09.67}$	7.40	...	$01.95^{+01.64}_{-01.64}$	$0.16^{+0.12}_{-0.12}$	$0.55^{+0.41}_{-0.41}$	$0.76^{+0.55}_{-0.55}$	...	24.80	...	...	...	...
022	Q2343-BX389	$02.99^{+03.66}_{-03.66}$	$46.06^{+56.35}_{-56.35}$	10.10	$14.46^{+02.08}_{-02.08}$	$16.14^{+19.75}_{-19.75}$	$0.25^{+0.18}_{-0.18}$	$0.83^{+0.62}_{-0.62}$	$1.15^{+0.83}_{-0.83}$	...	24.85	...	...	...	...
023	Q2343-BX390	$00.96^{+00.72}_{-00.72}$	$14.80^{+11.01}_{-11.01}$	10.80	$07.64^{+04.11}_{-04.70}$	$04.55^{+03.38}_{-03.38}$	$0.15^{+0.11}_{-0.11}$	$0.50^{+0.37}_{-0.37}$	$0.69^{+0.50}_{-0.50}$	...	24.36	...	...	...	...
024	Q2343-BX391	$00.89^{+00.84}_{-00.84}$	$13.66^{+13.02}_{-13.02}$	6.00	...	$02.52^{+02.41}_{-02.41}$	$0.20^{+0.14}_{-0.14}$	$0.65^{+0.48}_{-0.48}$	$0.90^{+0.64}_{-0.64}$	...	24.51	...	...	...	...
025	Q2343-BX418	$01.20^{+00.23}_{-00.23}$	$18.41^{+03.50}_{-03.50}$	3.60	$01.82^{+00.33}_{-00.33}$	$00.90^{+00.17}_{-00.17}$	$0.04^{+0.02}_{-0.02}$	$0.12^{+0.08}_{-0.08}$	$0.16^{+0.11}_{-0.11}$	...	23.99	...	...	...	...
026	Q2343-BX429	$00.98^{+00.90}_{-00.90}$	$15.16^{+13.83}_{-13.83}$	9.40	$02.84^{+01.78}_{-02.23}$	$02.47^{+02.25}_{-02.25}$	$0.18^{+0.13}_{-0.13}$	$0.62^{+0.46}_{-0.46}$	$0.85^{+0.62}_{-0.62}$	...	25.12	...	...	...	...
027	Q2343-BX435	$01.74^{+01.93}_{-01.93}$	$26.89^{+29.73}_{-29.73}$	8.90	$03.72^{+01.49}_{-01.74}$	$11.40^{+12.61}_{-12.61}$	$0.22^{+0.16}_{-0.16}$	$0.75^{+0.56}_{-0.56}$	$1.03^{+0.75}_{-0.75}$	...	24.23	...	...	...	...
028	Q2343-BX436	$01.23^{+00.44}_{-00.44}$	$18.88^{+06.73}_{-06.73}$	9.10	$04.20^{+01.33}_{-01.60}$	$05.21^{+01.86}_{-01.86}$	$0.07^{+0.05}_{-0.05}$	$0.23^{+0.17}_{-0.17}$	$0.32^{+0.23}_{-0.23}$	...	23.07	...	...	...	...
029	Q2343-BX461	$02.63^{+03.22}_{-03.22}$	$40.46^{+49.63}_{-49.63}$	7.70	$17.29^{+05.47}_{-05.97}$	$05.56^{+06.82}_{-06.82}$	$0.25^{+0.18}_{-0.18}$	$0.83^{+0.62}_{-0.62}$	$1.15^{+0.83}_{-0.83}$	...	24.40	...	...	...	...
030	Q2343-BX493	$01.61^{+02.02}_{-02.02}$	$24.81^{+31.14}_{-31.14}$	6.50	$18.15^{+09.14}_{-09.84}$	$04.99^{+06.27}_{-06.27}$	$0.26^{+0.18}_{-0.18}$	$0.85^{+0.63}_{-0.63}$	$1.17^{+0.84}_{-0.84}$	...	23.63	...	...	...	...
031	Q2343-BX529	$00.59^{+00.43}_{-00.43}$	$09.10^{+06.65}_{-06.65}$	< 1.9	...	$03.37^{+02.46}_{-02.46}$	$0.14^{+0.10}_{-0.10}$	$0.48^{+0.36}_{-0.36}$	$0.67^{+0.48}_{-0.48}$	...	24.42	...	...	...	...
032	Q2343-BX537	$01.08^{+00.69}_{-00.69}$	$16.60^{+10.66}_{-10.66}$	5.30	...	$04.35^{+02.80}_{-02.80}$	$0.13^{+0.09}_{-0.09}$	$0.43^{+0.32}_{-0.32}$	$0.60^{+0.43}_{-0.43}$	...	24.44	...	...	...	...
033	Q2343-BX660	$01.12^{+00.12}_{-00.12}$	$17.33^{+01.91}_{-01.91}$	6.20	< 01.15	$03.49^{+00.38}_{-00.38}$	$0.01^{+0.01}_{-0.01}$	$0.03^{+0.02}_{-0.02}$	$0.05^{+0.03}_{-0.03}$	...	24.36	...	...	...	...
034	Q2343-MD80	$00.33^{+00.05}_{-00.05}$	$05.04^{+00.83}_{-00.83}$	2.60	$01.66^{+00.72}_{-00.72}$	$01.94^{+00.32}_{-00.32}$	$0.02^{+0.01}_{-0.01}$	$0.07^{+0.05}_{-0.05}$	$0.09^{+0.07}_{-0.07}$	...	24.81	...	...	...	...
035	Q2346-BX220	$01.11^{+00.32}_{-00.32}$	$17.06^{+04.90}_{-04.90}$	6.50	$15.45^{+03.02}_{-03.02}$	$03.58^{+01.03}_{-01.03}$	$0.06^{+0.04}_{-0.04}$	$0.18^{+0.13}_{-0.13}$	$0.25^{+0.18}_{-0.18}$	...	23.57	...	...	...	...
036	Q2346-BX404	$01.82^{+00.86}_{-00.86}$	$28.04^{+13.18}_{-13.18}$	3.60	$04.35^{+00.26}_{-00.26}$	$09.22^{+04.33}_{-04.33}$	$0.10^{+0.07}_{-0.07}$	$0.32^{+0.23}_{-0.23}$	$0.44^{+0.31}_{-0.31}$	...	23.39	...	...	...	...
037	Q2346-BX405	$01.42^{+00.15}_{-00.15}$	$21.82^{+02.30}_{-02.30}$	5.80	$01.68^{+00.27}_{-00.27}$	$05.72^{+00.60}_{-00.60}$	$0.01^{+0.01}_{-0.01}$	$0.03^{+0.02}_{-0.02}$	$0.05^{+0.03}_{-0.03}$	...	23.36	...	...	...	...
038	Q2346-BX416	$02.75^{+02.62}_{-02.62}$	$42.37^{+40.42}_{-40.42}$	4.30	$07.94^{+01.51}_{-01.76}$	$13.56^{+12.94}_{-12.94}$	$0.20^{+0.14}_{-0.14}$	$0.65^{+0.48}_{-0.48}$	$0.90^{+0.64}_{-0.64}$	...	23.49	...	...	...	...
039	HDF-BX1322	$00.40^{+00.18}_{-00.18}$	$06.19^{+02.71}_{-02.71}$	4.60	< 01.18	$02.62^{+01.15}_{-01.15}$	$0.08^{+0.06}_{-0.06}$	$0.28^{+0.21}_{-0.21}$	$0.39^{+0.28}_{-0.28}$	...	23.72	...	20.95[c]	...	...
040	Q1623-BX376	$01.35^{+01.17}_{-01.17}$	$20.85^{+18.03}_{-18.03}$	7.00	$55.43^{+22.94}_{-22.94}$	$06.20^{+05.36}_{-05.36}$	$0.18^{+0.12}_{-0.12}$	$0.58^{+0.43}_{-0.43}$	$0.81^{+0.58}_{-0.58}$	...	23.31	...	20.84[c]	...	...

Continuation on the next page.

Table 2

Index	Name	L(Hβ) Corrected	SFR(Hβ) Corrected	r_e (kpc)	M_{dyn} (10^{10} $M_\odot$)	M_* (10^8 $M_\odot$)	$E(B-V)$ (mag)	A(Hα)	A(Hβ)	M_B (mag)	R (AB)	H (AB)	K (AB)	12 + log(O/H)	Method
041	Q1623-BX447	$00.74^{+00.20}_{-00.20}$	$11.34^{+03.01}_{-03.01}$	5.30	$18.65^{+03.22}_{-03.22}$	$06.07^{+01.61}_{-01.61}$	$0.05^{+0.04}_{-0.04}$	$0.17^{+0.12}_{-0.12}$	$0.23^{+0.16}_{-0.16}$	...	24.48	...	20.55[c]	...	...
042	Q1623-BX449	$00.74^{+00.44}_{-00.44}$	$11.40^{+06.85}_{-06.85}$	< 1.9	< 01.14	$04.83^{+02.90}_{-02.90}$	$0.11^{+0.08}_{-0.08}$	$0.37^{+0.27}_{-0.27}$	$0.51^{+0.36}_{-0.36}$	...	24.86	...	21.35[c]	...	...
043	Q1623-BX453	$03.76^{+05.04}_{-05.04}$	$57.83^{+77.58}_{-77.58}$	4.10	$01.77^{+00.23}_{-00.23}$	$25.07^{+33.63}_{-33.63}$	$0.28^{+0.19}_{-0.19}$	$0.91^{+0.68}_{-0.68}$	$1.26^{+0.91}_{-0.91}$	...	23.38	...	19.76[c]	...	...
044	Q1623-BX586	$00.99^{+00.95}_{-00.95}$	$15.31^{+14.63}_{-14.63}$	5.30	$09.47^{+02.75}_{-03.06}$	$06.49^{+06.20}_{-06.20}$	$0.20^{+0.14}_{-0.14}$	$0.65^{+0.48}_{-0.48}$	$0.90^{+0.64}_{-0.64}$	...	24.58	...	20.84[c]	...	...
045	Q1700-BX523	$01.67^{+02.12}_{-02.12}$	$25.66^{+32.73}_{-32.73}$	7.70	$15.13^{+06.05}_{-06.05}$	$12.08^{+15.41}_{-15.41}$	$0.26^{+0.18}_{-0.18}$	$0.86^{+0.64}_{-0.64}$	$1.20^{+0.86}_{-0.86}$	...	24.51	...	20.93[c]	...	...
046	Q1700-BX536	$01.48^{+00.85}_{-00.85}$	$22.78^{+13.11}_{-13.11}$	7.90	$07.27^{+02.29}_{-02.45}$	$12.61^{+07.26}_{-07.26}$	$0.12^{+0.08}_{-0.08}$	$0.38^{+0.28}_{-0.28}$	$0.53^{+0.38}_{-0.38}$	...	23.00	...	19.71[c]	...	...
047	Q1700-BX794	$01.28^{+00.82}_{-00.82}$	$19.66^{+12.64}_{-12.64}$	4.80	$03.57^{+01.25}_{-01.25}$	$08.84^{+05.68}_{-05.68}$	$0.13^{+0.09}_{-0.09}$	$0.43^{+0.32}_{-0.32}$	$0.60^{+0.43}_{-0.43}$	...	23.60	...	20.53[c]	...	...
048	Q2343-BX169	$00.83^{+00.52}_{-00.52}$	$12.83^{+07.99}_{-07.99}$	3.10	...	$07.11^{+04.42}_{-04.42}$	$0.12^{+0.09}_{-0.09}$	$0.42^{+0.31}_{-0.31}$	$0.57^{+0.42}_{-0.42}$	...	23.11	...	20.75[c]	...	...
049	Q2343-BX182	$00.43^{+00.22}_{-00.22}$	$06.61^{+03.38}_{-03.38}$	2.60	...	$03.14^{+01.61}_{-01.61}$	$0.10^{+0.07}_{-0.07}$	$0.33^{+0.25}_{-0.25}$	$0.46^{+0.33}_{-0.33}$	...	23.74	...	21.60[c]	...	...
050	Q2343-BX236	$00.62^{+00.29}_{-00.29}$	$09.51^{+04.45}_{-04.45}$	4.80	$12.22^{+06.61}_{-06.94}$	$05.26^{+02.46}_{-02.46}$	$0.08^{+0.06}_{-0.06}$	$0.28^{+0.21}_{-0.21}$	$0.39^{+0.28}_{-0.28}$	...	24.28	...	21.25[c]	...	...
051	Q2343-BX513	$01.65^{+01.09}_{-01.09}$	$25.37^{+16.81}_{-16.81}$	4.10	$10.72^{+01.29}_{-01.29}$	$10.75^{+07.13}_{-07.13}$	$0.14^{+0.09}_{-0.09}$	$0.45^{+0.33}_{-0.33}$	$0.62^{+0.44}_{-0.44}$	...	23.93	...	20.10[c]	...	...
052	Q2343-BX601	$01.57^{+00.98}_{-00.98}$	$24.18^{+15.02}_{-15.02}$	5.30	$06.79^{+01.55}_{-01.55}$	$10.25^{+06.37}_{-06.37}$	$0.12^{+0.09}_{-0.09}$	$0.42^{+0.31}_{-0.31}$	$0.57^{+0.42}_{-0.42}$	...	23.48	...	20.55[c]	...	...
053	DEEP2-1	...	...	...	...	...	...	...	...	-19.90	...	...	...	8.10±0.10	Te
054	DEEP2-2	...	...	...	...	...	...	...	...	-19.24	...	...	...	7.90±0.10	Te
055	DEEP2-3	...	...	...	...	...	...	...	...	-19.23	...	...	...	7.80±0.10	Te
056	DEEP2-4	...	...	...	...	...	...	...	...	-19.27	...	...	...	8.00±0.15	Te
057	DEEP2-5	...	...	...	...	...	...	...	...	-19.24	...	...	...	8.20±0.15	Te
058	DEEP2-6	...	...	...	...	...	...	...	...	...	...	...	...	8.10±0.15	Te
059	DEEP2-7	...	...	...	...	...	...	...	...	-20.10	...	...	...	8.10±0.15	Te
060	DEEP2-8	...	...	...	...	...	...	...	...	-19.97	...	...	...	8.10±0.15	Te
061	DEEP2-9	...	...	...	...	...	...	...	...	-20.55	...	...	...	8.10±0.10	Te
062	DEEP2-10	...	...	...	...	...	...	...	...	-21.40	...	...	...	8.30±0.15	Te
063	DEEP2-11	...	...	...	...	...	...	...	...	-18.48	...	...	...	8.00±0.15	Te
064	DEEP2-12	...	...	...	...	...	...	...	...	-21.00	...	...	...	8.20±0.15	Te
065	DEEP2-13	...	...	...	...	...	...	...	...	-19.94	...	...	...	8.30±0.15	Te
066	DEEP2-14	...	...	...	...	...	...	...	...	-19.53	...	...	...	7.80±0.15	Te
067	TKRS-1	...	...	1.00	$00.38^{+00.08}_{-00.08}$	...	...	...	...	...	...	...	...	8.00±0.10	Te
068	TKRS-2	...	...	0.70	$00.19^{+00.03}_{-00.03}$	...	...	...	...	-19.35	...	...	...	7.80±0.10	Te
069	Q0201-B13	$00.30^{+00.07}_{-00.07}$	$04.57^{+01.09}_{-01.09}$	...	...	$02.44^{+00.58}_{-00.58}$	0.004	$0.01^{+0.00}_{-0.00}$	$0.02^{+0.00}_{-0.00}$	...	23.34	...	...	~8.55	R23
070	Q1700-MD103	$00.93^{+00.25}_{-00.25}$	$14.33^{+03.79}_{-03.79}$	...	...	$03.95^{+01.04}_{-01.04}$	0.224	$0.74^{+0.18}_{-0.18}$	$1.03^{+0.18}_{-0.18}$	...	24.23	...	...	~8.55	R23
071	CDFaC1	$02.71^{+00.22}_{-00.22}$	$41.74^{+03.34}_{-03.34}$	...	...	$17.69^{+01.42}_{-01.42}$	0.110	$0.37^{+0.09}_{-0.09}$	$0.51^{+0.09}_{-0.09}$	...	23.53	...	...	~8.55	R23
072	Q0347-383C5	$01.49^{+00.11}_{-00.11}$	$22.95^{+01.68}_{-01.68}$	...	...	$09.73^{+00.71}_{-00.71}$	0.052	$0.17^{+0.04}_{-0.04}$	$0.24^{+0.04}_{-0.04}$	...	23.82	...	...	~8.55	R23
073	SSA22a-MD46	$01.79^{+00.13}_{-00.13}$	$27.58^{+02.06}_{-02.06}$	...	...	$10.20^{+00.76}_{-00.76}$	0.024	$0.08^{+0.02}_{-0.02}$	$0.11^{+0.02}_{-0.02}$	...	23.30	...	...	~8.55	R23
074	B20902+343C6	$02.33^{+00.80}_{-00.80}$	$35.94^{+12.28}_{-12.28}$	...	...	$11.05^{+03.77}_{-03.77}$	0.062	$0.21^{+0.05}_{-0.05}$	$0.28^{+0.05}_{-0.05}$	...	24.13	...	...	~8.55	R23
075	B20902+343C12	$02.64^{+00.35}_{-00.35}$	$40.68^{+05.38}_{-05.38}$	...	...	$13.38^{+01.77}_{-01.77}$	...	...	...	-22.84	23.63	...	22.89	8.70±0.08	R23
076	Q1422+231D81	$03.25^{+00.40}_{-00.40}$	$50.04^{+06.14}_{-06.14}$	...	...	$14.87^{+01.82}_{-01.82}$	...	...	...	-22.91	23.41	...	22.67	8.62±0.07	R23
077	SSA22aD3	$01.00^{+00.24}_{-00.24}$	$15.44^{+03.74}_{-03.74}$	...	...	$06.94^{+01.68}_{-01.68}$	...	...	...	-22.59	23.37	...	22.97	8.39±0.16	R23
078	DSF2237+116aC2	$03.26^{+00.44}_{-00.44}$	$50.18^{+06.78}_{-06.78}$	...	...	$22.55^{+03.05}_{-03.05}$	...	...	...	...	23.55	...	...	...	R23
079	MS1512-cB58	$00.78^{+00.13}_{-00.13}$	$12.06^{+02.02}_{-02.02}$	...	...	$05.23^{+00.88}_{-00.88}$	...	...	...	-22.04	24.10	...	23.30	8.49±0.10	R23
080	2QZC-C1-HAE19	$01.08^{+00.09}_{-00.09}$ [a]	$16.59^{+01.46}_{-01.46}$ [a]	...	...	$01.30^{+00.11}_{-00.11}$ [b]	...	...	...	...	...	...	> 22.15	...	...

Continuation on the next page.

Table 2

Index	Name	L(Hβ) Corrected	SFR(Hβ) Corrected	r_e (kpc)	M_{dyn} (10^{10} $M_\odot$)	M_* (10^8 $M_\odot$)	E($B-V$) (mag)	A(Hα)	A(Hβ)	M_B (mag)	R (AB)	H (AB)	K (AB)	12 + log(O/H)	Method
081	2QZC-C1-HAE20	$00.78^{+00.07}_{-00.07}$ [a]	$12.31^{+01.08}_{-01.08}$ [a]	...	...	$04.55^{+00.40}_{-00.40}$ [b]	...	...	...	...	...	...	21.25	...	...
082	2QZC-C1-HAE21	$00.94^{+00.08}_{-00.08}$ [a]	$14.44^{+01.27}_{-01.27}$ [a]	...	...	$01.52^{+00.13}_{-00.13}$ [b]	...	...	...	...	...	...	> 22.15	...	...
083	2QZC-C2-HAE1	$15.22^{+01.34}_{-01.34}$ [a]	$234.38^{+20.56}_{-20.56}$ [a]	...	...	$82.15^{+07.21}_{-07.21}$ [b]	...	...	...	...	...	...	18.14	...	...
084	2QZC-C2-HAE3	$02.30^{+00.20}_{-00.20}$ [a]	$35.47^{+03.11}_{-03.11}$ [a]	...	...	$07.68^{+00.67}_{-00.67}$ [b]	...	...	...	...	...	...	20.67	...	...
085	2QZC-C2-HAE4	$01.96^{+00.17}_{-00.17}$ [a]	$30.19^{+02.65}_{-02.65}$ [a]	...	...	$08.61^{+00.76}_{-00.76}$ [b]	...	...	...	...	...	...	20.58	...	...
086	2QZC-C2-HAE13	$00.90^{+00.08}_{-00.08}$ [a]	$13.79^{+01.21}_{-01.21}$ [a]	...	...	$05.30^{+00.46}_{-00.46}$ [b]	...	...	...	...	...	...	21.05	...	...
087	2QZC-C2-HAE14	$00.92^{+00.08}_{-00.08}$ [a]	$14.12^{+01.24}_{-01.24}$ [a]	...	...	$04.03^{+00.35}_{-00.35}$ [b]	...	...	...	...	...	...	21.43	...	...
088	2QZC-C2-HAE15	$00.94^{+00.08}_{-00.08}$ [a]	$14.44^{+01.27}_{-01.27}$ [a]	...	...	$03.12^{+00.27}_{-00.27}$ [b]	...	...	...	...	...	...	21.61	...	...
089	2QZC-C2-HAE16	$00.84^{+00.07}_{-00.07}$ [a]	$12.88^{+01.13}_{-01.13}$ [a]	...	...	$03.11^{+00.27}_{-00.27}$ [b]	...	...	...	...	...	...	21.66	...	...
090	2QZC-C2-HAE17	$00.82^{+00.07}_{-00.07}$ [a]	$12.59^{+01.10}_{-01.10}$ [a]	...	...	$03.47^{+00.30}_{-00.30}$ [b]	...	...	...	...	...	...	21.59	...	...
091	2QZC-C2-HAE18	$00.90^{+00.08}_{-00.08}$ [a]	$13.79^{+01.21}_{-01.21}$ [a]	...	...	$01.58^{+00.14}_{-00.14}$ [b]	...	...	...	...	...	...	> 22.15	...	...
092	2QZC-C3-HAE8	$01.26^{+00.11}_{-00.11}$ [a]	$19.49^{+01.71}_{-01.71}$ [a]	...	...	$07.49^{+00.66}_{-00.66}$ [b]	...	...	...	...	...	...	20.71	...	...
093	2QZC-C3-HAE9	$01.56^{+00.14}_{-00.14}$ [a]	$23.98^{+02.10}_{-02.10}$ [a]	...	...	...	...	...	...	...	...	...	> 22.15	...	...
094	2QZC-C3-HAE11	$01.33^{+00.12}_{-00.12}$ [a]	$20.42^{+01.79}_{-01.79}$ [a]	...	...	$03.04^{+00.27}_{-00.27}$ [b]	...	...	...	...	...	...	21.56	...	...
095	2QZC-C3-HAE12	$01.33^{+00.12}_{-00.12}$ [a]	$20.42^{+01.79}_{-01.79}$ [a]	...	...	$02.94^{+00.26}_{-00.26}$ [b]	...	...	...	...	...	...	21.59	...	...
096	2QZC-C3-HAE14	$00.86^{+00.08}_{-00.08}$ [a]	$13.18^{+01.16}_{-01.16}$ [a]	...	...	$05.72^{+00.50}_{-00.50}$ [b]	...	...	...	...	...	...	20.99	...	...
097	2QZC-C3-HAE15	$00.94^{+00.08}_{-00.08}$ [a]	$14.44^{+01.27}_{-01.27}$ [a]	...	...	$04.62^{+00.41}_{-00.41}$ [b]	...	...	...	...	...	...	21.28	...	...
098	2QZC-C3-HAE19	$00.80^{+00.07}_{-00.07}$ [a]	$12.31^{+01.08}_{-01.08}$ [a]	...	...	$05.22^{+00.46}_{-00.46}$ [b]	...	...	...	...	...	...	21.11	...	...
099	2QZC-C4-HAE3	$01.13^{+00.10}_{-00.10}$ [a]	$17.37^{+01.52}_{-01.52}$ [a]	...	...	$04.56^{+00.40}_{-00.40}$ [b]	...	...	...	...	...	...	21.27	...	...
100	2QZC-C4-HAE4	$00.88^{+00.08}_{-00.08}$ [a]	$13.49^{+01.18}_{-01.18}$ [a]	...	...	$05.85^{+00.51}_{-00.51}$ [b]	...	...	...	...	...	...	20.95	...	...
101	2QZC-C4-HAE6	$00.90^{+00.08}_{-00.08}$ [a]	$13.79^{+01.21}_{-01.21}$ [a]	...	...	$01.58^{+00.14}_{-00.14}$ [b]	...	...	...	...	...	...	> 22.15	...	...
102	0200-C1-HAE4	$02.10^{+00.18}_{-00.18}$ [a]	$32.35^{+02.84}_{-02.84}$ [a]	...	...	$13.71^{+01.20}_{-01.20}$ [b]	...	...	...	...	...	...	20.09	...	...
103	0200-C1-HAE6	$01.49^{+00.13}_{-00.13}$ [a]	$22.90^{+02.01}_{-02.01}$ [a]	...	...	$10.29^{+00.90}_{-00.90}$ [b]	...	...	...	...	...	...	20.36	...	...
104	0200-C1-HAE7	$01.75^{+00.15}_{-00.15}$ [a]	$26.90^{+02.36}_{-02.36}$ [a]	...	...	$05.41^{+00.47}_{-00.47}$ [b]	...	...	...	...	...	...	21.05	...	...
105	0200-C1-HAE8	$01.63^{+00.14}_{-00.14}$ [a]	$25.11^{+02.20}_{-02.20}$ [a]	...	...	$05.43^{+00.48}_{-00.48}$ [b]	...	...	...	...	...	...	21.06	...	...
106	0200-C1-HAE9	$01.36^{+00.12}_{-00.12}$ [a]	$20.88^{+01.83}_{-01.83}$ [a]	...	...	$09.05^{+00.79}_{-00.79}$ [b]	...	...	...	...	...	...	20.48	...	...
107	0200-C1-HAE10	$01.67^{+00.15}_{-00.15}$ [a]	$25.70^{+02.25}_{-02.25}$ [a]	...	...	$02.19^{+00.19}_{-00.19}$ [b]	...	...	...	...	...	...	21.63	...	...
108	0200-C1-HAE11	$01.26^{+00.11}_{-00.11}$ [a]	$19.49^{+01.71}_{-01.71}$ [a]	...	...	$06.41^{+00.56}_{-00.56}$ [b]	...	...	...	...	...	...	20.88	...	...
109	0200-C1-HAE12	$01.42^{+00.12}_{-00.12}$ [a]	$21.87^{+01.92}_{-01.92}$ [a]	...	...	$02.18^{+00.19}_{-00.19}$ [b]	...	...	...	...	...	...	> 22.75	...	...
110	0200-C2-HAE7	$02.15^{+00.19}_{-00.19}$ [a]	$33.11^{+02.90}_{-02.90}$ [a]	...	...	$05.94^{+00.52}_{-00.52}$ [b]	...	...	...	...	...	...	20.90	...	...
111	0200-C2-HAE9	$01.45^{+00.13}_{-00.13}$ [a]	$22.38^{+01.96}_{-01.96}$ [a]	...	...	$08.23^{+00.72}_{-00.72}$ [b]	...	...	...	...	...	...	20.61	...	...
112	0200-C2-HAE11	$01.36^{+00.12}_{-00.12}$ [a]	$20.88^{+01.83}_{-01.83}$ [a]	...	...	$08.85^{+00.78}_{-00.78}$ [b]	...	...	...	...	...	...	20.54	...	...
113	0200-C2-HAE12	$01.39^{+00.12}_{-00.12}$ [a]	$21.37^{+01.88}_{-01.88}$ [a]	...	...	$06.35^{+00.56}_{-00.56}$ [b]	...	...	...	...	...	...	20.90	...	...
114	0200-C2-HAE13	$01.42^{+00.12}_{-00.12}$ [a]	$21.87^{+01.92}_{-01.92}$ [a]	...	...	$02.18^{+00.19}_{-00.19}$ [b]	...	...	...	...	...	...	> 22.75	...	...
115	0200-C2-HAE16	$01.18^{+00.10}_{-00.10}$ [a]	$18.19^{+01.60}_{-01.60}$ [a]	...	...	$05.19^{+00.46}_{-00.46}$ [b]	...	...	...	...	...	...	21.12	...	...
116	0200-C4-HAE7	$01.45^{+00.13}_{-00.13}$ [a]	$22.38^{+01.96}_{-01.96}$ [a]	...	...	$06.65^{+00.58}_{-00.58}$ [b]	...	...	...	...	...	...	20.87	...	...
117	0200-C4-HAE8	$01.49^{+00.13}_{-00.13}$ [a]	$22.90^{+02.01}_{-02.01}$ [a]	...	...	$04.81^{+00.42}_{-00.42}$ [b]	...	...	...	...	...	...	21.15	...	...
118	0200-C4-HAE11	$01.05^{+00.09}_{-00.09}$ [a]	$16.21^{+01.42}_{-01.42}$ [a]	...	...	$07.03^{+00.62}_{-00.62}$ [b]	...	...	...	...	...	...	20.77	...	...
119	COSMOS-15144	...	...	0.99±0.06	$00.22^{+00.09}_{-00.09}$	...	...	...	...	...	...	...	...	...	...
120	COSMOS-13848	...	...	1.10±0.13	$00.28^{+00.17}_{-00.17}$	...	...	...	...	...	...	...	...	...	...

Continuation on the next page.

Table 2

Index	Name	L(Hβ) Corrected	SFR(Hβ) Corrected	r$_e$ (kpc)	M$_{dyn}$ (10^{10} M$_\odot$)	M$_*$ (10^8 M$_\odot$)	E($B-V$) (mag)	A(Hα)	A(Hβ)	M$_B$ (mag)	R (AB)	H (AB)	K (AB)	12 + log(O/H)	Method
121	COSMOS-12807	...	...	0.75±0.11	$00.13^{+00.07}_{-00.07}$	...	...	...	...	...	...	...	...	...	...
122	UDS-7444	...	...	...	...	...	...	...	...	...	...	...	...	...	...
123	COSMOS-16207	...	...	1.60±0.05	$00.42^{+00.17}_{-00.17}$	...	...	...	...	...	...	...	...	...	...
124	UDS-3760	...	...	0.67±0.04	$00.18^{+00.04}_{-00.04}$	...	...	...	...	...	...	...	...	...	...
125	UDS-3646	...	...	1.40±0.42	$00.49^{+00.11}_{-00.11}$	...	...	...	...	...	...	...	...	...	...
126	GOODS-S-17892	...	...	0.68±0.62	$00.22^{+00.05}_{-00.05}$	...	...	...	...	...	...	...	...	...	...
127	GOODS-S-26816	...	...	0.35±0.06	$00.12^{+00.02}_{-00.02}$	...	...	...	...	...	...	...	...	...	...
128	UDS-11484	...	...	1.10±0.20	$00.38^{+00.13}_{-00.13}$	...	...	...	...	...	...	...	...	...	...
129	COSMOS-11212	...	...	0.53±0.10	$00.10^{+00.04}_{-00.04}$	...	...	...	...	...	...	...	...	...	...
130	COSMOS-8991	...	...	0.67±0.16	$00.07^{+00.04}_{-00.04}$	...	...	...	...	...	...	...	...	...	...
131	UDS-14655	...	...	1.80±0.16	$00.78^{+00.28}_{-00.28}$	...	...	...	...	...	...	...	...	...	...
132	UDS-4501	...	...	0.51±0.08	$00.20^{+00.07}_{-00.07}$	...	...	...	...	...	...	...	...	...	...
133	COSMOS-12102	...	...	1.60±0.08	$09.91^{+01.26}_{-01.26}$	...	...	...	...	...	...	...	...	...	...
134	COSMOS-17118	...	...	4.80±0.33	$01.21^{+00.46}_{-00.46}$	...	...	...	...	...	...	...	...	...	...
135	WISP159-134	$00.52^{+00.70}_{-00.16}$	$08.01^{+10.84}_{-02.47}$	...	...	$02.38^{+03.22}_{-00.73}$	$0.04^{+0.20}_{-0.04}$	$0.13^{+0.66}_{-0.14}$	$0.18^{+0.92}_{-0.19}$	...	...	...	...	< 8.04	N2
136	WISP134-171	...	...	2.40	$01.43^{+00.08}_{-00.08}$	...	...	...	...	...	...	...	...	8.35±0.04	N2
137	WISP50-65	$04.27^{+10.36}_{-09.58}$	$65.73^{+159.52}_{-147.48}$	2.70	$06.64^{+00.35}_{-00.35}$	$27.87^{+67.63}_{-62.53}$	$0.76^{+0.33}_{-0.30}$	$2.53^{+1.25}_{-1.17}$	$3.49^{+1.63}_{-1.51}$	...	...	...	...	~8.4	R23
138	WISP173-205	$00.52^{+00.19}_{-00.12}$	$07.96^{+02.88}_{-01.92}$	1.50	$00.66^{+00.03}_{-00.03}$	$01.35^{+00.49}_{-00.33}$	$0.03^{+0.05}_{-0.03}$	$0.10^{+0.17}_{-0.10}$	$0.14^{+0.23}_{-0.14}$	...	...	...	...	...	...
139	WISP9-73	$02.01^{+00.97}_{-00.97}$	$30.93^{+14.95}_{-14.95}$	1.50	$01.09^{+00.03}_{-00.03}$	$11.89^{+05.75}_{-05.75}$	$0.30^{+0.04}_{-0.04}$	$1.00^{+0.27}_{-0.27}$	$1.38^{+0.30}_{-0.30}$	...	...	...	...	8.44±0.04	R23
140	WISP43-75	$02.04^{+01.59}_{-01.59}$	$31.45^{+24.52}_{-24.52}$	3.20	...	$19.11^{+14.90}_{-14.90}$	$0.14^{+0.11}_{-0.11}$	$0.46^{+0.38}_{-0.38}$	$0.64^{+0.52}_{-0.52}$	...	...	...	...	8.57±0.08	N2
141	WISP25-53	$00.68^{+00.16}_{-00.08}$	$10.45^{+2.46}_{-01.26}$	2.20	$01.47^{+00.05}_{-00.05}$	$06.83^{+01.61}_{-00.83}$	$0.00^{+0.03}_{-0.00}$	$0.00^{+0.10}_{-0.00}$	$0.00^{+0.14}_{-0.00}$	...	...	...	...	8.81±0.02	R23
142	WISP46-75	$00.74^{+00.71}_{-00.28}$	$11.38^{+10.87}_{-04.24}$	...	...	$03.99^{+03.81}_{-01.48}$	$0.05^{+0.14}_{-0.05}$	$0.17^{+0.47}_{-0.17}$	$0.23^{+0.64}_{-0.23}$	...	...	...	...	8.87±0.09	R23
143	WISP126-90	...	...	2.40	$01.70^{+00.06}_{-00.06}$	...	$0.61^{+0.15}_{-0.15}$	0.17	...	...	...	...	...	8.67±0.04	N2
144	WISP22-111	$00.38^{+00.41}_{-00.04}$	$05.78^{+6.26}_{-00.64}$	2.60	$01.41^{+00.08}_{-00.08}$	...	$0.00^{+0.16}_{-0.00}$	$0.00^{+0.53}_{-0.00}$	$0.00^{+0.74}_{-0.00}$	...	...	...	...	8.56±0.05	N2
145	WISP22-216	$00.48^{+00.14}_{-00.06}$	$07.33^{+02.16}_{-00.87}$	2.20	$00.59^{+00.04}_{-00.04}$	...	$0.00^{+0.04}_{-0.00}$	$0.00^{+0.13}_{-0.00}$	$0.00^{+0.18}_{-0.00}$	...	...	...	...	< 7.82	N2
146	WISP64-2056	...	...	...	...	...	...	...	...	...	...	...	...	< 8.09	N2
147	WISP81-83	...	...	2.80	...	...	...	...	...	...	...	...	...	...	...
148	WISP138-173	$06.97^{+07.86}_{-07.86}$	$107.36^{+121.11}_{-121.11}$	2.20	$00.94^{+00.20}_{-00.20}$	...	$0.61^{+0.12}_{-0.12}$	$2.03^{+0.63}_{-0.63}$	$2.80^{+0.74}_{-0.74}$	...	...	...	...	~8.4	R23
149	WISP170-106	$01.99^{+01.44}_{-01.44}$	$30.59^{+22.11}_{-22.11}$	1.60	$00.57^{+00.06}_{-00.06}$	...	$0.30^{+0.09}_{-0.09}$	$1.00^{+0.38}_{-0.38}$	$1.38^{+0.48}_{-0.48}$	...	...	...	...	~8.4	R23
150	WISP64-210	$02.49^{+01.59}_{-01.59}$	$38.34^{+24.51}_{-24.51}$	1.60	$01.03^{+00.13}_{-00.13}$	...	$0.33^{+0.07}_{-0.07}$	$1.10^{+0.35}_{-0.35}$	$1.52^{+0.42}_{-0.42}$	...	...	...	...	~8.4	R23
151	WISP204-133	$00.43^{+00.06}_{-00.06}$	$06.58^{+00.88}_{-0.88}$	1.70	$00.60^{+00.24}_{-00.24}$	...	$0.00^{+0.00}_{-0.00}$	$0.00^{+0.00}_{-0.00}$	$0.00^{+0.00}_{-0.00}$	...	...	...	...	8.00±0.11	R23
152	WISP27-95	$03.79^{+01.88}_{-01.88}$	$58.40^{+29.04}_{-29.04}$	2.00	$02.79^{+00.15}_{-00.15}$	...	$0.32^{+0.04}_{-0.04}$	$1.06^{+0.29}_{-0.29}$	$1.47^{+0.32}_{-0.32}$	...	...	...	...	~8.4	R23
153	WISP147-72	...	...	1.60	$06.48^{+00.50}_{-00.50}$	...	...	...	...	...	...	...	...	...	...
154	WISP90-58	$03.90^{+01.63}_{-01.63}$	$59.98^{+25.07}_{-25.07}$	1.60	$02.33^{+00.12}_{-00.12}$	...	$0.24^{+0.04}_{-0.04}$	$0.80^{+0.23}_{-0.23}$	$1.10^{+0.26}_{-0.26}$	...	...	...	...	8.62±0.03	R23
155	WISP70-253	$00.41^{+00.04}_{-00.04}$	$06.33^{+00.61}_{-00.61}$	1.60	$00.49^{+00.06}_{-00.06}$	...	$0.00^{+0.00}_{-0.00}$	$0.00^{+0.00}_{-0.00}$	$0.00^{+0.00}_{-0.00}$	...	...	...	...	7.96±0.03	R23
156	WISP175-124	...	...	2.00	$01.68^{+00.18}_{-00.18}$	...	...	...	...	...	...	...	...	8.33±0.05	N2
157	WISP96-158	$03.29^{+04.09}_{-04.09}$	$50.70^{+62.98}_{-62.98}$	2.40	$00.72^{+00.09}_{-00.09}$	...	$0.48^{+0.16}_{-0.16}$	$1.60^{+0.66}_{-0.66}$	$2.21^{+0.83}_{-0.83}$	...	...	...	...	~8.4	R23
158	WISP138-160	$02.70^{+01.91}_{-01.91}$	$41.63^{+29.35}_{-29.35}$	1.60	$00.59^{+00.02}_{-00.02}$	...	$0.15^{+0.10}_{-0.10}$	$0.50^{+0.35}_{-0.35}$	$0.69^{+0.48}_{-0.48}$	...	...	...	...	8.29±0.02	N2
159	WISP56-210	$01.38^{+01.51}_{-00.24}$	$21.26^{+23.19}_{-03.78}$	2.10	$01.72^{+00.96}_{-00.96}$	...	$0.00^{+0.16}_{-0.00}$	$0.000^{+0.532}_{-0.000}$	$0.00^{+0.74}_{-0.00}$	...	...	...	...	~8.4	R23
160	WISP206-261	$01.89^{+01.07}_{-01.07}$	$29.16^{+16.44}_{-16.44}$	1.90	$00.34^{+00.03}_{-00.03}$	...	$0.30^{+0.06}_{-0.06}$	$1.00^{+0.31}_{-0.31}$	$1.38^{+0.36}_{-0.36}$	...	...	...	...	8.37±0.06	R23

Continuation on the next page.

Table 2

Index	Name	L(Hβ) Corrected	SFR(Hβ) Corrected	r_e (kpc)	M_{dyn} (10^{10} $M_\odot$)	M_* (10^8 $M_\odot$)	E($B-V$) (mag)	A(Hα)	A(Hβ)	M_B (mag)	R (AB)	H (AB)	K (AB)	12 + log(O/H)	Method
161	TKRS7889	...	...	...	...	...	...	...	...	-19.52	22.68	...	...	8.74±0.15	R23
162	TKRS10625	...	...	...	...	...	...	...	...	-19.69	22.44	...	...	8.44±0.15	R23
163	TKRS7887	...	...	...	...	...	...	...	...	-18.87	22.95	...	...	8.52±0.15	R23
164	TKRS7878	...	...	...	...	...	...	...	...	-20.06	23.54	...	...	8.84±0.15	R23
165	TKRS2882	...	...	...	...	...	...	...	...	-20.10	23.61	...	...	8.83±0.15	R23
166	TKRS10350	...	...	...	...	...	...	...	...	-20.86	22.89	...	...	8.75±0.15	R23
167	TKRS7105	...	...	...	...	...	...	...	...	-17.33	23.58	...	...	8.51±0.15	R23
168	TKRS2246	...	...	...	...	...	...	...	...	-17.73	23.84	...	...	8.16±0.20	R23
169	TKRS2336	...	...	...	...	...	...	...	...	-17.27	24.15	...	...	8.23±0.19	R23
170	TKRS4648	...	...	...	...	...	...	...	...	-18.30	23.20	...	...	8.64±0.15	R23
171	TKRS3741	...	...	...	...	...	...	...	...	-17.87	24.08	...	...	8.59±0.15	R23
172	TKRS5621	...	...	...	...	...	...	...	...	-20.16	21.69	...	...	8.74±0.15	R23
173	TKRS5634	...	...	...	...	...	...	...	...	-19.69	22.20	...	...	8.74±0.15	R23
174	TKRS3272	...	...	...	...	...	...	...	...	-18.15	23.89	...	...	8.40±0.15	R23
175	TKRS7843	...	...	...	...	...	...	...	...	-19.37	22.76	...	...	8.65±0.15	R23
176	TKRS3130	...	...	...	...	...	...	...	...	-19.02	23.19	...	...	8.46±0.15	R23
177	TKRS10183	...	...	...	...	...	...	...	...	-18.93	23.51	...	...	8.73±0.15	R23
178	TKRS4375	...	...	...	...	...	...	...	...	-19.95	23.05	...	...	8.64±0.15	R23
179	TKRS1953	...	...	...	...	...	...	...	...	-19.08	23.97	...	...	8.61±0.15	R23
180	TKRS4389	...	...	...	...	...	...	...	...	-21.84	21.15	...	...	8.76±0.15	R23
181	TKRS8126	...	...	...	...	...	...	...	...	-19.46	23.69	...	...	8.65±0.15	R23
182	TKRS5167	...	...	...	...	...	...	...	...	-19.34	24.06	...	...	8.77±0.16	R23
183	TKRS1468	...	...	...	...	...	...	...	...	-20.34	23.18	...	...	8.77±0.15	R23
184	TKRS11643	...	...	...	...	...	...	...	...	-20.44	23.15	...	...	8.52±0.15	R23
185	TKRS4332	...	...	...	...	...	...	...	...	-19.68	24.01	...	...	8.66±0.15	R23
186	TKRS3021	...	...	...	...	...	...	...	...	-20.80	22.97	...	...	8.74±0.15	R23
187	TKRS6786	...	...	...	...	...	...	...	...	-21.10	22.52	...	...	8.81±0.15	R23
188	TKRS7075	...	...	...	...	...	...	...	...	-19.66	24.00	...	...	8.61±0.15	R23
189	TKRS9211	...	...	...	...	...	...	...	...	-20.04	23.81	...	...	8.83±0.15	R23
190	TKRS6596	...	...	...	...	...	...	...	...	-20.50	23.37	...	...	8.99±0.15	R23
191	PEARS123301	$09.36^{+06.52}_{-06.52}$	$144.09^{+100.38}_{-100.38}$	8.10	...	$31.18^{+21.72}_{-21.72}$	$0.30^{+0.30}_{-0.30}$	$1.00^{+1.03}_{-1.03}$	$1.38^{+1.40}_{-1.40}$	-19.74	...	...	...	$8.10^{+0.20}_{-0.16}$	R23
192	PEARS119341	$04.47^{+01.34}_{-01.34}$	$68.91^{+20.72}_{-20.72}$	1.97	...	$01.95^{+00.59}_{-00.59}$	$0.03^{+0.06}_{-0.03}$	$0.10^{+0.20}_{-0.10}$	$0.14^{+0.28}_{-0.14}$	-17.57	...	...	...	$7.71^{+0.28}_{-0.27}$	R23
193	PEARS122206	$35.24^{+17.88}_{-17.88}$	$542.64^{+275.30}_{-275.30}$	2.20	...	$16.85^{+08.55}_{-08.55}$	$0.03^{+0.06}_{-0.03}$	$0.10^{+0.20}_{-0.10}$	$0.14^{+0.28}_{-0.14}$	-18.99	...	...	...	$7.49^{+0.00}_{-0.17}$	R23
194	PEARS-364	$08.06^{+02.05}_{-02.05}$	$124.18^{+31.56}_{-31.56}$	1.72	...	$39.76^{+10.11}_{-10.11}$	$0.03^{+0.18}_{-0.03}$	$0.10^{+0.60}_{-0.10}$	$0.14^{+0.83}_{-0.14}$	-19.19	...	...	...	$8.22^{+0.16}_{-0.13}$	R23
195	PEARS-103	$17.33^{+13.87}_{-13.87}$	$266.91^{+213.63}_{-213.63}$	1.07	...	$76.15^{+60.95}_{-60.95}$	$0.06^{+0.13}_{-0.06}$	$0.20^{+0.44}_{-0.21}$	$0.28^{+0.60}_{-0.28}$	-19.41	...	...	...	$7.97^{+0.00}_{-0.22}$	R23
196	PEARS-242	$39.44^{+25.50}_{-25.50}$	$607.31^{+392.64}_{-392.64}$	2.09	...	$272.95^{+176.47}_{-176.47}$	$0.19^{+0.17}_{-0.17}$	$0.63^{+0.58}_{-0.58}$	$0.87^{+0.80}_{-0.80}$	-21.42	...	...	...	$8.32^{+0.00}_{-0.29}$	R23
197	GSD1	...	...	...	...	...	...	...	...	...	...	24.67±0.07	...	...	...
198	GSD2	...	...	...	...	...	...	...	...	...	...	25.63±0.07	...	...	...
199	GSD3	...	...	...	...	...	...	...	...	...	...	25.88±0.11	...	...	...
200	GSD4	...	...	...	...	...	...	...	...	...	...	26.20±0.11	...	...	...

Continuation on the next page.

Table 2

Index	Name	L(Hβ) Corrected	SFR(Hβ) Corrected	r_e (kpc)	M_{dyn} (10^{10} $M_\odot$)	M_* (10^8 $M_\odot$)	E($B-V$) (mag)	A(Hα)	A(Hβ)	M_B (mag)	R (AB)	H (AB)	K (AB)	12 + log(O/H)	Method
201	GSD5	...	...	...	...	...	...	...	...	...	...	25.05±0.08	...	...	...
202	GSD6	...	...	...	...	...	...	...	...	...	...	24.99±0.05	...	...	...
203	GSD7	...	...	...	...	...	...	...	...	...	...	25.44±0.12	...	...	...
204	GSD8	...	...	...	...	...	...	...	...	...	...	24.26±0.04	...	...	...
205	GSD9	...	...	...	...	...	...	...	...	...	...	24.86±0.04	...	...	...
206	GSD10	...	...	...	...	...	...	...	...	...	...	26.37±0.09	...	...	...
207	GSD11	...	...	...	...	...	...	...	...	...	...	25.97±0.09	...	...	...
208	GSD12	...	...	...	...	...	...	...	...	...	...	25.80±0.12	...	...	...
209	GSD13	...	...	...	...	...	...	...	...	...	...	24.77±0.03	...	...	...
210	GSD14	...	...	...	...	...	...	...	...	...	...	26.00±0.08	...	...	...
211	GSD15	...	...	...	...	...	...	...	...	...	...	26.64±0.15	...	...	...
212	GSD16	...	...	...	...	...	...	...	...	...	...	26.10±0.08	...	...	...
213	GSD17	...	...	...	...	...	...	...	...	...	...	25.41±0.05	...	...	...
214	GSD18	...	...	...	...	...	...	...	...	...	...	25.24±0.04	...	...	...
215	GSD19	...	...	...	...	...	...	...	...	...	...	25.71±0.06	...	...	...
216	GSD20	...	...	...	...	...	...	...	...	...	...	26.23±0.10	...	...	...
217	GSD21	...	...	...	...	...	...	...	...	...	...	24.76±0.10	...	...	...
218	GSD22	...	...	...	...	...	...	...	...	...	...	26.76±0.13	...	...	...
219	GSD23	...	...	...	...	...	...	...	...	...	...	26.81±0.17	...	...	...
220	GSD24	...	...	...	...	...	...	...	...	...	...	27.77±0.30	...	...	...
221	GSD25	...	...	...	...	...	...	...	...	...	...	27.29±0.15	...	...	...
222	GSD26	...	...	...	...	...	...	...	...	...	...	26.65±0.10	...	...	...
223	GSD27	...	...	...	...	...	...	...	...	...	...	26.91±0.13	...	...	...
224	GSD28	...	...	...	...	...	...	...	...	...	...	27.13±0.16	...	...	...
225	GSD29	...	...	...	...	...	...	...	...	...	...	27.79±0.21	...	...	...
226	UDS1	...	...	...	...	...	...	...	...	...	...	25.38±0.09	...	...	...
227	UDS2	...	...	...	...	...	...	...	...	...	...	25.74±0.09	...	...	...
228	UDS3	...	...	...	...	...	...	...	...	...	...	25.28±0.08	...	...	...
229	UDS4	...	...	...	...	...	...	...	...	...	...	25.44±0.10	...	...	...
230	UDS5	...	...	...	...	...	...	...	...	...	...	25.69±0.11	...	...	...
231	UDS6	...	...	...	...	...	...	...	...	...	...	25.10±0.07	...	...	...
232	UDS7	...	...	...	...	...	...	...	...	...	...	24.32±0.04	...	...	...
233	UDS8	...	...	...	...	...	...	...	...	...	...	26.44±0.17	...	...	...
234	UDS9	...	...	...	...	...	...	...	...	...	...	25.94±0.09	...	...	...
235	UDS10	...	...	...	...	...	...	...	...	...	...	25.48±0.07	...	...	...
236	UDS11	...	...	...	...	...	...	...	...	...	...	26.36±0.10	...	...	...
237	UDS12	...	...	...	...	...	...	...	...	...	...	24.15±0.03	...	...	...
238	UDS13	...	...	...	...	...	...	...	...	...	...	25.35±0.07	...	...	...
239	UDS14	...	...	...	...	...	...	...	...	...	...	25.69±0.11	...	...	...
240	UDS15	...	...	...	...	...	...	...	...	...	...	25.45±0.09	...	...	...

Continuation on the next page.

Table 2

Index	Name	L(Hβ) Corrected	SFR(Hβ) Corrected	r$_e$ (kpc)	M$_{dyn}$ (10^{10} M$_\odot$)	M$_*$ (10^8 M$_\odot$)	E($B-V$) (mag)	A(Hα)	A(Hβ)	M$_B$ (mag)	R (AB)	H (AB)	K (AB)	12 + log(O/H)	Method
241	UDS6	...	...	...	...	...	...	...	...	...	...	25.39±0.08	...	...	...
242	UDS17	...	...	...	...	...	...	...	...	...	...	25.95±0.10	...	...	...
243	UDS18	...	...	...	...	...	...	...	...	...	...	25.83±0.13	...	...	...
244	UDS19	...	...	...	...	...	...	...	...	...	...	26.25±0.15	...	...	...
245	UDS20	...	...	...	...	...	...	...	...	...	...	25.16±0.06	...	...	...
246	UDS21	...	...	...	...	...	...	...	...	...	...	25.15±0.07	...	...	...
247	UDS22	...	...	...	...	...	...	...	...	...	...	26.34±0.19	...	...	...
248	UDS123	...	...	...	...	...	...	...	...	...	...	25.59±0.07	...	...	...
249	UDS24	...	...	...	...	...	...	...	...	...	...	26.02±0.13	...	...	...
250	UDS25	...	...	...	...	...	...	...	...	...	...	24.47±0.05	...	...	...
251	UDS26	...	...	...	...	...	...	...	...	...	...	25.34±0.08	...	...	...
252	UDS27	...	...	...	...	...	...	...	...	...	...	26.40±0.17	...	...	...
253	UDS28	...	...	...	...	...	...	...	...	...	...	25.89±0.14	...	...	...
254	UDS29	...	...	...	...	...	...	...	...	...	...	26.35±0.13	...	...	...
255	UDS30	...	...	...	...	...	...	...	...	...	...	25.66±0.14	...	...	...
256	UDS31	...	...	...	...	...	...	...	...	...	...	25.95±0.12	...	...	...
257	UDS32	...	...	...	...	...	...	...	...	...	...	25.83±0.12	...	...	...
258	UDS33	...	...	...	...	...	...	...	...	...	...	26.06±0.11	...	...	...
259	UDS34	...	...	...	...	...	...	...	...	...	...	24.83±0.05	...	...	...
260	UDS35	...	...	...	...	...	...	...	...	...	...	26.42±0.21	...	...	...
261	UDS36	...	...	...	...	...	...	...	...	...	...	25.32±0.08	...	...	...
262	UDS37	...	...	...	...	...	...	...	...	...	...	26.54±0.22	...	...	...
263	UDS38	...	...	...	...	...	...	...	...	...	...	26.60±0.19	...	...	...
264	UDS39	...	...	...	...	...	...	...	...	...	...	26.99±0.18	...	...	...
265	UDS40	...	...	...	...	...	...	...	...	...	...	26.86±0.17	...	...	...
266	GMASS-167	$01.82^{+00.85}_{-00.83}$	$28.09^{+13.09}_{-12.81}$	1.80±1.10	$00.97^{+00.40}_{-00.48}$	$07.75^{+03.61}_{-03.53}$	$0.15^{+0.06}_{-0.06}$	$0.49^{+0.22}_{-0.22}$	$0.68^{+0.29}_{-0.29}$	...	...	...	21.13^c	...	...
267	GMASS-2562	$01.26^{+00.86}_{-00.85}$	$19.47^{+13.28}_{-13.07}$	2.00±1.50	$01.76^{+01.09}_{-01.34}$	$09.96^{+06.80}_{-06.69}$	$0.30^{+0.08}_{-0.08}$	$0.98^{+0.35}_{-0.35}$	$1.36^{+0.42}_{-0.42}$	...	...	...	20.72^c	...	...
268	Q1623-BX528	$02.31^{+01.01}_{-01.01}$	$35.63^{+15.59}_{-15.59}$	4.60±1.30	$10.63^{+01.21}_{-01.21}$	$23.29^{+10.19}_{-10.19}$	$0.15^{+0.06}_{-0.06}$	$0.49^{+0.22}_{-0.22}$	$0.68^{+0.29}_{-0.29}$	...	...	...	19.75^c	...	...
269	Q1623-BX663	$04.69^{+02.36}_{-02.36}$	$72.27^{+36.38}_{-36.38}$	4.70±1.10	$16.16^{+04.13}_{-04.13}$	$21.48^{+10.81}_{-10.81}$	$0.20^{+0.06}_{-0.06}$	$0.66^{+0.26}_{-0.26}$	$0.91^{+0.33}_{-0.33}$	...	...	...	19.92^c	...	...
270	SSA22a-MD41	$03.55^{+02.02}_{-02.02}$	$54.69^{+31.15}_{-31.15}$	4.30±1.00	$06.96^{+00.71}_{-00.82}$	$10.42^{+05.94}_{-05.94}$	$0.25^{+0.07}_{-0.07}$	$0.82^{+0.30}_{-0.30}$	$1.14^{+0.37}_{-0.37}$	...	...	...	20.42^c	...	...
271	Q2343-BX610	$06.77^{+03.41}_{-03.40}$	$104.26^{+52.45}_{-52.39}$	4.60±1.00	$16.56^{+01.88}_{-02.07}$	$34.29^{+17.25}_{-17.23}$	$0.20^{+0.06}_{-0.06}$	$0.66^{+0.26}_{-0.26}$	$0.91^{+0.33}_{-0.33}$	...	...	...	19.21^c	...	...
272	K20-ID5	$15.02^{+14.61}_{-14.61}$	$231.26^{+224.92}_{-224.92}$	4.70±1.10	$43.14^{+08.90}_{-09.21}$	$37.66^{+36.62}_{-36.62}$	$0.49^{+0.11}_{-0.11}$	$1.64^{+0.54}_{-0.54}$	$2.27^{+0.64}_{-0.64}$	...	...	...	19.04^c	...	...
273	K20-ID6	$01.43^{+00.82}_{-00.82}$	$22.03^{+12.62}_{-12.62}$	3.10±1.00	$02.98^{+00.92}_{-00.46}$	$12.20^{+06.98}_{-06.98}$	$0.25^{+0.07}_{-0.07}$	$0.82^{+0.30}_{-0.30}$	$1.14^{+0.37}_{-0.37}$	...	...	...	20.28^c	...	...
274	K20-ID7	$05.16^{+02.94}_{-02.94}$	$79.46^{+45.21}_{-45.21}$	5.30±1.20	$18.44^{+01.71}_{-01.92}$	$23.61^{+13.44}_{-13.44}$	$0.25^{+0.07}_{-0.07}$	$0.82^{+0.30}_{-0.30}$	$1.14^{+0.37}_{-0.37}$	...	...	...	19.61^c	...	...
275	K20-ID8	$02.41^{+01.22}_{-01.22}$	$37.12^{+18.72}_{-18.72}$	4.60±1.10	$09.32^{+01.41}_{-01.55}$	$16.75^{+08.44}_{-08.44}$	$0.20^{+0.06}_{-0.06}$	$0.66^{+0.26}_{-0.26}$	$0.91^{+0.33}_{-0.33}$	...	...	...	19.92^c	...	...
276	K20-ID9	$02.68^{+01.94}_{-01.94}$	$41.21^{+29.92}_{-29.96}$	6.90±1.50	$22.37^{+04.02}_{-03.48}$	$09.55^{+06.93}_{-06.94}$	$0.35^{+0.08}_{-0.08}$	$1.15^{+0.39}_{-0.39}$	$1.59^{+0.48}_{-0.48}$	...	...	...	20.40^c	...	...
277	Deep3a-4751	$01.86^{+01.07}_{-01.07}$	$28.70^{+16.49}_{-16.43}$	3.40±0.80	$02.92^{+00.88}_{-00.68}$	$15.89^{+09.13}_{-09.10}$	$0.25^{+0.07}_{-0.07}$	$0.82^{+0.30}_{-0.30}$	$1.14^{+0.37}_{-0.37}$	...	...	...	20.01^c	...	...
278	Deep3a-6004	$11.10^{+09.88}_{-09.88}$	$171.01^{+152.14}_{-152.10}$	5.90±1.40	$11.41^{+01.24}_{-01.24}$	$47.16^{+41.96}_{-41.95}$	$0.44^{+0.10}_{-0.10}$	$1.48^{+0.49}_{-0.49}$	$2.04^{+0.58}_{-0.58}$	...	...	...	19.10^c	...	...
279	Deep3a-15504	$07.72^{+04.39}_{-04.39}$	$118.92^{+67.62}_{-67.59}$	5.00±1.10	$12.73^{+01.55}_{-01.55}$	$39.11^{+22.24}_{-22.23}$	$0.25^{+0.07}_{-0.07}$	$0.82^{+0.30}_{-0.30}$	$1.14^{+0.37}_{-0.37}$	...	...	...	19.42^c	...	...
280	GMASS-1084	$01.02^{+01.44}_{-01.44}$	$15.78^{+22.25}_{-22.25}$	3.10±1.00	$04.68^{+01.31}_{-00.90}$	$06.06^{+08.55}_{-08.55}$	$0.74^{+0.15}_{-0.15}$	$2.46^{+0.78}_{-0.78}$	$3.41^{+0.92}_{-0.92}$	...	...	...	19.31^c	...	...

Continuation on the next page.

Table 2

Index	Name	L(Hβ) Corrected	SFR(Hβ) Corrected	r_e (kpc)	M_{dyn} (10^{10} $M_\odot$)	M_* (10^8 $M_\odot$)	E($B-V$) (mag)	A(Hα)	A(Hβ)	M_B (mag)	R (AB)	H (AB)	K (AB)	12 + log(O/H)	Method
281	GMASS-1146	$01.12^{+01.10}_{-01.09}$	$17.25^{+16.91}_{-16.84}$	< 4.7	< 09.66	$04.92^{+04.82}_{-04.81}$	$0.49^{+0.11}_{-0.11}$	$1.64^{+0.54}_{-0.54}$	$2.27^{+0.64}_{-0.64}$	...	...	...	20.01^{c}	...	...
282	GMASS-2113W	$00.58^{+00.66}_{-00.66}$	$08.89^{+10.24}_{-10.24}$	1.30±1.20	$07.12^{+13.64}_{-04.26}$	$06.51^{+07.50}_{-07.50}$	$0.59^{+0.13}_{-0.13}$	$1.97^{+0.63}_{-0.63}$	$2.72^{+0.75}_{-0.75}$	...	...	...	19.84^{c}	...	...
283	GMASS-2252	$02.26^{+01.30}_{-01.29}$	$34.82^{+19.97}_{-19.91}$	3.70±1.30	$08.55^{+03.03}_{-03.03}$	$13.38^{+07.68}_{-07.65}$	$0.25^{+0.07}_{-0.07}$	$0.82^{+0.30}_{-0.30}$	$1.14^{+0.37}_{-0.37}$	...	...	...	20.29^{c}	...	...
284	GMASS-2303	$01.39^{+00.55}_{-00.55}$	$21.46^{+08.42}_{-08.42}$	1.80±0.40	$02.48^{+00.36}_{-00.36}$	$08.25^{+03.23}_{-03.23}$	$0.10^{+0.05}_{-0.05}$	$0.33^{+0.19}_{-0.19}$	$0.46^{+0.26}_{-0.26}$	...	...	...	20.92^{c}	...	...
285	GMASS-2363	$01.12^{+00.75}_{-00.74}$	$17.26^{+11.55}_{-11.41}$	2.30±1.20	$04.87^{+04.40}_{-03.54}$	$08.13^{+05.44}_{-05.37}$	$0.30^{+0.08}_{-0.08}$	$0.98^{+0.35}_{-0.35}$	$1.36^{+0.42}_{-0.42}$	...	...	...	20.81^{c}	...	...
286	GMASS-2438	$01.42^{+01.14}_{-01.14}$	$21.80^{+17.57}_{-17.57}$	2.90±1.30	$09.74^{+01.83}_{-02.06}$	$07.64^{+06.16}_{-06.16}$	$0.40^{+0.09}_{-0.09}$	$1.31^{+0.44}_{-0.44}$	$1.82^{+0.53}_{-0.53}$	...	...	...	20.02^{c}	...	...
287	GMASS-2540	$00.92^{+00.42}_{-00.41}$	$14.15^{+06.41}_{-06.32}$	7.50±1.80	$05.58^{+01.67}_{-01.25}$	$09.59^{+04.34}_{-04.29}$	$0.15^{+0.06}_{-0.06}$	$0.49^{+0.22}_{-0.22}$	$0.68^{+0.29}_{-0.29}$	...	...	...	19.94^{c}	...	...
288	GMASS-2550	$00.41^{+00.22}_{-00.22}$	$06.33^{+03.37}_{-03.42}$	5.30±1.10	$02.52^{+10.45}_{-03.94}$	$04.81^{+02.56}_{-02.60}$	$0.20^{+0.06}_{-0.06}$	$0.66^{+0.26}_{-0.26}$	$0.91^{+0.33}_{-0.33}$	...	...	...	20.60^{c}	...	...
289	zCOSMOS-772759	$05.16^{+03.79}_{-03.76}$	$79.47^{+58.35}_{-57.88}$	...	...	$13.91^{+10.21}_{-10.13}$	$0.35^{+0.08}_{-0.08}$	$1.15^{+0.39}_{-0.39}$	$1.59^{+0.48}_{-0.48}$	...	...	...	20.15^{c}	...	...
290	zCOSMOS-782941	$06.53^{+04.23}_{-04.23}$	$100.53^{+65.19}_{-65.16}$	3.10±0.70	$10.54^{+01.48}_{-00.99}$	$21.75^{+14.11}_{-14.10}$	$0.30^{+0.08}_{-0.08}$	$0.98^{+0.35}_{-0.35}$	$1.36^{+0.42}_{-0.42}$	...	...	...	19.65^{c}	...	...
291	GDDSSA12-6339	$07.37^{+07.17}_{-07.16}$	$113.50^{+110.38}_{-110.33}$	2.40±0.70	$02.41^{+00.36}_{-00.31}$	$13.90^{+13.52}_{-13.51}$	$0.49^{+0.11}_{-0.11}$	$1.64^{+0.54}_{-0.54}$	$2.27^{+0.64}_{-0.64}$	...	...	...	20.15^{c}	...	...
292	zCOSMOS-400528	$05.38^{+02.31}_{-02.36}$	$82.86^{+35.62}_{-36.31}$	2.40±1.00	$13.63^{+08.88}_{-07.64}$	$48.78^{+20.97}_{-21.37}$	$0.49^{+0.03}_{-0.03}$	$0.93^{+0.24}_{-0.24}$	$1.29^{+0.26}_{-0.26}$	...	...	21.75±0.04	21.08±0.03	...	...
293	zCOSMOS-400569	$06.26^{+03.31}_{-03.33}$	$96.37^{+51.00}_{-51.35}$	5.80±1.40	$28.89^{+09.49}_{-10.88}$	$50.32^{+26.63}_{-26.81}$	$0.37^{+0.03}_{-0.03}$	$1.23^{+0.31}_{-0.31}$	$1.70^{+0.33}_{-0.33}$	...	...	21.29±0.03	20.69±0.02	...	...
294	zCOSMOS-403741	$01.83^{+01.07}_{-01.07}$	$28.25^{+16.50}_{-16.50}$	3.10±1.10	$02.66^{+00.43}_{-00.25}$	$12.25^{+07.15}_{-07.15}$	$0.42^{+0.03}_{-0.03}$	$1.40^{+0.35}_{-0.35}$	$1.93^{+0.36}_{-0.36}$	...	...	21.30±0.02	21.02±0.02	...	...
295	zCOSMOS-404221	$01.58^{+00.45}_{-00.46}$	$24.30^{+06.91}_{-07.11}$	2.30±1.70	$02.46^{+01.90}_{-00.98}$	$08.99^{+02.55}_{-02.63}$	$0.13^{+0.03}_{-0.03}$	$0.43^{+0.14}_{-0.14}$	$0.60^{+0.17}_{-0.17}$	...	...	22.83±0.08	22.44±0.09	...	...
296	zCOSMOS-404987	$01.56^{+00.62}_{-00.70}$	$24.06^{+09.50}_{-10.77}$	1.50±1.30	$02.99^{+01.96}_{-02.79}$	$06.86^{+02.71}_{-03.07}$	$0.23^{+0.03}_{-0.03}$	$0.76^{+0.21}_{-0.21}$	$1.06^{+0.23}_{-0.23}$	...	...	23.19±0.11	22.77±0.13	...	...
297	zCOSMOS-405081	$01.05^{+00.40}_{-00.42}$	$16.14^{+06.19}_{-06.49}$	5.50±1.40	$02.62^{+01.96}_{-01.72}$	$05.66^{+02.17}_{-02.27}$	$0.17^{+0.04}_{-0.04}$	$0.56^{+0.19}_{-0.19}$	$0.78^{+0.23}_{-0.23}$	...	...	23.40±0.15	22.91±0.16	...	...
298	zCOSMOS-405501	$02.28^{+00.81}_{-00.79}$	$35.07^{+12.54}_{-12.20}$	4.40±1.00	$07.86^{+04.06}_{-02.28}$	$10.78^{+03.86}_{-03.75}$	$0.19^{+0.03}_{-0.03}$	$0.63^{+0.18}_{-0.18}$	$0.87^{+0.21}_{-0.21}$	...	...	23.12±0.14	22.25±0.11	...	...
299	zCOSMOS-406690	$14.35^{+05.13}_{-05.13}$	$221.05^{+79.06}_{-79.00}$	4.90±1.40	$10.85^{+00.63}_{-00.63}$	$55.95^{+20.01}_{-19.99}$	$0.22^{+0.03}_{-0.03}$	$0.73^{+0.20}_{-0.20}$	$1.01^{+0.22}_{-0.22}$	...	...	21.11±0.02	20.81±0.03	...	...
300	zCOSMOS-407928	$03.04^{+01.56}_{-01.57}$	$46.86^{+24.01}_{-24.12}$	2.80±0.90	$10.31^{+21.44}_{-09.96}$	$12.29^{+06.30}_{-06.33}$	$0.30^{+0.04}_{-0.04}$	$1.00^{+0.27}_{-0.27}$	$1.38^{+0.30}_{-0.30}$	...	...	23.25±0.12	22.63±0.13	...	...
301	zCOSMOS-410041	$03.64^{+01.40}_{-01.37}$	$56.03^{+21.50}_{-21.04}$	5.90±1.50	$16.26^{+16.90}_{-12.67}$	$05.92^{+02.27}_{-02.22}$	$0.18^{+0.03}_{-0.03}$	$0.60^{+0.18}_{-0.18}$	$0.83^{+0.20}_{-0.20}$	...	...	22.77±0.08	23.16±0.18	...	...
302	zCOSMOS-410542	$02.70^{+01.62}_{-01.64}$	$41.60^{+25.00}_{-25.21}$	4.10±1.50	$38.98^{+10.63}_{-17.45}$	$18.04^{+10.84}_{-10.93}$	$0.43^{+0.03}_{-0.03}$	$1.43^{+0.36}_{-0.36}$	$1.98^{+0.37}_{-0.37}$	...	...	20.86±0.02	20.60±0.02	...	...
303	zCOSMOS-411737	$02.51^{+00.81}_{-00.79}$	$38.68^{+12.50}_{-12.23}$	2.00±0.80	$02.61^{+01.48}_{-00.74}$	$09.79^{+03.16}_{-03.09}$	$0.17^{+0.03}_{-0.03}$	$0.56^{+0.17}_{-0.17}$	$0.78^{+0.19}_{-0.19}$	...	...	23.00±0.12	22.81±0.15	...	...
304	zCOSMOS-412369	$06.02^{+02.95}_{-02.95}$	$92.73^{+45.40}_{-45.40}$	2.30±1.00	$04.73^{+00.64}_{-00.64}$	$30.50^{+14.93}_{-14.93}$	$0.34^{+0.03}_{-0.03}$	$1.13^{+0.30}_{-0.30}$	$1.56^{+0.30}_{-0.30}$	...	...	21.85±0.04	21.39±0.05	...	...
305	zCOSMOS-413507	$01.96^{+01.16}_{-00.94}$	$30.21^{+17.88}_{-14.46}$	4.10±1.00	$01.89^{+07.45}_{-02.10}$	$11.61^{+06.87}_{-05.56}$	$0.31^{+0.03}_{-0.03}$	$1.03^{+0.27}_{-0.27}$	$1.42^{+0.28}_{-0.28}$	...	...	22.77±0.08	22.52±0.11	...	...
306	zCOSMOS-413597	$02.85^{+01.38}_{-01.37}$	$43.84^{+21.21}_{-21.08}$	2.50±1.00	$01.55^{+00.93}_{-02.04}$	$13.03^{+06.30}_{-06.26}$	$0.31^{+0.03}_{-0.03}$	$1.03^{+0.27}_{-0.27}$	$1.42^{+0.28}_{-0.28}$	...	...	22.96±0.09	22.58±0.11	...	...
307	zCOSMOS-415087	$00.70^{+00.40}_{-00.36}$	$10.77^{+06.16}_{-05.51}$	< 2.2	< 02.36	$09.48^{+05.42}_{-04.85}$	$0.25^{+0.04}_{-0.04}$	$0.83^{+0.24}_{-0.24}$	$1.15^{+0.27}_{-0.27}$	...	...	22.94±0.11	22.87±0.16	...	...
308	zCOSMOS-415876	$01.36^{+00.64}_{-00.62}$	$20.88^{+09.91}_{-09.57}$	2.70±0.90	$04.22^{+02.04}_{-01.67}$	$15.30^{+07.26}_{-07.01}$	$0.30^{+0.03}_{-0.03}$	$1.00^{+0.26}_{-0.26}$	$1.38^{+0.28}_{-0.28}$	...	...	22.73±0.08	22.38±0.11	...	...
309	zCOSMOS-700882	...	...	1.02	...	...	...	...	...	-18.90	...	...	...	...	...
310	zCOSMOS-701051	...	...	1.48	...	...	...	...	...	-18.06	...	...	...	...	...
311	zCOSMOS-701741	...	...	...	...	...	...	...	...	-18.94	...	...	...	$7.46^{+0.15}_{-0.15}$	Te
312	zCOSMOS-800984	...	...	1.54	...	...	...	...	...	-19.04	...	...	...	$7.95^{+0.07}_{-0.07}$	Te
313	zCOSMOS-801094	...	...	...	...	...	...	...	...	-19.27	...	...	...	$8.14^{+0.10}_{-0.10}$	R23
314	zCOSMOS-802275	...	...	2.22	...	...	...	...	...	-19.93	...	...	...	$8.18^{+0.06}_{-0.06}$	R23
315	zCOSMOS-803226	...	...	1.72	...	...	...	...	...	-19.50	...	...	...	$7.87^{+0.10}_{-0.10}$	Te
316	zCOSMOS-803892	...	...	1.43	...	...	...	...	...	-18.96	...	...	...	...	...
317	zCOSMOS-804130	...	...	2.21	...	...	...	...	...	-20.08	...	...	...	$8.53^{+0.12}_{-0.12}$	N2
318	zCOSMOS-804791	...	...	2.02	...	...	...	...	...	-20.65	...	...	...	$8.29^{+0.16}_{-0.16}$	R23
319	zCOSMOS-805200	...	...	0.48	...	...	...	...	...	-19.30	...	...	...	$8.01^{+0.09}_{-0.09}$	Te-Z calibration
320	zCOSMOS-806881	...	...	1.00	...	...	...	...	...	-20.38	...	...	...	$8.21^{+0.05}_{-0.05}$	Te

Continuation on the next page.

Table 2

Index	Name	L(Hβ) Corrected	SFR(Hβ) Corrected	r_e (kpc)	M_{dyn} (10^{10} $M_\odot$)	M_* (10^8 $M_\odot$)	$E(B-V)$ (mag)	A(Hα)	A(Hβ)	M_B (mag)	R (AB)	H (AB)	K (AB)	12 + log(O/H)	Method
321	zCOSMOS-806958	...	...	1.17	...	...	...	...	...	-20.82	...	...	...	$8.11^{+0.03}_{-0.03}$	Te
322	zCOSMOS-807965	...	...	...	...	...	...	...	...	...	...	...	...	$8.33^{+0.14}_{-0.14}$	R23
323	zCOSMOS-807990	...	...	1.86	...	...	...	...	...	-19.19	...	...	...	$8.14^{+0.20}_{-0.20}$	R23
324	zCOSMOS-809215	...	...	1.49	...	...	...	...	...	-17.18	...	...	...	$7.65^{+0.07}_{-0.07}$	N2
325	zCOSMOS-809399	...	...	1.04	...	...	...	...	...	-20.08	...	...	...	$7.99^{+0.08}_{-0.08}$	Te-Z calibration
326	zCOSMOS-809463	...	...	2.06	...	...	...	...	...	-20.89	...	...	...	$8.22^{+0.08}_{-0.08}$	Te
327	zCOSMOS-809944	...	...	1.06	...	...	...	...	...	-16.51	...	...	...	$8.09^{+0.07}_{-0.07}$	N2
328	zCOSMOS-810153	...	...	0.70	...	...	...	...	...	-19.82	...	...	...	$8.10^{+0.08}_{-0.08}$	Te
329	zCOSMOS-810220	...	...	1.76	...	...	...	...	...	-20.35	...	...	...	$8.14^{+0.09}_{-0.09}$	R23
330	zCOSMOS-810304	...	...	1.24	...	...	...	...	...	-18.62	...	...	...	$8.44^{+0.07}_{-0.07}$	N2
331	zCOSMOS-810646	...	...	2.58	...	...	...	...	...	-17.91	...	...	...	$8.14^{+0.04}_{-0.04}$	N2
332	zCOSMOS-811012	...	...	0.72	...	...	...	...	...	-21.16	...	...	...	$8.40^{+0.10}_{-0.10}$	R23
333	zCOSMOS-811024	...	...	1.13	...	...	...	...	...	-20.66	...	...	...	$8.17^{+0.24}_{-0.24}$	R23
334	zCOSMOS-811075	...	...	1.71	...	...	...	...	...	-20.47	...	...	...	$8.18^{+0.21}_{-0.21}$	R23
335	zCOSMOS-811415	...	...	1.46	...	...	...	...	...	-20.29	...	...	...	$8.15^{+0.10}_{-0.10}$	R23
336	zCOSMOS-811842	...	...	0.64	...	...	...	...	...	-20.70	...	...	...	$8.27^{+0.10}_{-0.10}$	Te
337	zCOSMOS-812047	...	...	3.30	...	...	...	...	...	-19.87	...	...	...	$7.85^{+0.04}_{-0.04}$	N2
338	zCOSMOS-812087	...	...	2.80	...	...	...	...	...	-18.05	...	...	...	$8.18^{+0.13}_{-0.13}$	N2
339	zCOSMOS-812195	...	...	2.03	...	...	...	...	...	-20.09	...	...	...	$8.16^{+0.08}_{-0.08}$	Te-Z calibration
340	zCOSMOS-812207	...	...	1.18	...	...	...	...	...	-16.67	...	...	...	$8.06^{+0.07}_{-0.07}$	N2
341	zCOSMOS-812599	...	...	1.25	...	...	...	...	...	-17.56	...	...	...	$8.27^{+0.08}_{-0.08}$	N2
342	zCOSMOS-812879	...	...	1.80	...	...	...	...	...	-19.80	...	...	...	$8.30^{+0.02}_{-0.02}$	N2
343	zCOSMOS-812971	...	...	3.84	...	...	...	...	...	-17.51	...	...	...	$7.89^{+0.04}_{-0.04}$	N2
344	zCOSMOS-813334	...	...	1.38	...	...	...	...	...	-20.15	...	...	...	$8.18^{+0.07}_{-0.07}$	Te-Z calibration
345	zCOSMOS-813400	...	...	0.67	...	...	...	...	...	-19.09	...	...	...	...	...
346	zCOSMOS-813444	...	...	0.66	...	...	...	...	...	-16.19	...	...	...	$7.93^{+0.10}_{-0.10}$	N2
347	zCOSMOS-813723	...	...	1.23	...	...	...	...	...	-19.00	...	...	...	$8.23^{+0.07}_{-0.07}$	N2
348	zCOSMOS-813894	...	...	1.56	...	...	...	...	...	-19.57	...	...	...	$8.08^{+0.07}_{-0.07}$	Te-Z calibration
349	zCOSMOS-814092	...	...	0.66	...	...	...	...	...	-19.47	...	...	...	$8.07^{+0.07}_{-0.07}$	Te-Z calibration
350	zCOSMOS-814148	...	...	2.17	...	...	...	...	...	-18.79	...	...	...	...	...
351	zCOSMOS-814386	...	...	0.52	...	...	...	...	...	-17.30	...	...	...	$8.19^{+0.05}_{-0.05}$	N2
352	zCOSMOS-815797	...	...	2.10	...	...	...	...	...	-20.30	...	...	...	$7.93^{+0.06}_{-0.06}$	Te
353	zCOSMOS-815800	...	...	0.98	...	...	...	...	...	-20.74	...	...	...	$8.46^{+0.05}_{-0.05}$	R23
354	zCOSMOS-815804	...	...	0.81	...	...	...	...	...	-19.38	...	...	...	$8.33^{+0.05}_{-0.05}$	R23
355	zCOSMOS-816839	...	...	3.09	...	...	...	...	...	-18.69	...	...	...	...	...
356	zCOSMOS-817226	...	...	1.47	...	...	...	...	...	-19.46	...	...	...	$8.38^{+0.05}_{-0.05}$	R23
357	zCOSMOS-817306	...	...	1.81	...	...	...	...	...	-18.66	...	...	...	$8.37^{+0.08}_{-0.08}$	N2
358	zCOSMOS-817804	...	...	0.50	...	...	...	...	...	-20.86	...	...	...	$8.36^{+0.03}_{-0.03}$	R23
359	zCOSMOS-817820	...	...	1.80	...	...	...	...	...	-19.98	...	...	...	$8.20^{+0.15}_{-0.15}$	R23
360	zCOSMOS-819298	...	...	1.40	...	...	...	...	...	-18.44	...	...	...	$7.82^{+0.07}_{-0.07}$	N2

Continuation on the next page.

Table 2

Index	Name	L(Hβ) Corrected	SFR(Hβ) Corrected	r$_e$ (kpc)	M$_{dyn}$ (10^{10} M$_\odot$)	M$_*$ (10^8 M$_\odot$)	E($B-V$) (mag)	A(Hα)	A(Hβ)	M$_B$ (mag)	R (AB)	H (AB)	K (AB)	12 + log(O/H)	Method
361	zCOSMOS-819574	...	...	0.80	...	...	...	...	...	-20.86	...	...	...	$8.13^{+0.05}_{-0.05}$	Te
362	zCOSMOS-820061	...	...	2.16	...	...	...	...	...	-20.10	...	...	...	$8.15^{+0.10}_{-0.10}$	R23
363	zCOSMOS-820087	...	...	2.79	...	...	...	...	...	-20.44	...	...	...	$8.16^{+0.10}_{-0.10}$	R23
364	zCOSMOS-820163	...	...	1.22	...	...	...	...	...	-20.44	...	...	...	$8.40^{+0.05}_{-0.05}$	R23
365	zCOSMOS-820424	...	...	1.13	...	...	...	...	...	-19.22	...	...	...	$8.00^{+0.08}_{-0.08}$	N2
366	zCOSMOS-820575	...	...	0.88	...	...	...	...	...	-18.85	...	...	...	$7.93^{+0.06}_{-0.06}$	Te
367	zCOSMOS-820600	...	...	1.17	...	...	...	...	...	-19.64	...	...	...	$8.17^{+0.12}_{-0.12}$	R23
368	zCOSMOS-821098	...	...	0.65	...	...	...	...	...	-18.39	...	...	...	$8.26^{+0.03}_{-0.03}$	N2
369	zCOSMOS-821693	...	...	...	...	...	...	...	...	-20.24	...	...	...	$8.14^{+0.03}_{-0.03}$	Te
370	zCOSMOS-822429	...	...	1.31	...	...	...	...	...	-19.93	...	...	...	$8.18^{+0.14}_{-0.14}$	R23
371	zCOSMOS-822504	...	...	1.03	...	...	...	...	...	-20.61	...	...	...	$8.19^{+0.18}_{-0.18}$	R23
372	zCOSMOS-822723	...	...	2.46	...	...	...	...	...	-17.68	...	...	...	$8.10^{+0.05}_{-0.05}$	N2
373	zCOSMOS-822960	...	...	1.74	...	...	...	...	...	-20.75	...	...	...	$8.18^{+0.10}_{-0.10}$	R23
374	zCOSMOS-823087	...	...	1.14	...	...	...	...	...	-20.77	...	...	...	$8.16^{+0.11}_{-0.11}$	R23
375	zCOSMOS-823693	...	...	0.37	...	...	...	...	...	-21.14	...	...	...	$8.16^{+0.04}_{-0.04}$	R23
376	zCOSMOS-823694	...	...	...	...	...	...	...	...	...	...	...	...	$8.17^{+0.05}_{-0.05}$	R23
377	zCOSMOS-824210	...	...	1.50	...	...	...	...	...	-15.53	...	...	...	$7.90^{+0.06}_{-0.06}$	N2
378	zCOSMOS-824225	...	...	2.00	...	...	...	...	...	-17.94	...	...	...	$8.10^{+0.04}_{-0.04}$	N2
379	zCOSMOS-824503	...	...	1.35	...	...	...	...	...	-20.40	...	...	...	$8.18^{+0.12}_{-0.12}$	R23
380	zCOSMOS-824584	...	...	1.15	...	...	...	...	...	-19.27	...	...	...	...	...
381	zCOSMOS-825278	...	...	2.30	...	...	...	...	...	-16.49	...	...	...	$8.00^{+0.11}_{-0.11}$	N2
382	zCOSMOS-825921	...	...	0.98	...	...	...	...	...	-20.01	...	...	...	$7.75^{+0.08}_{-0.08}$	Te
383	zCOSMOS-825959	...	...	0.89	...	...	...	...	...	-20.04	...	...	...	$7.56^{+0.12}_{-0.12}$	Te
384	zCOSMOS-826050	...	...	0.73	...	...	...	...	...	-20.75	...	...	...	$8.16^{+0.16}_{-0.16}$	R23
385	zCOSMOS-826076	...	...	2.58	...	...	...	...	...	-17.37	...	...	...	$7.91^{+0.07}_{-0.07}$	N2
386	zCOSMOS-826191	...	...	0.75	...	...	...	...	...	-19.66	...	...	...	$8.03^{+0.06}_{-0.06}$	N2
387	zCOSMOS-826195	...	...	1.14	...	...	...	...	...	-20.54	...	...	...	$8.34^{+0.05}_{-0.05}$	R23
388	zCOSMOS-827073	...	...	1.64	...	...	...	...	...	-17.59	...	...	...	$8.22^{+0.05}_{-0.05}$	N2
389	zCOSMOS-827326	...	...	1.60	...	...	...	...	...	-20.75	...	...	...	$8.40^{+0.04}_{-0.04}$	R23
390	zCOSMOS-828338	...	...	2.53	...	...	...	...	...	-20.36	...	...	...	$8.47^{+0.03}_{-0.03}$	R23
391	zCOSMOS-829725	...	...	0.74	...	...	...	...	...	-20.50	...	...	...	$8.39^{+0.13}_{-0.13}$	R23
392	zCOSMOS-829868	...	...	0.17	...	...	...	...	...	-18.63	...	...	...	$7.79^{+0.03}_{-0.03}$	Te
393	zCOSMOS-829923	...	...	1.27	...	...	...	...	...	-17.80	...	...	...	$8.29^{+0.06}_{-0.06}$	N2
394	zCOSMOS-830132	...	...	2.42	...	...	...	...	...	-20.52	...	...	...	$7.89^{+0.12}_{-0.12}$	Te-Z calibration
395	zCOSMOS-830321	...	...	1.04	...	...	...	...	...	-20.79	...	...	...	$8.11^{+0.12}_{-0.12}$	R23
396	zCOSMOS-830751	...	...	0.68	...	...	...	...	...	-18.91	...	...	...	$7.88^{+0.04}_{-0.04}$	N2
397	zCOSMOS-831158	...	...	1.23	...	...	...	...	...	-18.56	...	...	...	$8.49^{+0.02}_{-0.02}$	N2
398	zCOSMOS-831178	...	...	0.77	...	...	...	...	...	-17.65	...	...	...	...	...
399	zCOSMOS-831397	...	...	1.30	...	...	...	...	...	-20.77	...	...	...	$8.30^{+0.10}_{-0.10}$	R23
400	zCOSMOS-831498	...	...	1.56	...	...	...	...	...	-19.56	...	...	...	$7.96^{+0.06}_{-0.06}$	Te

Continuation on the next page.

Table 2

Index	Name	L(Hβ) Corrected	SFR(Hβ) Corrected	r_e (kpc)	M_{dyn} (10^{10} $M_\odot$)	M_* (10^8 $M_\odot$)	$E(B-V)$ (mag)	A(Hα)	A(Hβ)	M_B (mag)	R (AB)	H (AB)	K (AB)	12 + log(O/H)	Method
401	zCOSMOS-831622	...	...	2.10	...	...	...	...	...	-21.74	...	...	...	$7.76^{+0.09}_{-0.09}$	Te
402	zCOSMOS-831713	...	...	2.26	...	...	...	...	...	-19.00	...	...	...	...	...
403	zCOSMOS-831791	...	...	4.05	...	...	...	...	...	-18.52	...	...	...	$8.33^{+0.04}_{-0.04}$	N2
404	zCOSMOS-831824	...	...	0.88	...	...	...	...	...	-20.89	...	...	...	$8.17^{+0.07}_{-0.07}$	R23
405	zCOSMOS-831940	...	...	0.78	...	...	...	...	...	-16.34	...	...	...	$8.00^{+0.07}_{-0.07}$	N2
406	zCOSMOS-832077	...	...	1.09	...	...	...	...	...	-19.50	...	...	...	$8.17^{+0.07}_{-0.07}$	R23
407	zCOSMOS-832097	...	...	9.31	...	...	...	...	...	-18.66	...	...	...	$8.11^{+0.07}_{-0.07}$	N2
408	zCOSMOS-832539	...	...	0.52	...	...	...	...	...	-20.44	...	...	...	$8.41^{+0.10}_{-0.10}$	R23
409	zCOSMOS-832898	...	...	1.22	...	...	...	...	...	-19.53	...	...	...	$7.86^{+0.11}_{-0.11}$	Te-Z calibration
410	zCOSMOS-833022	...	...	0.11	...	...	...	...	...	-18.91	...	...	...	...	...
411	zCOSMOS-833044	...	...	2.83	...	...	...	...	...	-19.42	...	...	...	$8.03^{+0.08}_{-0.08}$	N2
412	zCOSMOS-833222	...	...	1.51	...	...	...	...	...	-19.01	...	...	...	$8.28^{+0.15}_{-0.15}$	R23
413	zCOSMOS-834100	...	...	0.20	...	...	...	...	...	-20.73	...	...	...	$8.44^{+0.03}_{-0.03}$	R23
414	zCOSMOS-834172	...	...	2.22	...	...	...	...	...	-20.38	...	...	...	$8.15^{+0.11}_{-0.11}$	R23
415	zCOSMOS-834906	...	...	1.17	...	...	...	...	...	-18.19	...	...	...	$7.91^{+0.09}_{-0.09}$	Te-Z calibration
416	zCOSMOS-836042	...	...	1.46	...	...	...	...	...	-20.63	...	...	...	$8.17^{+0.10}_{-0.10}$	R23
417	zCOSMOS-836108	...	...	1.72	...	...	...	...	...	-18.46	...	...	...	$7.47^{+0.10}_{-0.10}$	Te-Z calibration
418	zCOSMOS-836228	...	...	0.67	...	...	...	...	...	-17.11	...	...	...	$8.19^{+0.03}_{-0.03}$	N2
419	zCOSMOS-836232	...	...	1.30	...	...	...	...	...	-18.33	...	...	...	$8.07^{+0.08}_{-0.08}$	Te-Z calibration
420	zCOSMOS-836338	...	...	1.18	...	...	...	...	...	-20.42	...	...	...	...	...
421	zCOSMOS-836632	...	...	1.11	...	...	...	...	...	-20.53	...	...	...	$7.77^{+0.09}_{-0.09}$	Te-Z calibration
422	zCOSMOS-837240	...	...	2.25	...	...	...	...	...	-20.47	...	...	...	$8.02^{+0.07}_{-0.07}$	Te-Z calibration
423	zCOSMOS-837330	...	...	2.77	...	...	...	...	...	-18.53	...	...	...	$7.76^{+0.12}_{-0.12}$	N2
424	zCOSMOS-837582	...	...	0.96	...	...	...	...	...	-20.43	...	...	...	$8.13^{+0.12}_{-0.12}$	R23
425	zCOSMOS-837610	...	...	1.17	...	...	...	...	...	-19.21	...	...	...	$7.93^{+0.09}_{-0.09}$	Te
426	zCOSMOS-838357	...	...	0.89	...	...	...	...	...	-20.35	...	...	...	$8.18^{+0.19}_{-0.19}$	R23
427	zCOSMOS-838843	...	...	...	...	...	...	...	...	...	...	...	...	$7.99^{+0.08}_{-0.08}$	Te-Z calibration
428	zCOSMOS-839293	...	...	2.49	...	...	...	...	...	-17.36	...	...	...	$8.08^{+0.03}_{-0.03}$	N2
429	zCOSMOS-839458	...	...	0.90	...	...	...	...	...	-20.78	...	...	...	$8.43^{+0.04}_{-0.04}$	R23
430	zCOSMOS-839488	...	...	2.20	...	...	...	...	...	-18.40	...	...	...	$8.33^{+0.06}_{-0.06}$	N2
431	zCOSMOS-839539	...	...	1.29	...	...	...	...	...	-18.62	...	...	...	$8.34^{+0.06}_{-0.06}$	N2
432	zCOSMOS-840004	...	...	2.36	...	...	...	...	...	-19.55	...	...	...	$8.06^{+0.08}_{-0.08}$	Te-Z calibration
433	zCOSMOS-840051	...	...	1.36	...	...	...	...	...	-17.79	...	...	...	$7.69^{+0.08}_{-0.08}$	R23
434	zCOSMOS-840109	...	...	0.35	...	...	...	...	...	-17.14	...	...	...	...	...
435	zCOSMOS-840247	...	...	0.38	...	...	...	...	...	-20.51	...	...	...	$7.87^{+0.13}_{-0.13}$	Te
436	zCOSMOS-840599	...	...	...	...	...	...	...	...	-19.12	...	...	...	...	...
437	zCOSMOS-840688	...	...	...	...	...	...	...	...	-19.47	...	...	...	$7.96^{+0.10}_{-0.10}$	Te-Z calibration
438	zCOSMOS-840845	...	...	1.99	...	...	...	...	...	-18.29	...	...	...	$7.78^{+0.08}_{-0.08}$	N2
439	zCOSMOS-840962	...	...	0.73	...	...	...	...	...	-16.51	...	...	...	$7.35^{+0.11}_{-0.11}$	N2
440	zCOSMOS-840971	...	...	0.97	...	...	...	...	...	-19.38	...	...	...	$8.11^{+0.08}_{-0.08}$	Te-Z calibration

Continuation on the next page.

Table 2

Index	Name	L(Hβ) Corrected	SFR(Hβ) Corrected	r$_e$ (kpc)	M$_{dyn}$ (10^{10} M$_\odot$)	M$_*$ (10^8 M$_\odot$)	E($B-V$) (mag)	A(Hα)	A(Hβ)	M$_B$ (mag)	R (AB)	H (AB)	K (AB)	12 + log(O/H)	Method
441	zCOSMOS-840973	...	...	1.66	...	...	...	...	...	-17.12	...	...	...	$8.13^{+0.07}_{-0.07}$	N2
442	zCOSMOS-841104	...	...	2.29	...	...	...	...	...	-16.86	...	...	...	...	...
443	zCOSMOS-841150	...	...	6.21	...	...	...	...	...	-21.23	...	...	...	$8.16^{+0.07}_{-0.07}$	Te-Z calibration
444	zCOSMOS-841493	...	...	2.57	...	...	...	...	...	-17.28	...	...	...	$8.24^{+0.06}_{-0.06}$	N2
445	zCOSMOS-841554	...	...	1.18	...	...	...	...	...	-17.79	...	...	...	$8.33^{+0.05}_{-0.05}$	N2
446	zCOSMOS-841564	...	...	0.97	...	...	...	...	...	-16.50	...	...	...	$8.12^{+0.08}_{-0.08}$	N2
447	zCOSMOS-841642	...	...	2.64	...	...	...	...	...	-21.49	...	...	...	$8.34^{+0.14}_{-0.14}$	R23
448	zCOSMOS-841690	...	...	0.54	...	...	...	...	...	-20.62	...	...	...	$8.17^{+0.07}_{-0.07}$	Te
449	zCOSMOS-842700	...	...	2.04	...	...	...	...	...	-16.85	...	...	...	$8.07^{+0.08}_{-0.08}$	N2
450	zCOSMOS-842947	...	...	1.26	...	...	...	...	...	-17.47	...	...	...	$7.93^{+0.10}_{-0.10}$	N2
451	zCOSMOS-843208	...	...	1.30	...	...	...	...	...	-19.39	...	...	...	$8.52^{+0.08}_{-0.08}$	N2
452	zCOSMOS-843329	...	...	0.93	...	...	...	...	...	-20.99	...	...	...	$8.11^{+0.02}_{-0.02}$	Te
453	zCOSMOS-843573	...	...	1.57	...	...	...	...	...	-21.41	...	...	...	$7.92^{+0.08}_{-0.08}$	Te
454	zCOSMOS-843933	...	...	1.76	...	...	...	...	...	-21.51	...	...	...	$8.16^{+0.04}_{-0.04}$	R23
455	zCOSMOS-844465	...	...	1.28	...	...	...	...	...	-20.12	...	...	...	$8.31^{+0.09}_{-0.09}$	R23
456	zCOSMOS-844480	...	...	2.70	...	...	...	...	...	-20.98	...	...	...	$8.16^{+0.05}_{-0.05}$	R23
457	zCOSMOS-844783	...	...	1.45	...	...	...	...	...	-20.66	...	...	...	$8.15^{+0.03}_{-0.03}$	Te
458	zCOSMOS-844972	...	...	0.67	...	...	...	...	...	-19.79	...	...	...	$7.96^{+0.05}_{-0.05}$	Te
459	zCOSMOS-845045	...	...	2.00	...	...	...	...	...	-18.10	...	...	...	$8.16^{+0.10}_{-0.10}$	N2
460	zCOSMOS-845785	...	...	1.91	...	...	...	...	...	-19.04	...	...	...	...	...
461	zCOSMOS-845804	...	...	2.26	...	...	...	...	...	-20.30	...	...	...	$8.16^{+0.05}_{-0.05}$	R23
462	zCOSMOS-846604	...	...	0.47	...	...	...	...	...	-21.00	...	...	...	$8.02^{+0.07}_{-0.07}$	Te
463	zCOSMOS-846749	...	...	...	...	...	...	...	...	-16.88	...	...	...	$8.07^{+0.12}_{-0.12}$	N2
464	zCOSMOS-846799	...	...	1.01	...	...	...	...	...	-20.81	...	...	...	$8.45^{+0.06}_{-0.06}$	R23
465	zCOSMOS-847264	...	...	0.60	...	...	...	...	...	-19.66	...	...	...	...	...
466	zCOSMOS-847277	...	...	1.85	...	...	...	...	...	-19.44	...	...	...	$8.37^{+0.16}_{-0.16}$	R23
467	zCOSMOS-847434	...	...	0.46	...	...	...	...	...	-20.34	...	...	...	$8.33^{+0.22}_{-0.22}$	R23
468	zCOSMOS-847735	...	...	1.22	...	...	...	...	...	-20.22	...	...	...	$7.90^{+0.08}_{-0.08}$	Te-Z calibration
469	zCOSMOS-848170	...	...	1.42	...	...	...	...	...	-21.80	...	...	...	$8.20^{+0.15}_{-0.15}$	R23
470	zCOSMOS-849222	...	...	...	...	...	...	...	...	-21.05	...	...	...	$8.31^{+0.09}_{-0.09}$	R23
471	zCOSMOS-849272	...	...	...	...	...	...	...	...	-20.13	...	...	...	$8.17^{+0.05}_{-0.05}$	Te
472	zCOSMOS-849619	...	...	1.62	...	...	...	...	...	-18.51	...	...	...	$8.28^{+0.03}_{-0.03}$	N2
473	zCOSMOS-850262	...	...	1.80	...	...	...	...	...	-20.62	...	...	...	$8.17^{+0.11}_{-0.11}$	R23
474	VUDS520276545	$00.26^{+00.07}_{-00.07}$ [a]	$03.98^{+01.09}_{-01.09}$ [a]	...	...	$01.14^{+00.31}_{-00.31}$ [b]	...	...	...	-17.90	...	...	24.90^{d}	$8.06^{+0.23}_{-0.23}$	R23
475	VUDS520281627	$00.07^{+00.02}_{-00.02}$ [a]	$01.06^{+00.34}_{-00.34}$ [a]	...	...	$00.35^{+00.11}_{-00.11}$ [b]	...	...	...	-17.30	...	...	23.59^{d}	$8.21^{+0.14}_{-0.14}$	R23
476	VUDS520290391	$00.19^{+00.04}_{-00.04}$ [a]	$02.95^{+00.60}_{-00.60}$ [a]	...	...	$00.48^{+00.10}_{-00.10}$ [b]	...	...	...	-17.50	...	...	24.93^{d}	$7.79^{+0.15}_{-0.15}$	R23
477	VUDS520246239	$00.11^{+00.03}_{-00.03}$ [a]	$01.66^{+00.40}_{-00.40}$ [a]	...	...	$00.64^{+00.15}_{-00.15}$ [b]	...	...	...	-17.70	...	...	24.24^{d}	$8.22^{+0.16}_{-0.16}$	R23
478	VUDS520327062	$00.18^{+00.05}_{-00.05}$ [a]	$02.78^{+00.76}_{-00.76}$ [a]	...	...	$00.91^{+00.25}_{-00.25}$ [b]	...	...	...	-18.20	...	...	23.93^{d}	$7.96^{+0.16}_{-0.16}$	R23
479	VUDS520388031	$00.13^{+00.03}_{-00.03}$ [a]	$01.98^{+00.54}_{-00.54}$ [a]	...	...	$00.56^{+00.15}_{-00.15}$ [b]	...	...	...	-17.10	...	...	24.19^{d}	$8.24^{+0.16}_{-0.16}$	R23
480	VUDS520420821	$00.20^{+00.05}_{-00.05}$ [a]	$03.09^{+00.76}_{-00.76}$ [a]	...	...	$00.31^{+00.08}_{-00.08}$ [b]	...	...	...	-17.50	...	...	23.54^{d}	$8.03^{+0.08}_{-0.08}$	Te

Continuation on the next page.

Table 2

Index	Name	L(Hβ) Corrected	SFR(Hβ) Corrected	r$_e$ (kpc)	M$_{dyn}$ (10^{10} M$_\odot$)	M$_*$ (10^8 M$_\odot$)	E($B-V$) (mag)	A(Hα)	A(Hβ)	M$_B$ (mag)	R (AB)	H (AB)	K (AB)	12 + log(O/H)	Method
481	VUDS520349673	$00.14^{+00.04}_{-00.04}$ [a]	$02.09^{+00.55}_{-00.55}$ [a]	...	...	$00.80^{+00.21}_{-00.21}$ [b]	...	...	...	-17.80	...	...	23.62[d]	$7.79^{+0.17}_{-0.17}$	Te
482	VUDS520316717	$00.20^{+00.04}_{-00.04}$ [a]	$03.04^{+00.62}_{-00.62}$ [a]	...	...	$00.87^{+00.18}_{-00.18}$ [b]	...	...	...	-18.10	...	...	24.21[d]	$7.96^{+0.16}_{-0.16}$	R23
483	VUDS520433508	$00.23^{+00.07}_{-00.07}$ [a]	$03.62^{+01.07}_{-01.07}$ [a]	...	...	...	...	...	...	-18.00	...	...	24.78[d]	$8.06^{+0.21}_{-0.21}$	R23
484	VUDS520344687	$00.25^{+00.09}_{-00.09}$ [a]	$03.84^{+01.33}_{-01.33}$ [a]	...	...	$00.77^{+00.27}_{-00.27}$ [b]	...	...	...	-17.60	...	...	24.97[d]	$7.92^{+0.21}_{-0.21}$	R23
485	VUDS530076899	$00.01^{+00.00}_{-00.00}$ [a]	$00.11^{+00.04}_{-00.04}$ [a]	...	...	$00.02^{+00.01}_{-00.01}$ [b]	...	...	...	-15.60	...	...	25.39[d]	$8.23^{+0.23}_{-0.23}$	R23
486	VUDS530076254	$00.01^{+00.00}_{-00.00}$ [a]	$00.15^{+00.08}_{-00.08}$ [a]	...	...	$00.06^{+00.03}_{-00.03}$ [b]	...	...	...	-15.10	...	...	24.54[d]	$8.32^{+0.16}_{-0.16}$	R23
487	VUDS530080539	$00.57^{+00.11}_{-00.11}$ [a]	$08.82^{+01.72}_{-01.72}$ [a]	...	...	$02.13^{+00.42}_{-00.42}$ [b]	...	...	...	-18.80	...	...	24.43[d]	$8.31^{+0.20}_{-0.20}$	R23
488	VUDS530053182	$00.25^{+00.08}_{-00.08}$ [a]	$03.89^{+01.32}_{-01.32}$ [a]	...	...	$00.33^{+00.11}_{-00.11}$ [b]	...	...	...	-16.50	...	...	24.33[d]	$7.66^{+0.08}_{-0.08}$	Te
489	VUDS530046029	$00.10^{+00.03}_{-00.03}$ [a]	$01.59^{+00.46}_{-00.46}$ [a]	...	...	...	...	...	...	-17.30	...	...	24.58[d]	$8.30^{+0.27}_{-0.27}$	R23
490	VUDS530048721	$00.03^{+00.01}_{-00.01}$ [a]	$00.48^{+00.18}_{-00.18}$ [a]	...	...	$00.15^{+00.06}_{-00.06}$ [b]	...	...	...	-16.70	...	...	25.19[d]	$7.97^{+0.28}_{-0.28}$	R23
491	VUDS530043711	$00.25^{+00.13}_{-00.13}$ [a]	$03.87^{+02.02}_{-02.02}$ [a]	...	...	...	...	...	...	-18.10	...	...	24.14[d]	$8.22^{+0.34}_{-0.34}$	R23
492	VUDS530079125	$00.03^{+00.01}_{-00.01}$ [a]	$00.40^{+00.14}_{-00.14}$ [a]	...	...	$00.09^{+00.03}_{-00.03}$ [b]	...	...	...	-15.90	...	...	25.20[d]	$7.86^{+0.20}_{-0.20}$	R23
493	VUDS510830468	$00.47^{+00.10}_{-00.10}$ [a]	$07.24^{+01.53}_{-01.53}$ [a]	...	...	$00.21^{+00.04}_{-00.04}$ [b]	...	...	...	-17.00	...	...	24.30[d]	$7.58^{+0.09}_{-0.09}$	Te
494	VUDS510146174	$00.02^{+00.01}_{-00.01}$ [a]	$00.36^{+00.14}_{-00.14}$ [a]	...	...	$00.05^{+00.02}_{-00.02}$ [b]	...	...	...	-15.60	...	...	25.00[d]	$7.80^{+0.26}_{-0.26}$	R23
495	VUDS511475480	$00.26^{+00.06}_{-00.06}$ [a]	$04.04^{+00.92}_{-00.92}$ [a]	...	...	$00.14^{+00.03}_{-00.03}$ [b]	...	...	...	-16.70	...	...	24.34[d]	$7.55^{+0.14}_{-0.14}$	Te
496	VUDS510573089	$00.22^{+00.05}_{-00.05}$ [a]	$03.35^{+00.84}_{-00.84}$ [a]	...	...	$00.88^{+00.22}_{-00.22}$ [b]	...	...	...	-17.90	...	...	23.33[d]	$8.00^{+0.14}_{-0.14}$	Te
497	VUDS510809459	$00.03^{+00.01}_{-00.01}$ [a]	$00.53^{+00.12}_{-00.12}$ [a]	...	...	$00.09^{+00.02}_{-00.02}$ [b]	...	...	...	-17.20	...	...	24.45[d]	$7.81^{+0.13}_{-0.13}$	R23
498	VUDS510352169	$00.43^{+00.09}_{-00.09}$ [a]	$06.62^{+01.42}_{-01.42}$ [a]	...	...	$00.35^{+00.07}_{-00.07}$ [b]	...	...	...	-17.40	...	...	23.79[d]	$7.63^{+0.08}_{-0.08}$	R23
499	VUDS510229076	$00.01^{+00.00}_{-00.00}$ [a]	$00.11^{+00.06}_{-00.06}$ [a]	...	...	$00.04^{+00.02}_{-00.02}$ [b]	...	...	...	-14.50	...	...	24.87[d]	$8.33^{+0.24}_{-0.24}$	R23
500	VUDS510997797	$00.02^{+00.01}_{-00.01}$ [a]	$00.27^{+00.13}_{-00.13}$ [a]	...	...	$00.08^{+00.04}_{-00.04}$ [b]	...	...	...	-15.20	...	...	24.55[d]	$8.23^{+0.22}_{-0.22}$	R23
501	VUDS510175664	$00.08^{+00.03}_{-00.03}$ [a]	$01.22^{+00.51}_{-00.51}$ [a]	...	...	$00.15^{+00.06}_{-00.06}$ [b]	...	...	...	-15.90	...	...	24.98[d]	$7.82^{+0.24}_{-0.24}$	R23
502	VUDS5120568170	$00.01^{+00.00}_{-00.00}$ [a]	$00.18^{+00.07}_{-00.07}$ [a]	...	...	$00.04^{+00.02}_{-00.02}$ [b]	...	...	...	-15.20	...	...	24.98[d]	$8.18^{+0.27}_{-0.27}$	R23
503	VUDS5101659094	$00.05^{+00.02}_{-00.02}$ [a]	$00.82^{+00.26}_{-00.26}$ [a]	...	...	$00.45^{+00.14}_{-00.14}$ [b]	...	...	...	-17.90	...	...	24.18[d]	$8.24^{+0.27}_{-0.27}$	R23
504	VUDS5101657178	$00.09^{+00.02}_{-00.02}$ [a]	$01.43^{+00.37}_{-00.37}$ [a]	...	...	$00.31^{+00.08}_{-00.08}$ [b]	...	...	...	-17.40	...	...	24.23[d]	$7.76^{+0.12}_{-0.12}$	Te

Notes: Luminosity units in 10^{42} erg s^{-1} and SFR units in M$_\odot$ yr^{-1}.
[a] Observed luminosity or observed SFR of Hβ emission line.
[b] Stellar mass deduced from *Starburst99* model using the rest-frame EW(Hα) or EW(Hβ) and L(Hβ) observed.
[c] K-band magnitudes in the Vega system.
[d] I-band magnitudes in the AB system.

Chapter 4

Analysis and Results

Physical differences in HII regions with extreme star formation rates may have a deep impact on the star formation process and stellar IMF (Stolte et al., 2005). Therefore, to characterize the buildup of the stellar mass in the universe, we must have a full understanding of the physical conditions in star-forming regions in distant galaxies. Measurements of the redshift evolution in the observed relationships among metallicity, luminosity and stellar mass provide powerful constraints on models of galaxy formation and star formation feedback.

This chapter presents the results obtained using the different physical parameters previously deduced. Also, it presents a global comparison between HIIGx at high and low redshift, which is obtained combining our sample at high redshift with the local sample from Chávez et al. (2014). Such comparison is derived by analysing the different relationships: Luminosity vs Velocity Dispersion; Luminosity vs Redshift; Dynamical Mass vs Stellar Mass; Metallicity vs Stellar Mass and Metallicity vs Luminosity. The first one presents a remarkable flattening for HII-like Galaxies at high redshift with log $\sigma > 1.8$ km s^{-1}. Finally a BPT Diagram is plotted in order to discriminate a possible contamination due to the presence of AGN in the sample.

4.1 L(Hβ) - σ Relation

In order to assess the L(Hβ) - σ relation as a distance estimator, 117 HII-like starburst galaxies were selected from the total sample at high redshift, in a range of $1.3 < z < 3.4$. Also 114 HIIGx at low redshift, in a range of $0.008 < z < 0.165$, were taken from Chávez et al. (2014) in order to compare the behaviour in the relationship. Therefore, in total we have 231 objects between high and low redshift with available data.

The resulting L(Hβ) - σ relation is shown in Figure 4.1, from this we can see that even with large uncertainties for the high redshift data, a flattening that starts at approximately $\log(\sigma) = 1.8$ km s^{-1} is evident. The reason behind such flattening in

the relationship is not obvious. However it is clear that in the range of $0.008 < z < 0.165$ and $\log(\sigma) < 1.8$ km s^{-1} if the velocity dispersion increases, the luminosity also increases. This is not the case at high redshift ($1.3 < z < 3.4$) and $\log(\sigma) > 1.8$ km s^{-1}, where an increase in the velocity dispersion does not affect the luminosity.
A possible explanation for the observed flattening in the L(Hβ)-σ relation is that the objects with $\log(\sigma) > 1.8$ km s^{-1} are dominated by rotation. Therefore, the emission-line profile widths are the result of the motions in the gravitational potential and also of rotation effects. As a consequence, there is no longer a direct correlation between mass and velocity dispersion.

This flattening might have an impact into cosmology since we can use it as a standard candle, in which the HIIGx with $\log(\sigma) > 1.8$ km s^{-1} may be assumed to have an upper limit in their luminosities. As can be seen in Figure 4.1, this occurs for HIIGx in a range of $1.3 < z < 3.4$, though we need more data for HIIGx at higher redshift to confirm this trend. Besides, we need to have high resolution spectra in order to measure with accuracy the FWHM in the emission lines and therefore to obtain the velocity dispersion. We can also expect to have smaller uncertainties in the calculated fluxes and therefore in the luminosities.

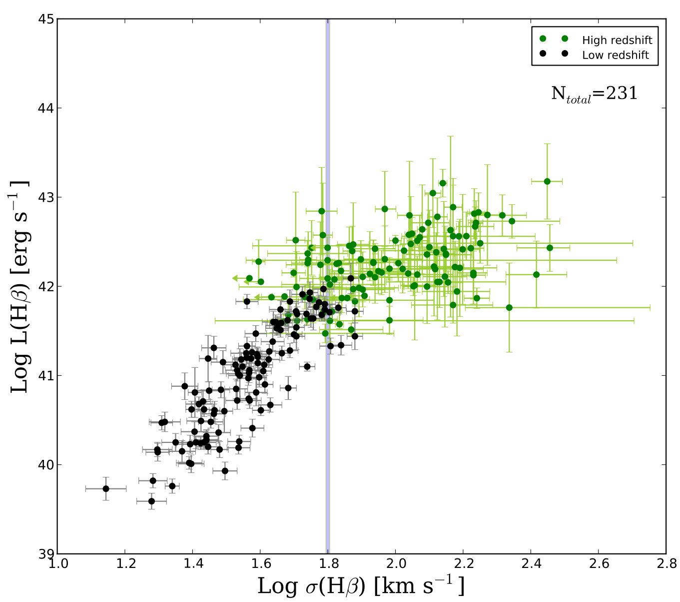

Figure 4.1: L(Hβ) - σ relation for 231 objects. From these 231 objects, 117 are HII-like starburst galaxies at high redshift (green symbols), in a range of $1.300 < z < 3.387$, and 114 are HIIGx at low redshift taken from Chávez et al. (2014) (black symbols), in a range of $0.008 < z < 0.165$. The blue band, at approximately $\log(\sigma) = 1.8$ km s^{-1}, indicates the approximate value where the flattening in the L-σ relation starts.

This result has not been reported before in the literature and the possibility that there is an upper limit to the luminosity of a burst of star formation has several important consequences. One of them is that if this is confirmed we would have a "standard candle" distance estimator similar to the SNIa, but capable of reaching up to the most distant star forming systems.

4.2 Luminosity vs Redshift

Motivated by the flattening observed in the L(Hβ)-σ relation for the sample at high redshift, we made the plot luminosity vs redshift for all objects with luminosities, which have been reported in Chapter 3 regardless of whether they have or not σ determinations. The result is shown in Figure 4.2, where the pink dots represent observed luminosities and the green dots represent the luminosities corrected by extinction. The principal characteristic in this plot is that in the range of 1.3 < z < 3.4 the luminosity effectively remains constant within the errors. The inset shows the luminosity distribution for such HII-like galaxies at high redshift, where the dashed line represents the median value of logL(Hβ)= 42.16 erg s^{-1}.

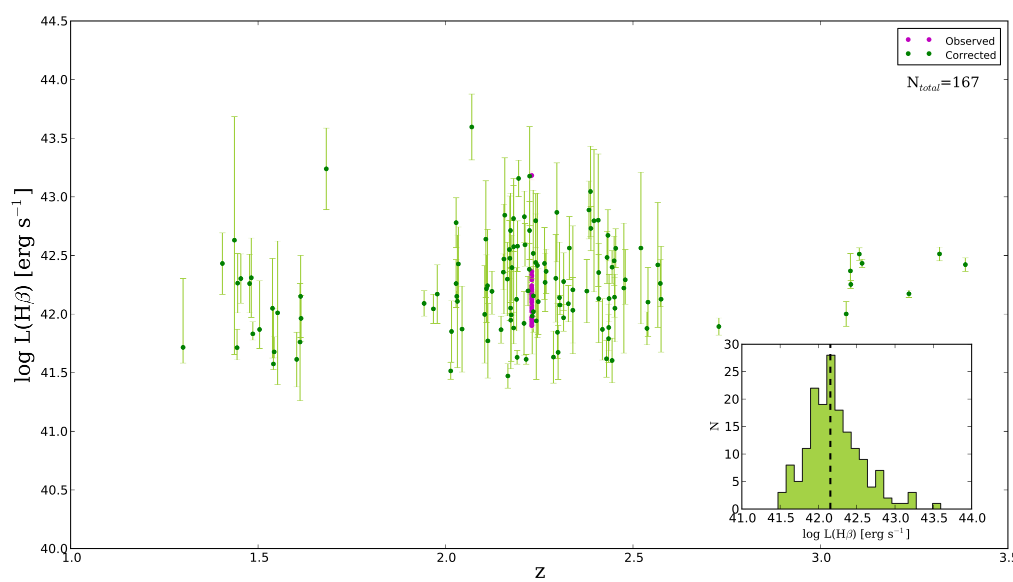

Figure 4.2: Hβ luminosity vs redshift for 167 HII-like starburst galaxies at z > 1.3. The pink dots are objects with observed L(Hβ) and green dots represent the L(Hβ) corrected by extinction. The inset shows the luminosity distribution where the dashed line represents the median.

The luminosity vs redshift relation for the 103 objects with log(σ) > 1.8 km s^{-1} is shown in Figure 4.3. Clearly the luminosity remains roughly constant within errors in this redshift range. I expect to further investigate this interesting aspect of the HIIGx behaviour in my PhD work. The inset shows the luminosity distribution for such HII-like galaxies at high redshift, where the dashed line represents the median value of logL(Hβ)= 42.26 erg s^{-1}.

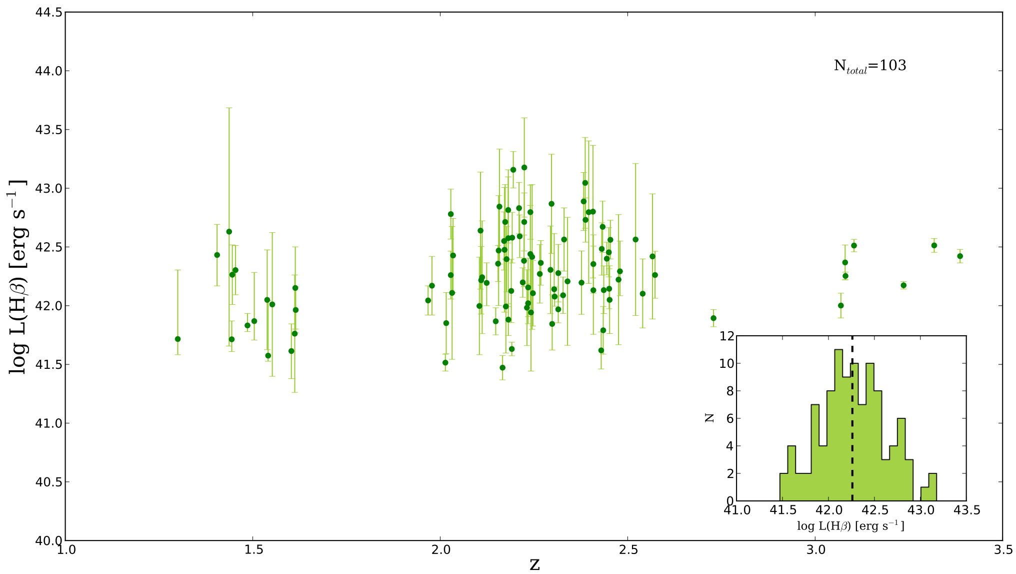

Figure 4.3: Hβ luminosity vs redshift for 103 HII-like starburst galaxies with logσ > 1.8 km s^{-1}. The inset shows the luminosity distribution where the dashed line represents the median.

4.3 Cosmological Parameters Solution Space

From the previous analysis, we clearly see that the luminosity remains roughly constant within errors for the 103 objects with log(σ) > 1.8 km s^{-1} and for 167 HIIGx at z > 1.3. Therefore, we can use this constant luminosity in HIIGx as a "Standard clandle" in order to constrain cosmological parameters.

Figure 4.4 shows the Hubble diagram for the joint sample of HIIGx at low and high redshift, where the red continuous line indicates the concordance ΛCDM cosmology with Ω_m = 0.3; w_0 = -1.0 and H$_0$ = 73.6 km s^{-1} Mpc^{-1}. The points correspond to individual HIIGx, where their distance moduli were obtained using the procedure explained in the section 2.4. For the sample at high redshift with log(σ) > 1.8 km s^{-1}, we propose to use a value of log L(Hβ)= 42.3 $\pm$ 0.3 erg s^{-1} as standard candle. The left panel of Figure 4.4 shows distance moduli as a function of redshift for 103 HIIGx at high redshift with $\log(\sigma) > 1.8$ km s^{-1}. While right panel of Figure 4.4 shows the same but adding the local sample of 156 HIIGx and GEHRs. It is important to note that the Hubble diagram obtained by combining HIIGx at high and low redshift covers a huge redshift range. In particular, it has galaxies in the Local Group up to z $\sim$ 3.4.

Adopting the value of $H_0 = 73.6 \pm 3.1$ km s^{-1} Mpc^{-1}, $w_1 = 0$ and our standard candle of log L(Hβ)= 42.3 ± 0.3 erg s^{-1}, we obtain reasonable strong restrictions on the plane Ω_m, w_0, which are shown in Figure 4.5 (Chávez et al. in preparation). The left panel of Figure 4.5 shows the solution for 103 HIIGx at high redshift with $\log(\sigma) > 1.8$ km s^{-1}. 1, 2 and 3σ contours (random) are shown. The right panel of Figure 4.5 shows the effect of including a local sample of 156 HIIGx and GEHRs (Terlevich et al., 2015; Chávez et al., 2014). By comparing both plots in Figure 4.4, we have verified that by using a few tens of HIIGx at high redshift (in the range 1.3 < z < 3.4), even with a relatively large distance modulus uncertainty, improves the constraints on the plane $\{\Omega_m, w_0\}$. This provides an indication of how much an increase in number can restrict the cosmological parameters solution space.

By comparing our results on the plane $\{\Omega_m, w_0\}$, in which we combine the high redshift with the local HIIGx samples (see right panel of Figure 4.5), with recent results from SNeIa, CMB and BAO (see right panel of Figure 2.14,) we can conclude that our results are not only in agreement with those of SNeIa but the surface covered by our simple approach is not much larger than that of the SNeIa solution. In fact our 1-σ area solution looks very similar to the 2-σ area of the SNeIa solution. Therefore, with a larger sample of HII galaxies at higher redshift with high quality data it may be possible to achieve similar results (and perhaps even better restrictions) for the cosmological parameters solution space obtained from SNeIa.

4.4 Luminosity - Radius and Velocity Dispersion - Radius Relations

As was explained in section 3.2, the nature of the L - σ relation for HIIGx is gravitational where the emission-line profile widths reflect the motions in the gravitational potential well (Terlevich & Melnick, 1981). Besides, the HIIGx define a fundamental plane that is similar to that defined by normal elliptical galaxies (Telles, 1995).

With the purpose of exploring if the radius can be a parameter that contributes to such observed flattening, I made the plots velocity dispersion vs radius and luminosity vs radius which are shown in Figure 4.6, where the half-light radius was obtained using curves-of-growth extracted from circular apertures. (see subsection 3.2.2).

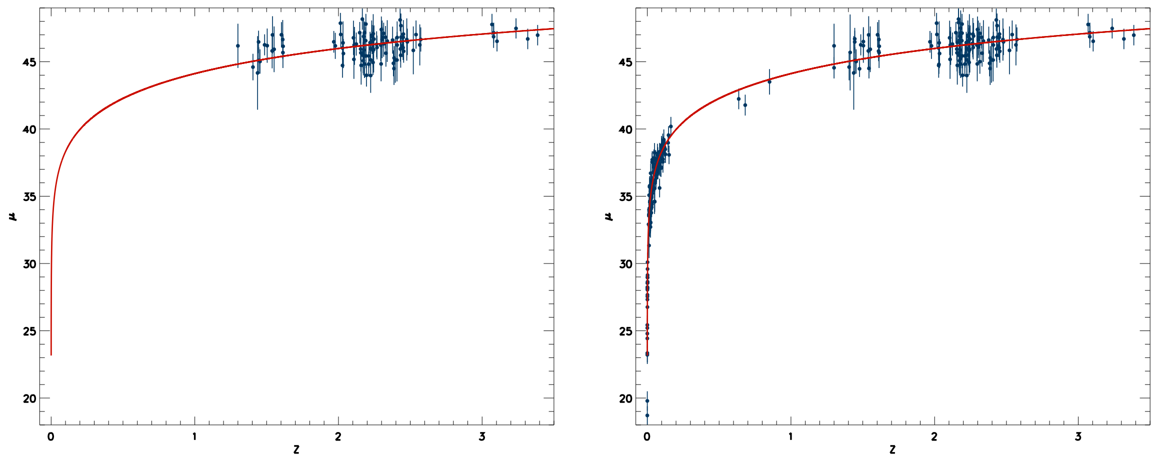

Figure 4.4: Distance moduli as a function of redshift. Left Panel: Our results for 103 HIIGx at high redshift with $\log(\sigma) > 1.8$ km s^{-1}. Right Panel: The same but for the combined 103 HIIGx at high redshift with $\log(\sigma) > 1.8$ km s^{-1} and the local sample of 156 HIIGx and GEHRs (Terlevich et al., 2015; Chávez et al., 2014).

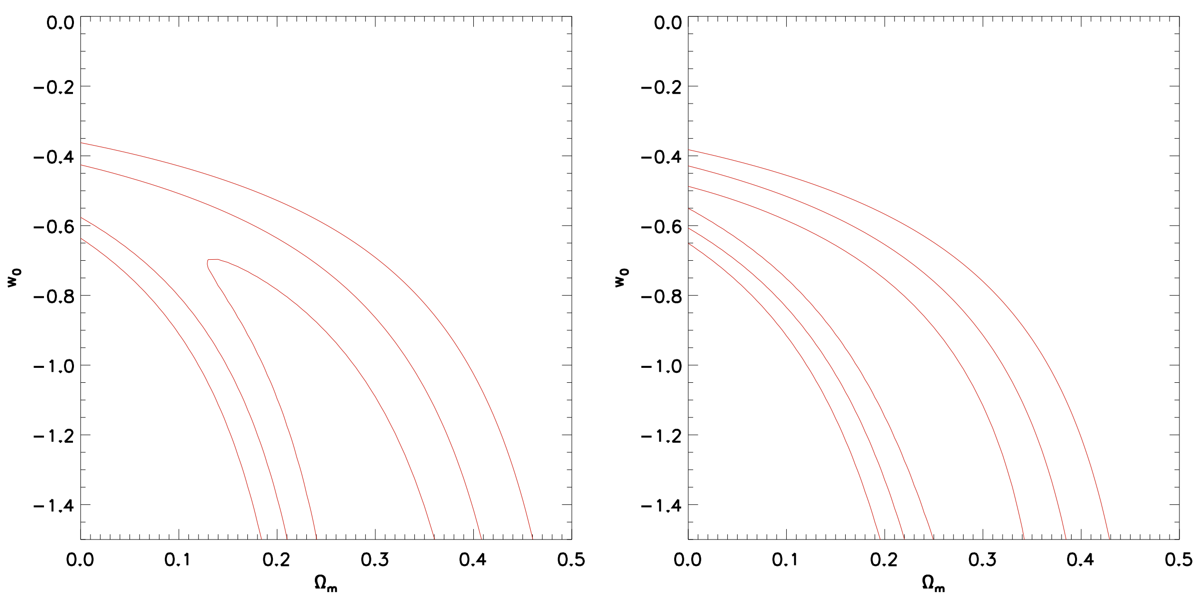

Figure 4.5: Cosmological Parameters Solution Space. Left Panel: Our results for 103 HIIGx at high redshift with $\log(\sigma) > 1.8$ km s^{-1}. Right Panel: The same but for the combined 103 HIIGx at high redshift with $\log(\sigma) > 1.8$ km s^{-1} and the local sample of 156 HIIGx and GEHRs (Terlevich et al., 2015; Chávez et al., 2014). 1, 2 and 3σ contours (random) are shown.

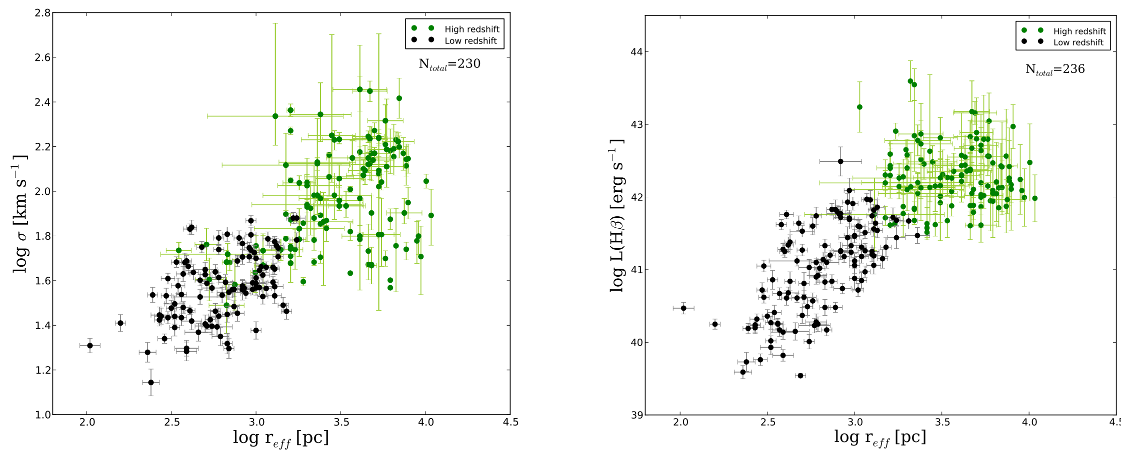

Figure 4.6: Left: Velocity Dispersion vs Radius for 230 objects, of which 124 are HII-like starburst galaxies at high redshift, in a range of $0.68 < z < 2.58$, and 106 are HIIGx at low redshift, in a range of $0.01 < z < 0.17$. Right: Luminosity of Hβ emission line vs Radius for 236 objects, of which 118 are HII-like starburst galaxies at high redshift, in a range of $0.60 < z < 2.58$, and 106 are HIIGx at low redshift, in a range of $0.01 < z < 0.20$.

In the left panel of Figure 4.6, we see that if the effective radius increases, the velocity dispersion also increases in both ranges of redshift $0.01 < z < 0.20$ and $0.60 < z < 2.58$ by approximately the same factor in velocity dispersion, while in the right panel there seems to be a flattening for high luminosity objects. This is in agreement with the L-σ behaviour in the sense that it also suggests that there is an upper limit in the luminosity of the HIIGx.

4.5 Dynamical Mass vs Stellar Mass

As was explained before, the dynamical mass for the sample at high redshift (as at low redshift) was calculated using the equation (3.4). Regarding the calculation of stellar mass, this was made using the stellar population synthesis model *Starburst99* [1] (Leitherer et al., 1999). The simulation used a Kroupa IMF (Initial Mass Function), instantaneous star formation and a metallicity of 0.004 of Padova AGB.

The EWs for the sample at high redshift were taken from the EWs delivered by the simulation and the luminosity and mass loss were examined for each object. The mass loss was subtracted from the initial mass in order to obtain the total mass. Finally with the total mass and the luminosity I estimated the constant of the stellar mass-to-light

[1] *Starburst99* is a stellar population synthesis model, which is available in the website http://www.stsci.edu/science/starburst99

ratio. In order to estimate the stellar mass for each object, I multiplied such constant by the L(Hβ) calculated as in subsection 3.2.5.

Comparing the Stellar Mass - Dynamical Mass relation for the high and low redshift samples, I obtain the result that such objects do not fall into the same correlation, as can be seen in Figure 4.7. It is important to note that for the objects at low redshift there is a difference of an order of magnitude between the dynamical mass and the stellar mass.

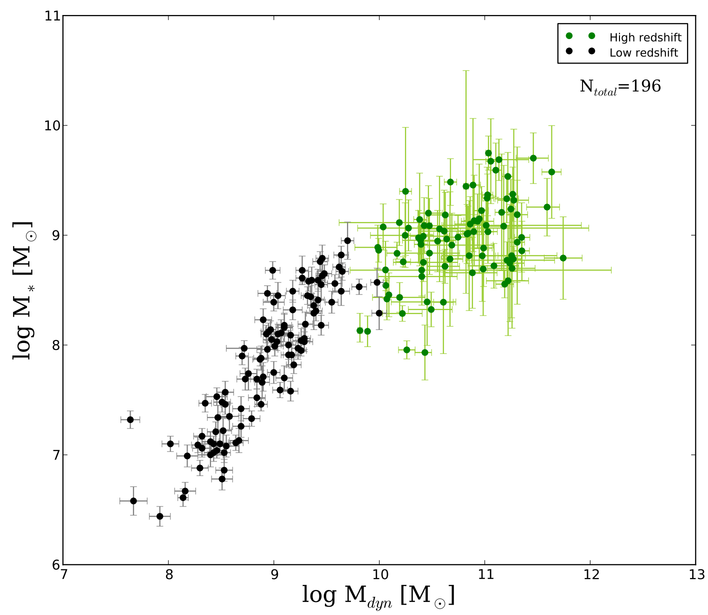

Figure 4.7: Stellar Mass - Dynamical Mass relation for 196 objects. 90 at high redshift, in a range of $1.40 < z < 2.57$ (green dots), and 106 at low redshift, in a range of $0.01 < z < 0.16$ (black dots). Note the similarity with the L - σ relation.

In order to confirm the results, I also calculate the M_{dyn} using the equation found in Chávez et al. 2014:

$$M_{dyn} = 7.1 \times 10^{-34} L(H\beta), \tag{4.1}$$

which was obtained using a *Starburst*99 model and an EW(Hβ) = 50 Å as lower limit. However, no major differences were found in the plot M_* vs M_{dyn} previously analysed.

A possible answer to the difference observed in the M_* - M_{dyn} relation between the samples at high and low redshift is the flattening found in the L(Hβ)-σ relation. We see in the L(Hβ)-σ relation that the velocity dispersion continues increasing while the luminosity is approximately constant for the objects with log $\sigma > 1.8$ km s^{-1} at high redshift. Therefore, the increase in σ indicates an increase in the dynamical mass (see equation 3.4) and that the luminosity is approximately constant means that the stellar mass increases very little. A drawback is that the definition of the radius is very important in the determination of dynamical mass (see subsection 3.2.3). I used the half-light radius, which was determined using curves-of-growth extracted from circular apertures (see subsection 3.2.2) for calculating the dynamical mass.

In order to obtain an unbiased estimate of the dynamical mass a good measurement of the effective radius of the ionising massive cluster is necessary. Therefore, the difference found between the objects at high and low redshift in the M_{dyn} vs M_* relation also can be due to estimation in the radii, which in both cases are affected by the seeing and by the instrumental resolution. For example, Chávez et al. (2014) compared the HST angular size with the Petrosian radius obtained from the SDSS u band photometry (corrected for seeing) and they found that the ionising cluster radius measured from the HST images is on average more than a factor of 5 smaller than the SDSS Petrosian radius. For the moment, for estimating the dynamical mass of the objects at low and high redshift I have not corrected in any way the radii reported in the literature. However, this correction must be contemplated also for the sample at high redshift since due to the instrumental resolution and the large redshift of the sample many of the objects are perhaps unresolved even under very good seeing conditions. As a consequence, the half-light radii can be overestimated and hence also the dynamical masses. The effects of rotation or multiplicity affecting the mass estimates have also to be taken into account. All this needs careful investigation in the future.

4.6 Metallicity - Mass Relation

The existence of a correlation between stellar mass and metallicity reflects the fundamental role that galaxy mass plays in galactic chemical evolution. However, it is still unclear whether this sequence is one of enrichment or depletion. If more massive galaxies form fractionally more stars in a Hubble time than their low-mass counterparts, then the observed mass-metallicity relation represents a sequence in astration. However, if galaxies form similar fractions of stars, then the relation could imply that metals are lost from galaxies with small potential wells via galactic winds. Using a sample of $\sim$ 53,000 star-forming galaxies selected from the SDSS, Tremonti et al. (2004) found that a striking correlation is observed, extending over three decades in stellar mass and a factor of 10 in metallicity. The correlation is roughly linear from $10^{8.5}$ to $10^{10.5}$ $M_{\odot}$, after which a gradual flattening occurs.

In order to test the possible existence of a Metallicity - Stellar Mass relation for HII galaxies, I used a sample of 53 HII-like starburst galaxies at high redshift and 117

HIIGx at low redshift for which the required data exists in the literature. The results are presented in Figure 4.8, which shows a large dispersion. This could be due to the fact that we are not dealing here with the properties of whole galaxies but instead with the properties of a young massive burst of starformation for which no correlation between size and metallicity is expected.

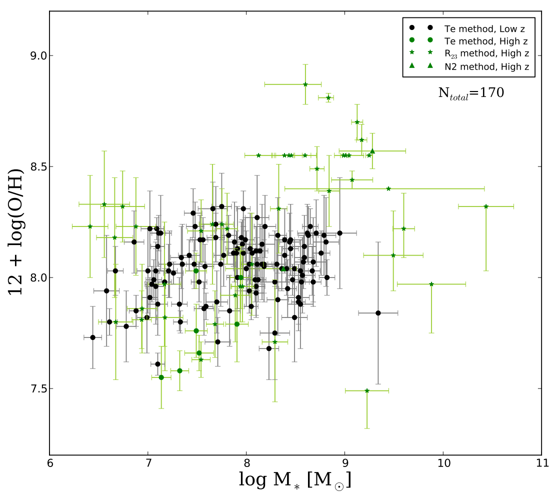

Figure 4.8: Relation between stellar mass, in units of solar masses, and gas-phase oxygen abundance for 170 objects, of which 53 (green symbols) are at high redshift, in a range of redshift of $0.21 < z < 3.39$, and 117 (black symbols) are at low redshift, in a range of redshift of $0.01 < z < 0.20$. The different symbols indicate the different metallicity calibrators (see subsection 3.2.8).

4.7 Metallicity-Luminosity Relation

It is well known that both star-forming and early-type galaxies in the local universe follow the correlation between rest-frame B-band luminosity and the degree of chemical enrichment (Lequeux et al., 1979; Skillman et al., 1989; Garnett & Shields, 1987). This relationship is expected because of the fundamental role that galaxy mass plays in determining the degree of chemical enrichment of the interstellar medium through the rate at which those elements are produced by star formation. Because of the relative difficulty of measuring the stellar mass of galaxies, nevertheless, most works have focused on the relationship between galaxy luminosity and metallicity.

For 231 HII-like starburst galaxies at high redshift and 100 HIIGx at low redshift, I plotted in Figure 4.9 metallicity vs rest-frame B-band luminosity. The relationship exists, albeit with large dispersion in the data which could be due to the large uncertainties in the estimates of metallicity based on different calibrators (see subsection 3.2.8) indicated by different symbols in Figure 4.9.

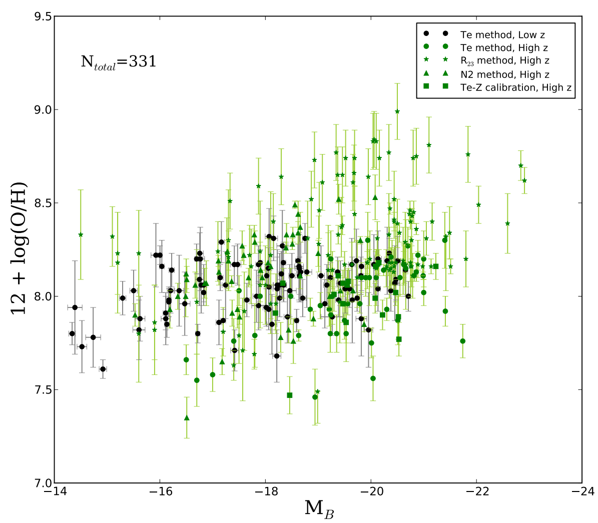

Figure 4.9: Relation between B-band luminosity and gas-phase oxygen abundance for 331 objects, of which 231 (green symbols) are at high redshift, in a range of redshift of $0.10 < z < 3.39$, and 100 (black symbols) are at low redshift, in a range of redshift of $0.01 < z < 0.17$. The different symbols shown in the inset indicate the calibrator used for the estimation of metallicity (see subsection 3.2.8).

The slight overall trend observed in Figure 4.9, in which objects with higher luminosities have higher metallicities, again supports the idea that with HIIG we are not dealing with the properties of whole galaxies but instead with the properties of a young massive burst of starformation for which no correlation between luminosity and metallicity is expected.

4.8 Starburst or AGN?

For this thesis I have assumed that star formation is primarily responsible for the narrow and intense emission lines. However, such result would be entirely coincidental in the case that the emission lines are powered by AGN since the width of AGN emission lines is not necessarily coupled to the stellar mass of the host galaxy. In other words, we observe narrow emission lines in these small systems (∼1 kpc) where the emission-line profile widths reflect the motions in the gravitational potential well, while typical AGN narrow line region (clouds of gas at low densities and velocities located farther away from the black hole) also have emission line widths, σ, from ∼ 200 - 1200 km/s (Osterbrock & Mathews, 1986).

Anyway, the most secure method to distinguish starburst galaxies from AGN is by using a diagnostic diagram, for example the BPT diagram (Baldwin, Phillips, & Terlevich, 1981), a diagnostic diagram that uses emission line ratios, e.g. [NII]λ6584/Hα and [OIII]λ5007/Hβ (In what follows I will use the term [NII]/Hα to refer to the measured ratio between [NII]λ6584 and Hα and [OIII]/Hβ for the measured ratio between [OIII]λ5007 and Hβ) to classify objects into groups corresponding to the predominant excitation mechanism. These groups are: normal HII regions (photoionization by O and B stars), narrow-line regions of Seyfert 1 galaxies (photoionization by a power-law continuum source) and LINERS, Low Ionization Nuclear Emission Line Regions, (shock-wave heating).

The BPT diagram locates star-forming galaxies in the lower left corner, in a region defined by decreasing excitation as a function of increasing metallicity. This physical sequence results in the empirical anticorrelation between [OIII]/Hβ and [NII]/Hα up to the point where [NII]/Hα saturates at [NII]/Hα $\sim$ 0.3. At the highest metallicities [OIII]/Hβ continues decreasing at relatively fixed [NII]/Hα. AGN are mostly located in the upper right corner of the diagram, typically described by both higher [NII]/Hα and [OIII]/Hβ ratios than those in star-forming galaxies. Several curves in the BPT diagram represent the theoretical upper limit on the location of star-forming galaxies (Kewley et al., 2001; Kauffmann et al., 2003).

An advantage of these BPT diagrams is that the measured line ratios, [NII]/Hα and [OIII]/Hβ, are not affected by uncertainties in flux calibration or dust extinction since each line ratio is calculated from emission lines very close in wavelength. Another common diagnostic diagram in the literature uses the log([OIII]λ5007/Hβ) vs log([SII]λ6716 + λ6731/Hα) ratios (Veilleux & Osterbrock, 1987).

In order to characterize the sample, a BPT diagram was made for the 25 HII-like starburst galaxies in a range of redshift of $1.30 < z < 2.135$ and 96 HIIGx in a range of redshift of $0.01 < z < 0.20$, which is illustrated in Figure 4.10. The stars in our BPT diagram indicate that the data were taken using the *Plot Digitizer* program [2], which allows us to take a scanned image of a plot and quickly digitize values off the plot just by clicking the mouse on each data point.
From the BPT diagram it can be seen that if we consider the uncertainties, most of the objects are located just below the transition line (Kewley et al., 2001), indicating high excitation and suggesting low metal content and photoionization due to the presence of hot main sequence stars, which is consistent with the expectations for young HII regions.

[2] The *Plot Digitizer* program is a Java program used for digitalizer scanner plots and it is available in the website http://plotdigitizer.sourceforge.net/.

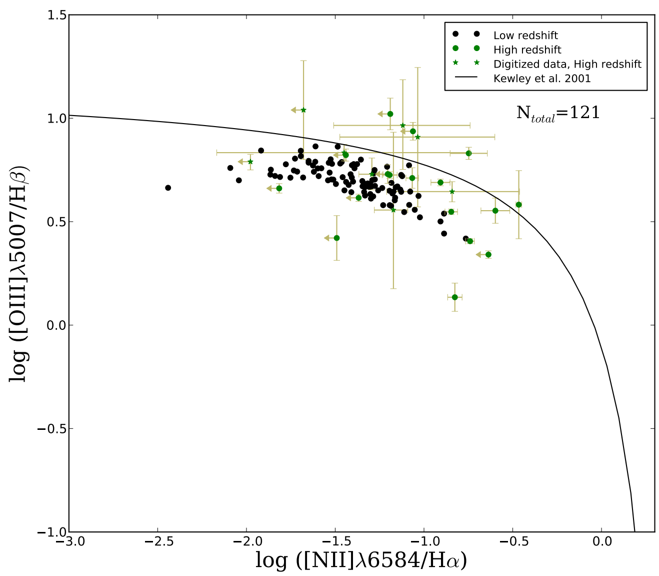

Figure 4.10: BPT diagram for 121 objects. From these 121, 25 are HII-like starburst galaxies at high redshift (green symbols), in a range of redshift of $1.30 < z < 2.135$, and 96 are HIIGx at low redshift (black symbols), in a range of redshift of $0.01 < z < 0.20$. The stars indicate that the data were taken using the *Plot Digitizer* program. The solid line represents the theoretical upper limit for stellar photoionization, from Kewley et al. (2001).

In the next Chapter, I will summarise the results of this work and set a scheme for future work.

Chapter 5

Conclusions and future work

We have selected a sample of 504 HII like-starburst galaxies in a range of redshift of 0.1 < z < 3.4 from the literature in order to assess the validity of the L(Hβ) - σ relation at high redshift and its use as an accurate distance estimator. The candidates were selected according to the equivalent widths in their emission lines. We also compared the physical parameters of the HII-like galaxies at high redshift with the nearby sample of HIIGx from Chávez et al. (2014).

The main conclusions obtained are:

1 There is a large enough number of appropriate objects at high redshift in the literature to measure cosmological parameters with high accuracy using the L(Hβ) - σ relation for HIIGx.

2 The objects at high redshift cover the following ranges in their physical parameters: 39.84 < L(Hβ) < 43.59, -0.97 < SFR(Hβ) < 2.78, 6.41 < Log M_* < 10.43, 8.87 < Log M_{dyn} < 11.75, 2.04 < Log r_{eff} < 4.04, 7.32 < 12 + log(O/H) < 8.99. These values, within the uncertainties, are consistent with the ones for the HIIGx at low redshift. This suggests that the physical properties for HIIGx at low and high redshift are similar.

3 I compared the low and high redshift L(Hβ) - σ relation, 117 HII-like starburst galaxies having the required data in a range of 1.3 < z < 3.4. By combining this subset with 114 HIIGx on the range 0.008 < z < 0.165 from Chávez et al. 2014, we find an evident flattening in the L(Hβ) - σ relation. This flattening starts at approximately log(σ) = 1.8 km s^{-1}, i.e there seems to be an upper limit to the luminosity of HIIGx.

4 The flattening or the existence of an upper limit in the luminosity of HIIGx has not been reported before. The fact that we see a constant luminosity could be the consequence of the existence of an upper limit for the luminosity of a burst of star formation combined with the limiting flux achievable with present day instrumentation.

5 If the HIIGx with $\log(\sigma) > 1.8$ km s^{-1} have an upper limit in their luminosities, we would have a "standard candle" distance estimator similar to the SNIa, but capable of reaching up to the most distant star forming systems.

6 By comparing the Stellar Mass vs Dynamical Mass relation for the high and low redshift samples, I found that the objects at low redshift have a difference of an order of magnitude between the dynamical mass and the stellar mass whereas for the objects at high redshift there is a difference of two orders of magnitude between them. This implies that such objects do not fall into the same correlation. A possible explanation to such result is related to the flattening in the L(Hβ)-σ relation since the estimated stellar mass depends on luminosity and the estimated dynamical mass depends on velocity dispersion. A drawback is that estimations of the dynamical mass also need a good measurement of the effective radius of the ionising massive cluster. Therefore, the difference found between the objects at high and low redshift in the M_* - M_{dyn} relation also can be related to the radii estimates, which are affected by the seeing and instrumental resolution of the observations.

7 The [OIII]/Hβ vs [NII]/Hα BPT diagnostic diagram was used to investigate the nature of the ionization source for the samples at high and low redshift. The result is that if we consider the uncertainties, most of the objects are located just below the transition line (Kewley et al., 2001), indicating high excitation and suggesting low metal content and photoionization by hot main sequence stars, which is consistent with the expectations for young HII regions.

8 Finally, we have applied the HIIGx standard candle method to the high redshift sample to constrain the cosmological parameters solution space. Adopting the value of log L(Hβ)= 42.2 ± 0.3 erg s^{-1} as a standard candle for 103 HIIGx at high redshift with $\log(\sigma) > 1.8$ km s^{-1}, we obtain strong restrictions on the plane $\{ \Omega_m, w_0 \}$.

The combination of our sample at high redshift with the local sample of 156 (HIIGx and GEHRs) from Chávez et al. (2014) and Terlevich et al. (2015) dramatically improves the constraints on the plane Ω_m, w_0. This provides a clear indication of how much an increase in number can restrict the cosmological parameters solution space.

These results are surprisingly good considering the high uncertainties in the data at high redshift, therefore we expect better constraints on the plane $\{\Omega_m, w_0\}$ with new high quality data from high resolution spectrographs at 8 m class telescopes.

5.1 Future work

The main aim of my future work is to investigate both HIIGx distance estimators for the accurate determination of cosmological parameters up to the highest redshift possible.

The main aspects are:

1 Observe the sample of 504 HII like-starburst galaxies at high redshift using high resolution spectrographs at 8 m class telescopes in order to measure with great accuracy the flux and the FWHM in the emission lines.

To observe the selected sample, the best option is to use multiples IFUs at large telescopes, e.g. VLT-KMOS and KECK-MOSFIRE, for which we have already been granted observing time. The reason for this is that several objects in the same field can be observed simultaneously ($\sim$ 40 objects/night), increasing notably the observation efficiency and in this way we take advantage of the high number density of the HIIGx.

2 I will compare the intrinsic properties of the new high precision data on this high-z sample with the low-z sample in order to have a better understanding of the nature of these starforming galaxies at high redshift and their relation with similar objects nearby.

3 Analyse critically the L - σ distance estimator and its application in cosmology.

4 I will explore in detail the observed flattening in the L - σ relation for objects with $\mathrm{Log}(\sigma) > 1.8$ km s^{-1} and its use as a standard candle, which is an independent method to determine cosmological parameters, in particular Ω_m and w_0.

5 Given the high redshift at which these methods seem to work, I will also explore the evolution of the dark energy equation of state to explore whether its is a cosmological constant or a field that provides a time varying equation of state.

6 Finally, I will do joint analysis of the HIIGx methods with the SNIa method as accurate distance estimators to learn about systematics affecting both approaches.

Bibliography

Albrecht, A., Bernstein, G., Cahn, R., et al. 2006, ArXiv Astrophysics e-prints

Alloin, D., Collin-Souffrin, S., Joly, M., & Vigroux, L. 1979, Astronomy and Astrophysics, 78, 200

Amanullah, R., Lidman, C., Rubin, D., et al. 2010, The Astrophysical Journal, 716, 712

Amorín, R., Sommariva, V., Castellano, M., et al. 2014, Astronomy & Astrophysics, 568, L8

Amorín, R., Pérez-Montero, E., Contini, T., et al. 2015, Astronomy & Astrophysics, 578, A105

Aubourg, É., Bailey, S., Bautista, J. E., et al. 2014, ArXiv e-prints

Baldwin, J. A., Phillips, M. M., & Terlevich, R. 1981, Publications of the Astronomical Society of the Pacific, 93, 5

Bassett, B. A. 2005, Physical Review D, 71, 083517

Bordalo, V., & Telles, E. 2011, The Astrophysical Journal, 735, 52

Bosch, G., Terlevich, E., & Terlevich, R. 2002, Monthly Notices of the Royal Astronomical Society, 329, 481

Bueno Sanchez, J. C., Nesseris, S., & Perivolaropoulos, L. 2009, Journal of Cosmology and Astroparticle Physics, 11, 29

Calzetti, D., Armus, L., Bohlin, R. C., et al. 2000, The Astrophysical Journal, 533, 682

Calzetti, D., Kinney, A. L., & Storchi-Bergmann, T. 1994, The Astrophysical Journal, 429, 582

Chávez, R., Terlevich, E., Terlevich, R., et al. 2012, Monthly Notices of the Royal Astronomical Society, 425, L56

Chávez, R., Terlevich, R., Terlevich, E., et al. 2014, Monthly Notices of the Royal Astronomical Society, 442, 3565

Chevallier, M., & Polarski, D. 2001, International Journal of Modern Physics D, 10, 213

Copetti, M. V. F., Pastoriza, M. G., & Dottori, H. A. 1986, Astronomy and Astrophysics, 156, 111

Denicoló, G., Terlevich, R., & Terlevich, E. 2002, Monthly Notices of the Royal Astronomical Society, 330, 69

Dicus, D. A., & Repko, W. W. 2004, Physical Review D, 70, 083527

Dottori, H. A. 1981, Astrophysics and Space Scienc, 80, 267

Dottori, H. A., & Bica, E. L. D. 1981, Astronomy and Astrophysics, 102, 245

Edmunds, M. G., & Pagel, B. E. J. 1984, Monthly Notices of the Royal Astronomical Society, 211, 507

Erb, D. K., Pettini, M., Shapley, A. E., et al. 2010, The Astrophysical Journal, 719, 1168

Erb, D. K., Shapley, A. E., Steidel, C. C., et al. 2003, The Astrophysical Journal, 591, 101

Erb, D. K., Steidel, C. C., Shapley, A. E., Pettini, M., & Adelberger, K. L. 2004, The Astrophysical Journal, 612, 122

Erb, D. K., Steidel, C. C., Shapley, A. E., et al. 2006a, The Astrophysical Journal, 647, 128

—. 2006b, The Astrophysical Journal, 646, 107

Förster Schreiber, N. M., Genzel, R., Bouché, N., et al. 2009, The Astrophysical Journal, 706, 1364

Freedman, W. L., Madore, B. F., Scowcroft, V., et al. 2012, The Astrophysical Journal, 758, 24

García-Benito, R. 2009, PhD thesis, Universidad Autonoma de Madrid

Garnett, D. R., & Shields, G. A. 1987, Astrophysical Journal, 317, 82

Gilliland, R. L., Nugent, P. E., & Phillips, M. M. 1999, The Astrophysical Journal, 521, 30

Gilliland, R. L., & Phillips, M. M. 1998, IAU Circ., 6810, 1

Haro, G. 1956, Boletin de los Observatorios Tonantzintla y Tacubaya, 2, 8

Hicken, M., Wood-Vasey, W. M., Blondin, S., et al. 2009, The Astrophysical Journal, 700, 1097

Hoyos, C., Koo, D. C., Phillips, A. C., Willmer, C. N. A., & Guhathakurta, P. 2005, The Astrophysical Journal, 635, L21

Kauffmann, G., Heckman, T. M., Tremonti, C., et al. 2003, Monthly Notices of the Royal Astronomical Society, 346, 1055

Kennicutt, R. C., & Evans, N. J. 2012, Annual Review of Astronomy and Astrophysics, 50, 531

Kennicutt, Jr., R. C., Bresolin, F., & Garnett, D. R. 2003, The Astrophysical Journal, 591, 801

Kennicutt, Jr., R. C., Edgar, B. K., & Hodge, P. W. 1989, The Astrophysical Journal, 337, 761

Kewley, L. J., & Dopita, M. A. 2002, The Astrophysical Journal Supplement Series, 142, 35

Kewley, L. J., Dopita, M. A., Sutherland, R. S., Heisler, C. A., & Trevena, J. 2001, The Astrophysical Journal, 556, 121

Kewley, L. J., & Ellison, S. L. 2008, The Astrophysical Journal, 681, 1183

Kobulnicky, H. A., Kennicutt, Jr., R. C., & Pizagno, J. L. 1999, The Astrophysical Journal, 514, 544

Kobulnicky, H. A., & Kewley, L. J. 2004, The Astrophysical Journal, 617, 240

Komatsu, E., Smith, K. M., Dunkley, J., et al. 2011, The Astrophysical Journal Supplement, 192, 18

Kroupa, P., & Weidner, C. 2003, The Astrophysical Journal, 598, 1076

Kunth, D., & Östlin, G. 2000, The Astronomy and Astrophysics Review, 10, 1

Leitherer, C., Schaerer, D., Goldader, J. D., et al. 1999, The Astrophysical Journal Supplement Series, 123, 3

Lequeux, J., Peimbert, M., Rayo, J. F., Serrano, A., & Torres-Peimbert, S. 1979, Astronomy and Astrophysics, 80, 155

Linder, E. V. 2003, Physical Review Letters, 90, 091301

Mancini, C., Förster Schreiber, N. M., Renzini, A., et al. 2011, The Astrophysical Journal, 743, 86

Maseda, M. V., van der Wel, A., da Cunha, E., et al. 2013, The Astrophysical Journal Letters, 778, L22

Maseda, M. V., van der Wel, A., Rix, H.-W., et al. 2014, The Astrophysical Journal, 791, 17

Masters, D., McCarthy, P., Siana, B., et al. 2014, The Astrophysical Journal, 785, 153

Matsuda, Y., Smail, I., Geach, J. E., et al. 2011, Monthly Notices of the Royal Astronomical Society, 416, 2041

McCall, M. L., Rybski, P. M., & Shields, G. A. 1985, Astrophysical Journal Supplement Series, 57, 1

Melnick, J. 1978, Astronomy and Astrophysics, 70, 157

Melnick, J. 1987, in Starbursts and Galaxy Evolution, ed. T. X. Thuan, T. Montmerle, & J. Tran Thanh van, 215–225

Melnick, J., Moles, M., Terlevich, R., & Garcia-Pelayo, J.-M. 1987, Monthly Notices of the Royal Astronomical Society, 226, 849

Melnick, J., Terlevich, R., & Moles, M. 1988, Monthly Notices of the Royal Astronomical Society, 235, 297

Melnick, J., Terlevich, R., & Terlevich, E. 2000, Monthly Notices of the Royal Astronomical Society, 311, 629

Osterbrock, D. E. 1989, Astrophysics of gaseous nebulae and active galactic nuclei

Osterbrock, D. E., & Mathews, W. G. 1986, Annual review of astronomy and astrophysics, 24, 171

Pagel, B. E. J., Edmunds, M. G., Blackwell, D. E., Chun, M. S., & Smith, G. 1979, Monthly Notices of the Royal Astronomical Society, 189, 95

Pagel, B. E. J., Simonson, E. A., Terlevich, R. J., & Edmunds, M. G. 1992, Monthly Notices of the Royal Astronomical Society, 255, 325

Peebles, P. J., & Ratra, B. 2003, Reviews of Modern Physics, 75, 559

Percival, W. J., Reid, B. A., Eisenstein, D. J., et al. 2010, Monthly Notices of the Royal Astronomical Society, 401, 2148

Pérez-Montero, E., & Díaz, A. I. 2003, Monthly Notices of the Royal Astronomical Society, 346, 105

Perlmutter, S., Aldering, G., Goldhaber, G., et al. 1999, The Astrophysical Journal, 517, 565

Pettini, M., & Pagel, B. E. J. 2004, Monthly Notices of the Royal Astronomical Society, 348, L59

Pettini, M., Shapley, A. E., Steidel, C. C., et al. 2001, The Astrophysical Journal, 554, 981

Pilyugin, L. S. 2001a, Astronomy and Astrophysics, 369, 594

—. 2001b, Astronomy and Astrophysics, 374, 412

—. 2001c, Astronomy and Astrophysics, 373, 56

Plionis, M., Terlevich, R., Basilakos, S., et al. 2011, Monthly Notices of the Royal Astronomical Society, 416, 2981

Poznanski, D., Butler, N., Filippenko, A. V., et al. 2009, The Astrophysical Journal, 694, 1067

Raimann, D., Storchi-Bergmann, T., Bica, E., Melnick, J., & Schmitt, H. 2000, Monthly Notices of the Royal Astronomical Society, 316, 559

Riess, A. G., Filippenko, A. V., Challis, P., et al. 1998, The Astronomical Journal, 116, 1009

Riess, A. G., Nugent, P. E., Gilliland, R. L., et al. 2001, The Astrophysical Journal, 560, 49

Riess, A. G., Macri, L., Casertano, S., et al. 2011, The Astrophysical Journal, 730, 119

Sargent, W. L. W., & Searle, L. 1970, The Astrophysical Journal, 162, L155

Schaefer, B. E. 2007, The Astrophysical Journal, 660, 16

Searle, L., & Sargent, W. L. W. 1972, The Astrophysical Journal, 173, 25

Shapley, A. E., Erb, D. K., Pettini, M., Steidel, C. C., & Adelberger, K. L. 2004, The Astrophysical Journal, 612, 108

Siegel, E. R., Guzmán, R., Gallego, J. P., Orduña López, M., & Rodríguez Hidalgo, P. 2005, Monthly Notices of the Royal Astronomical Society, 356, 1117

Skillman, E. D., Kennicutt, R. C., & Hodge, P. W. 1989, Astrophysical Journal, 347, 875

Stolte, A., Brandner, W., Grebel, E. K., Lenzen, R., & Lagrange, A.-M. 2005, The Astrophysical Journal, 628, L113

Storchi-Bergmann, T., Calzetti, D., & Kinney, A. L. 1994, The Astrophysical Journal, 429, 572

Suzuki, N., Rubin, D., Lidman, C., et al. 2012, The Astrophysical Journal, 746, 85

Swinbank, A. M., Smail, I., Chapman, S. C., et al. 2004, The Astrophysical Journal, 617, 64

Telles, E., Melnick, J., & Terlevich, R. 1997, Monthly Notices of the Royal Astronomical Society, 288, 78

Telles, J. E. 1995, PhD thesis, Univ. Cambridge, (1995)

Terlevich, R., & Melnick, J. 1981, Monthly Notices of the Royal Astronomical Society, 195, 839

Terlevich, R., Melnick, J., Masegosa, J., Moles, M., & Copetti, M. V. F. 1991, Astronomy and Astrophysics Supplement Series, 91, 285

Terlevich, R., Terlevich, E., Melnick, J., et al. 2015, Monthly Notices of the Royal Astronomical Society, 451, 3001

Terlevich, R., Terlevich, E., Rosa-González, D., & Silich, S. 2003, in Astronomical Society of the Pacific Conference Series, Vol. 297, Star Formation Through Time, ed. E. Perez, R. M. Gonzalez Delgado, & G. Tenorio-Tagle, 149

Tremonti, C. A., Heckman, T. M., Kauffmann, G., et al. 2004, The Astrophysical Journal, 613, 898

van der Wel, A., Straughn, A. N., Rix, H.-W., et al. 2011, The Astrophysical Journal, 742, 111

Veilleux, S., & Osterbrock, D. E. 1987, Astrophysical Journal Supplement Series, 63, 295

Wang, Y., & Mukherjee, P. 2006, The Astrophysical Journal, 650, 1

Weiner, B. J., Willmer, C. N. A., Faber, S. M., et al. 2006, The Astrophysical Journal, 653, 1027

Xia, L., Malhotra, S., Rhoads, J., et al. 2012, The Astronomical Journal, 144, 28

Zaritsky, D., Kennicutt, Jr., R. C., & Huchra, J. P. 1994, Astrophysical Journal,, 420, 87